Industrial Induction Heating - with a focus on multi coil solutions

Frogner, Kenneth

2014

Industrial Induction Heating – with a focus on multi coil solutions

Doctoral Thesis

Kenneth Frogner
Lund University, Division of Production and Materials Engineering

March 11, 2014

Abstract

Most types of materials and components use heating during the manufacturing process, with a large potential for cost and energy savings. Induction heating is the most energy efficient industrial heating technology for many applications, but so far technical limitations has delayed large scale introduction. The difficulties relate to heating of large flat and curved surfaces, and, perhaps most important of all, the difficulties in achieving a uniform heat distribution. The efficiency of existing industrial induction heating systems on the market is often low, with clear demands for improvement.

The first part of this work aims to improve the efficiency and manufacturability of induction heaters. By combining a newly developed core material, a silicon-iron powder composite, with litz wire for high frequency applications, very high efficiency heaters can be manufactured. The powder composite can be molded into any size and shape which allows building large, complex structures with integrated cooling. The results from this work have been commercialized and an increasing number of companies can benefit of substantial economical and energy savings in the production.

The second part of the work concerns investigating a type of induction heating based on several coils, in order to achieve uniform heating. The method is called travelling wave and characterized by a fast propagating electromagnetic field that moves along the workpiece. The challenges related to multi-coil solutions are many, because of the interaction between the currents in the coils. The work contains results of the system behavior based on analytical models, simulation results of the heating pattern, and above all, experimental validation of the models. The general accuracy of the analysis of travelling wave systems has been greatly improved. Solutions to the challenges limiting the practical use of travelling wave systems are presented.

Combining the new materials and production methods developed for induction heaters, with the technology of multi-coil heating has the potential to greatly improve the output from industrial processes in terms of cycle time, energy efficiency and product quality. For thermal cycling operations, the thermal mass is a huge problem. Given a method to supply uniform heating of thin workpieces provides entirely new conditions for many industrial processes; considerably reduced energy consumption, an increased production rate and products with new and improved properties.

Acknowledgements

The work presented in this thesis has been carried out during a number of years with many people, companies and organizations involved, contributing in different ways. First of all I would like to express my sincere gratitude to my supervisor Mats Andersson, who always takes his time to discuss any type of idea or problem, and with a light touch significantly improves the work. The co-supervisor Tord Cedell has contributed with valuable technical knowledge and always questioned the results, which have been very helpful. Also the contributions from my former supervisor, from the first year as a Ph.D. student, Jan-Eric Ståhl is acknowledged.

Other people involved in the projects are Peter Jeppsson and Leif Siesing (former Svensson) who developed the core material used in this work and helped producing many of the inductors tested, their results was crucial to complete this thesis. Oleksandr Gutnichenko made most of the analytical work related to travelling wave induction heating which is greatly appreciated. Ville Akujärvi helped implementing and calibrating the automatic thermography and made many of the experiments related to this, as well as other tasks, a significant help that is much appreciated. Lanny Kirkhorn has been a great support for the most crazy ideas, when everyone else has since long stopped listening. He has also supported with corrections, gratefully acknowledged. Other important people are the workshop personnel, Svante Bouvin and Ryszard Wierzbicki who produced many of the test platforms.

Furthermore, I would like to express my sincere gratitude towards all my colleagues at the Division of Production and Materials Engineering at Lund University for your support and interesting discussions. Also the help and contributions from cooperating companies are appreciated.

The present work was carried out with the financial support from the Swedish Foundation for Strategic Research (project RaUCH), from Mistra and SSF (project Greenheat) and from Vinnova within the Sustainable Production Initiative (SPI). Their support is gratefully acknowledged.

Contents

Symbols and Abbreviations

Abbreviations

EMC	Electromagnetic compatibility
CFRP	Carbon fiber reinforced plastic
TFIH	Transverse flux induction heating
LFIH	Longitudinal field induction heating
CVD	Chemical vapor deposition
SMC	Soft magnetic composite
MDM	Magnetodielectric materials
IH	Induction heating
SM^2C	Soft magnetic moldable composite
AC	Alternating current
DC	Direct current
VFD	Variable frequency drive
FPGA	Field programmable gate array
TWIH	Travelling-wave induction heating
FEA	Finite element analysis
FEM	Finite element method
PCB	Printed circuit board
LCR	Inductance, Capacitance, Resistance

List of Symbols

P	Power [W]
I	Current [A]
R	Resistance [Ω]
J	Current density [A/m^2]
E	Electric field [V/m]
f	Frequency [Hz]
B	Magnetic field [T]
H	Magnetic field strength [A/m]
V	Volume [m^3]
J_S	Surface current density [A/m^2]
d	Distance [m]
δ	Skin depth [m]
ρ	Resistivitet [Ωm]
μ_r	Relative magnetic permeability
μ_0	Magnetic permeability for vacuum [H/m]

l	Length [m]
A	Cross sectional area [m^2]
P_d	Power density [W/m^3]
f_{res}	Resonance frequency [Hz]
C	Capacitance [F]
L	Inductance [H]
V_{out}	Excitation voltage [V]
V_L	Voltage across an inductor [V]
Q	Quality factor
W	Losses [W]
k_0	Steinmetz coefficient
α	Steinmetz coefficient, frequency dependency
β	Steinmetz coefficient, flux density dependency
σ	Stefan-Boltzmanns constant [W/m^2K^4]
T	Temperature [K]
Q	Reactive power [VAr]
t	Time [s]
φ	Phase angle [rad]
Z	Length [m]
c_p	Specific heat capacity [kJ/kgK]
m	Mass [kg]
M	Mutual inductance [H]
k	Coupling factor
V	Voltage [V]
w	Angular frequency [rad/s]
σ	Electric conductivity [S/m]
ϵ	Permettivity [F/m]

1 Introduction

In the book *Catching Fire: How Cooking Made Us Human* [1], anthropologist Richard Wrangham presents a new theory of human evolution, starting almost two million years ago with knowledge of how to control fire. Fire allows the cooking of food, the single most important reason for the evolution of modern humans, according to the author. Food preparation reduces the time required for chewing and significantly improves food digestibility, according to research carried out at Harvard University into the eating habits of chimpanzees and humans. Though the theory that cooking accounts for humanoid evolution is fairly well substantiated, it is far from generally accepted and requires additional support from clear archaeological evidence. However, the importance of heating for the development of modern society is generally accepted by researchers. The production of most materials, from metals to ceramics and plastics, today relies on heating in one step or another. In addition, the digital revolution requires fast and precise heating to produce the semiconductors [2] [3] essential in all electronic equipment. *Fast and precise* are watchwords in the present work, together with *efficient* and *environmentally friendly*, words associated with sustainable production.

1.1 Background and aim

Industrial heating can be done in various ways, ranging from open flames, still used in many applications, to furnaces, infrared (IR) furnaces, hot gases or liquids, and induction or heat transfer in solids using, for example, temperature-controlled tools. Induction heating supplies most of the properties required for modern production, namely, low investment cost, high flexibility, fast operation, immediate startup, and freedom from pollutants. In addition, its potentially high efficiency and very wide application area make the technology especially attractive, motivating the present work. Although induction heating has been commercially used for about a hundred years [4] [5] [6], its efficiency is often relatively low and its application areas limited due to the non-uniform heating patterns produced, with parts of the necessary components being produced in the same way and of the same materials as when the process was introduced. The image used on the cover of the book *History of Induction Heating and Melting* (Figure 1) gives a telling impression not only of the history, but also of the present usual reality of induction heating—a few turns of copper tubing, without any kind of flux concentrator. The losses in the coil can easily be transferred away from the critical region using water cooling, which calls for very robust construction

but suffers from low efficiency, imposes design limitations, and usually gives rise to severe problems with stray magnetic fields. Efficient solutions exist, but are generally sensitive to high temperatures and often require complex and expensive manufacturing processes with geometrical limitations, and therefore are not commonly used for real applications.

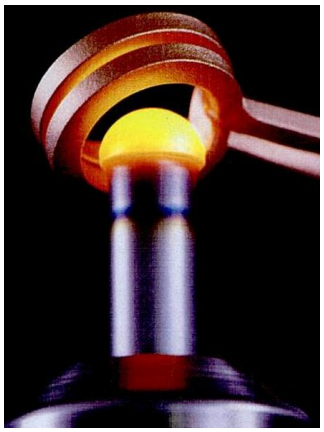

Figure 1: A common water-cooled induction coil made of copper tubing heating a steel rod [5].

After an introductory section summarizing industrial heating today as well as the basic theory of induction heating, this work treats two main areas: 1) material technology related to heating inductors and 2) various aspects of multi-coil heating, particularly as concerns *travelling-wave induction heating*, with a focus on methods to achieve uniform heating.

This work aims to describe induction heating solutions that can be implemented in industry and offer large advantages over existing alternatives. There are two ways to access an industrial market. The first is to come up with a very cost-effective solution with many parameters, ranging from the investment in the unit itself, through processing time, energy consumption, and cooling and space requirements, to environmental aspects such as noise, pollution, and electromagnetic compatibility, EMC issues. The second way is to provide a solution with unique properties that allows for new application areas. New applications can imply new products, often based on new combinations of materials not previously available, but may also involve a change in technology, for example, using heating where it has not been used before. The thesis will present examples of new applications in which the technology developed here has been used or successfully tested as well as applications in which it has cost-effectively replaced existing technology.

The uniform heating results produced by the method have great potential to boost the productivity of thermal-cycling processes by significantly reducing the thermal mass and also entail huge energy savings. In the final analysis, only two properties determine whether or not an industrial solution is profitable: the cost and quality of the items produced.

1.2 Problem description

Developing an induction heating system with a uniform heating pattern is a true challenge, both scientifically and technically. The problems related to the inductor and its control can be summarized in five areas, all of which must be considered in order to meet this challenge.

1. Efficiency: The total efficiency of an ideal induction heating process is very high; the challenge is to achieve this in a multi-coil arrangement.
2. Manufacturability and geometric flexibility: The induction heating of flat or curved surfaces calls for new ways to produce coils and flux concentrators.
3. Stray magnetic fields: These should be minimized and therefore must be considered when designing the inductor.
4. Solutions for uniform heating: This is the common problem in most induction-heating setups, and very few solutions have been demonstrated to work.
5. Controllability of spatial and absolute temperature: This problem is connected to uniform heating, but full control of the temperature in different zones would offer further advantages.

The three first problem areas are closely related to the selected materials and their properties, while the last two are fairly dependent on the control of the induction process. All the problem areas are linked and are related to the design and shape of the inductor.

1.3 Objectives

Given the complex of problems, the scientific objectives of this thesis are mainly related to the multi-coil concept and the control system. The overall objective of the work is to develop, analyze, and demonstrate a working laboratory-scale travelling-wave induction-heating (TWIH) unit; however, within this overall objective, several more detailed objectives can be defined:

- Elaborate a TWIH simulation model and verify its results experimentally.
- Develop methods to determine how current phase shift affects the heating results of multi-coil heating.
- Identify the working points of a TWIH setup and analyze their properties. This objective was added to the list after the first experimental iteration.
- Analyze ways to handle the mutual coupling of multi-phase inductors.
- Develop an automatic measurement tool for analyzing the efficiency and heating pattern of the developed setup.
- Identify the circumstances under which TWIH is a competitive heating alternative.
- Analyze ways to adapt single-sided TWIH to industrial applications.

1.4 Delimitations

This work covers the complete chain of development, from material development, simulation, and inductor design to manufacturing, testing, and verification. All these phases are interlinked and all must be understood to achieve proper results. The work takes a clear approach to the development of generic inductor design solutions and their electromagnetic control, in order to produce the desired heating patterns. Close cooperation with colleagues, focusing on material development and inductor manufacture, delimits the work significantly. Material aspects as well as electric and thermal interactions between materials are important factors in the development of induction units, though they are not treated here; the same applies to soft switching and fast current control. Industrial partners that have handled prototype testing in real applications and given feedback on testing results have provided valuable help, limiting the work further. Figure 2 illustrates the complete structure of the development process, the green-colored elements belonging to this work and the red ones being supplemental.

This work focuses on low-temperature applications, meaning processes using a maximum temperature of a few hundred degrees Celsius, but the results can also be applied to high-temperature and high-power applications, as explained later. Similarly, the work refers to the heating of flat surfaces, but curved surfaces, shafts, billets, and small components that are normally

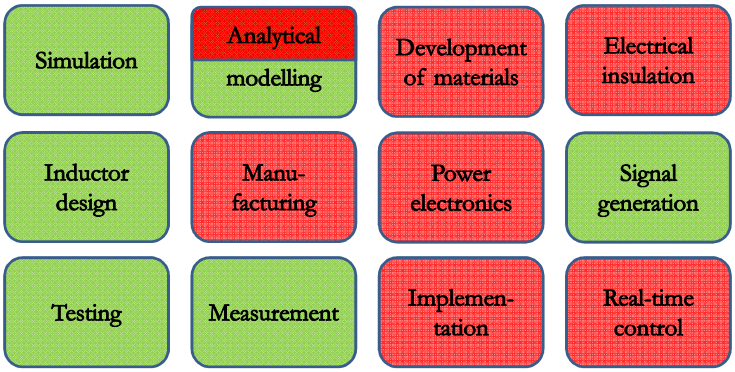

Figure 2: Elements of the development of the high-performance induction heater, the green boxes represent essential parts of this work, while the red ones were largely brought into the project by others.

heated using surrounding coils can also benefit from the findings. The inductors are exclusively based on one type of soft magnetic material, developed at Lund University and demonstrated to provide good properties for prototype manufacturing and laboratory testing, but the results are valid for any type of core material; to that end, a comparison of the properties of alternative materials is presented. As the industrial market can accept a fairly high heater price providing the technology yields production savings, the effort has concentrated on performance and manufacturability rather than cost optimization. It should also be noted that material properties not directly related to the electromagnetic and thermal design, for example, structural properties, have been neglected.

1.5 Methodology

The work is based on a top–down approach, starting with the applications or the expected demands placed on an induction heater and stepwise breaking the heater system into subsystems with specific requirements. The methodology was developed in close cooperation with industrial partners, which explains why functional prototypes were generally achieved. The industrial focus was not always a scientific advantage, however, as it sometimes resulted in complex design concepts difficult to analyze using simulations or analytical expressions and only testable experimentally. In hindsight, a more appropriate approach would have been to sometimes complement the complicated applied designs with simple axisymmetric or planar models easy to analyze in detail using computational tools. Later in the work, this lesson

was learnt and, for example, the examination of travelling-wave induction heaters disregards the core material at the ends and instead focuses on planar properties.

The research was based on iterative cycling among simulations, analytical models, and experiments, as shown in Figure 3. The start state varies depending on the complexity of the inductor. For heaters for which a 2D axisymmetric or planar simulation model can be easily built, this is the preferred choice. For complex 3D problems, manufacturing a simplified or full prototype followed by experimental testing is generally the fastest way to understand the design, while analytical solutions may be the best place to start if similar designs have been previously investigated.

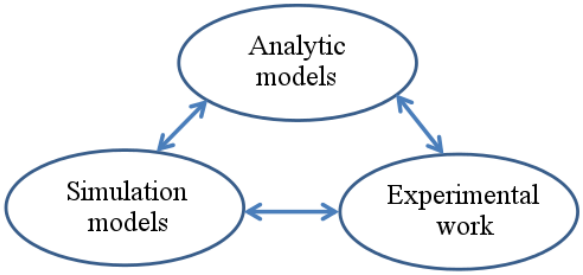

Figure 3: The iterative chain of inductor design.

The moldable soft magnetic material on which the present design work relied allowed us not only to produce large structures, but also to rapidly build prototypes, even those with complex shapes. Together with the automatic measurement tool developed in this work, this rapid prototyping ability was one reason why experiments may have been the best approach for investigating certain designs. For short-term experiments, the thermal design was not particularly critical, which shortened the production time.

1.6 Scope

The first part of this work focuses on alternative materials and production methods for heating inductors. Using a combination of materials with suitable properties allowing for effective production for each volume of the unit is a challenge. Important considerations in this are the electromagnetic design, loss distribution, interaction between different materials to allow for necessary cooling, heat transport within the inductor, and dielectric strength between coils and the surroundings. The properties of the developed materials must match the demands imposed by different applications. The goal is a

production method with a high degree of geometric flexibility that allows the creation of high-efficiency components also able to meet the requirements of industrial applications.

The second part continues the first, using the developed production method to build inductors designed to generate uniform and spatially controllable heating. This part focuses on multi-coil solutions, mainly for travelling-wave induction heating. The interaction between coils, the influence of current amplitudes and phase shift on the heating pattern, and the decoupling of the system are important aspects. The switching pattern and current control in this kind of system are important factors in achieving good results and relate to the combination of materials through saturation effects. The selection of materials can allow for new inductor designs by providing paths by which the electromagnetic fields can penetrate the wires as well as being focused in critical regions, which affects the control of the currents. The work also contains a section treating an alternative inductor design that is one of the few single-phase solutions that can compete in terms of uniform induction heating.

Instead of a deep focus on specific details, this work uses a higher abstraction level to encompass the complete chain ranging from analytical expressions, simulation models, and experimental verification to industrial implementation and analysis. This large scope links the academic work with industrial needs in a way that is unusual, though important for both academy and industry. It also highlights the differences between models and reality and emphasizes the difficulties of realizing ideas in working prototypes. In addition, the development of novel measurement and analytical tools has been an important component of this work.

2 Industrial heating

Heating is fundamental to many processes, from melting, curing, drying, and vaporization to heat treatment, joining, and many other applications. Induction can be used for many of these applications, either for directly heating the target material or for indirect heating, using some kind of tool. This section discusses and cites examples of heating methods related to a selection of processes in which it is possible to replace the current heating method with induction. As a major focus of this work is on efficiency, absolute and spatial control of temperature and cycle times, together with features related to these areas, are considered when evaluating a range of properties in a comparison of different heating methods. In addition, other properties, such as the complexity of industrial implementation, startup time, and cost, are briefly discussed. Since the properties of a certain method can vary significantly depending on the process and the actual design, it is difficult to provide exact numbers and to cite directly applicable references. Instead, the aim is to provide a simple overview and the author encourages the reader to create his or her own assessment based on unbiased sources.

2.1 Processes

Many processes are based on heating—chemical reactions and drying, shifting the state of matter, temporarily modifying material properties, metallurgical processing, catalyzing or separating substances, joining materials, etc. Most materials used today, whether metals, glass, plastics, semiconductors, gasses, or liquids, have their origins in various raw materials, often bound in ore, minerals, fossil materials, or biomaterials, and need to be extracted, purified, and further processed based on heating. The same applies to the recycling of materials. What can be defined as the *production of components* thus starts with materials or substances that have already been subjected to heating processes, usually in large-scale factories and often more than once. This work focuses on, but is not limited to, the processes that treat the elemental materials as input.

Processes that the author or cooperating companies have been involved in include food processing, component preheating, in-tool heating for manufacturing composites, thermal expansion, hardening, annealing, and melting. Other processes that use heating are hot rolling, beam straightening, component joining, oil evaporation, and thermoset curing. Production can comprise several steps and the output need not necessarily be the final product.

One area that has resulted in significant weight savings and product improvements in the vehicle industry is the production of high-strength steel using controlled-temperature processing. An example is Domex® high-strength steel, manufactured using thermomechanical rolling [7]. Another area with great potential is hot forming. Aluminum and magnesium alloys are difficult to form into bi-curved and other complex shapes at room temperature, but there is a large market for electronic equipment covers and larger components such as vehicles made of these materials. In addition, high-strength steels benefit from hot forming, though the process is still used only at a limited scale. Another large area with considerable potential and that also involves heating is the production of carbon-fiber-reinforced plastics (CFRP)—a field still in its infancy. All these combined heating and forming operations need not only a supply of energy but a complete cycle of heating and cooling.

2.2 Principles of industrial heating

There are many types of heating sources, ranging from nuclear power to thermoelectric or magnetocaloric effects, each with a range of suitable applications. When it comes to heating in industrial manufacturing processes, industrial demands significantly limit the most used heating sources. Some common industrial heating methods are:

- Open flame (e.g. gas burning)
- Furnace
- IR radiation
- Induction
- Resistance (e.g. heating cartridge)
- Hot oil or water
- Laser
- Chemical reaction

Some of these methods can supply energy directly to the target object while others require heat transfer using conduction, convection or radiation. Except for exclusive solutions such as lasers or electron beams, induction is the most power-dense heating source (Figure 4), and the one with the best

ability to create large thermal gradients. Induction heating, unlike most other heating principles, supplies power not only to the surface but also a well-defined distance into the material by adjusting the excitation frequency.

Type of heating	Power transmission (W/cm^2)
Convection (Carrying heat, by molecular movement)	5×10^{-1}
Radiation (electric furnace, box-type furnace)	8
Thermal conduction, touch (hot plate, salt bath)	20
Infrared point emitters	2×10^{2}
Flame (burner)	10^{3}
Induction heating	10^{4}
Laser (CO2)	10^{8}
Electron jet	10^{10}

Figure 4: Maximum power transmission of different heating principles.

2.3 Challenges and bottlenecks

Many targets to be heated are freely moving: travelling on a conveyor belt, transported through the air in the gripper of a robot, or continuously rotating (e.g. a roller). Although there are ways to transfer gas or liquid media as well as electricity into moving components, additional costs and complexity are related to doing so. Furnaces, IR furnaces, flames, and induction heating have a completely wireless transfer of energy and are frequently used in such applications. The emissivity of unpainted metal components is generally low at IR wavelengths, making this type of heating inefficient. For painted components and non-reflective materials IR heating works well but, although several times better than traditional furnaces, it still requires significant time to heat objects, which means huge space requirements for large-scale manufacturing. The long startup time and idle-time power consumption of furnaces are drawbacks as well. Flames and induction both allow for fast heating, short startup times, and low idle power consumption. However, flames can easily damage thermally sensitive materials and most of the supplied energy is lost to the surroundings. Induction heating is limited to metals and other electrically conductive materials and its efficiency in

industrial applications is generally only slightly better than that of flames. Depending on the component geometry, overheating might be a problem along edges in induction-heating setups. While gas burning can, depending on the type of gas, potentially pollute the air with carbon dioxide and other compounds, the pollutants from induction heating are high-frequency electromagnetic stray fields that can interfere with surrounding equipment—though these can be nearly eliminated using a properly designed inductor. For inefficient processing, cooling of the environment is sometimes a severe problem that is rarely discussed in public.

Electrical cartridges or hot oil flowing in channel systems are common methods for in tool heating. The widely-spaced distribution of these heaters often provides a fairly non-uniform temperature profile that must be equalized before reaching the tool surface. To distribute the temperature uniformly on the surface, an excessive amount of material is required, which increases the thermal mass and slows down the dynamics. For temperature cycling operations, this is fatal. A method for uniform heating of the tool surface only, would significantly improve productivity and introduce new application areas for the technology.

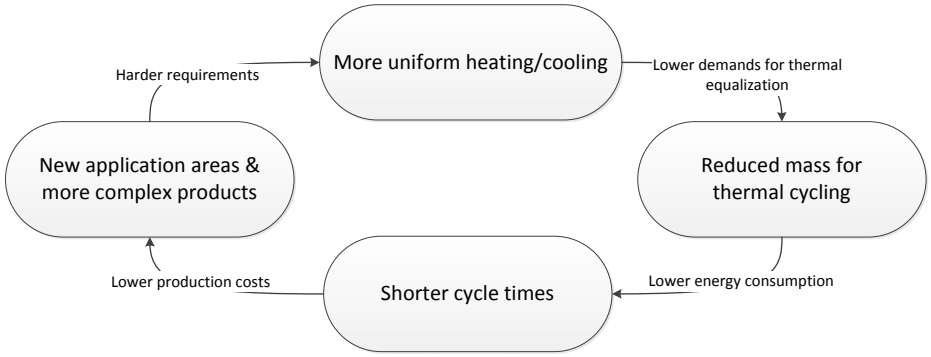

Figure 5: Uniform heating leads to a positive development, where cycle times can be reduced and new application areas can be exploited.

The investment cost for induction heating is usually higher than open flame, and resistive heating while in the same region for furnaces and hot oil. For a multi kW-system the investment cost for induction heating is in the order of 1 euro per net watt. Since induction heating is power dense, the cost for the factory space occupied by the heating equipment should also be considered in the grand total. Induction heating is not the most generic of heating principles; if products with a large variation in material, size and shape are to be heated with the same induction coil, the heating

result is bound to be non-uniform and the overall efficiency poor. On the other hand, the result obtained will be very repetitive with small temperature variations. With conservative dimensioning of the induction heating system, maintenance can be kept to a minimum. For water cooled copper-tube inductors, the water needs to be kept free from ions. If air/fluid heat exchanger or coolers are used, fan filters must be changed on regular basis. Also, thermal isolation material close to the heated object can sometimes need to be changed due to wear. This is a drawback for induction heating because in order to get good system efficiency, the coil should be kept close to the heated object thus increasing the wear of the isolation material.

3 Basic theory of induction heating

This section gives a brief overview of the theory of induction heating and points out a few important matters that are crucial for understanding this work. The technology is characterized by the non-contact supply of power due to currents induced in a workpiece by an alternating magnetic field. The resistive losses, proportional to the square of the current, according to Equation 1, are generally the dominant power source, but for some materials magnetic hysteresis losses also provide a significant contribution. The hysteresis losses are determined mainly by the coercivity, but also by the remanence, and increase linearly with the frequency and the integral of the enclosed area of the magnetic field, as shown in Figure 6. The total hysteresis losses are obtained by integrating the result over the entire volume; see Equation 3.

$$P = I^2 \cdot R \tag{1}$$

$$P_d = \vec{J} \cdot \vec{E} \tag{2}$$

$$P = f \cdot \iint B \cdot dH \cdot dV \tag{3}$$

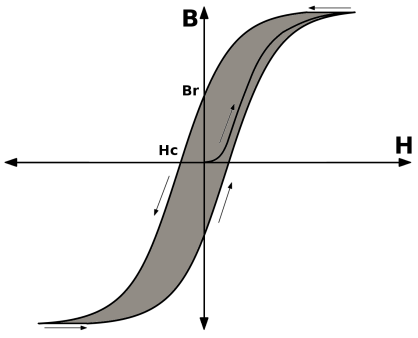

Figure 6: Magnetization curve, hysteresis.

The alternating electromagnetic field is usually generated by coils carrying a high-frequency current, although permanent magnet solutions do exist [8] [9]. The coils can be grouped in several configurations, the most common of which are shown in Figure 7. Longitudinal-field (LF) inductors usually surround the workpiece and are commonly used to heat rods, tubes, billets, etc. with good electromagnetic coupling. For flat or curved surfaces,

the transverse-flux (TF) coil is probably the most frequently used, for example, in cooktops and for heating sheets, strips, and large rolls. The face inductors shown in Figure 7 and bifilar inductors are generally less efficient than the other types but are used in applications that require a uniform heating pattern.

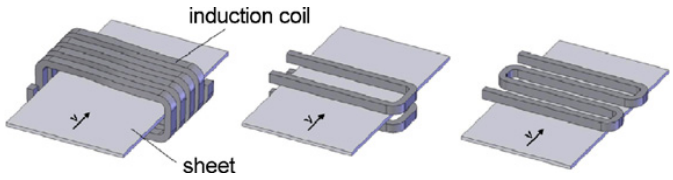

Figure 7: Different types of coils [10].

Other heating topologies discussed in this thesis are zone-control induction heating (ZCIH) and travelling-wave induction heating (TWIH). ZCIH typically refers to LF or TF heating with more than one coil (Figure 8), with the aim of providing spatial control of the heating pattern. TWIH is defined as a system of two or more coils the currents of which have different phase shifts in such a way that a travelling magnetic field is generated (Figure 8).

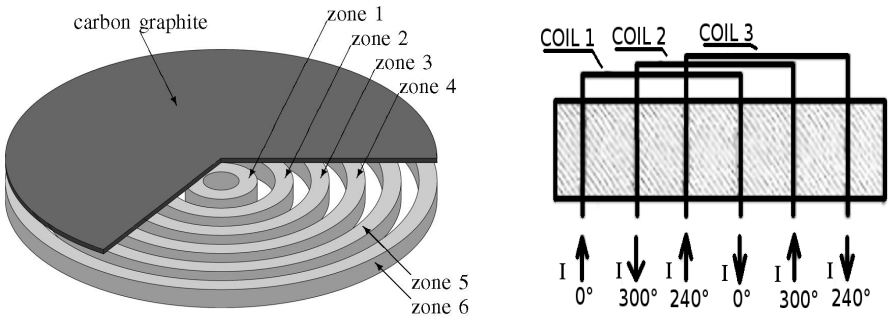

Figure 8: Heating topologies: Left: ZCIH with six coils [11]. Right: TWIH with three coils [12].

One of the most important matters related to induction heating is the skin effect. Equation 4 describes how the current density, J, diminishes from the surface current density, J_S, with increased distance, d, into a material with the skin depth δ. The skin depth is a frequency- and material-dependent variable determined by Equation 5. The influence of the electrical resistivity, ρ, and relative magnetic permeability, μ_r, on the efficiency due to the skin effect, however, is rarely considered. Figure 9 shows four plots, 9a and 9b were calculated analytically and 9c and 9d were using numerical

tools. Figure 9a illustrates the skin depth as a function of the frequency for different materials: iron has by far the smallest values of the selected materials due to its high permeability, followed by the best electrical conductors. The AC resistance of an object much thicker than the skin depth δ corresponds to the DC resistance of a flat or hollow piece with the wall thickness δ. By considering a TF coil lying above a thick plate and applying the law of resistance in uniform conductors (equation 6), an equivalent resistance can be calculated. The equivalent resistance for the different materials as a function of the frequency, proportional to the efficiency of an ideal induction-heating system, is illustrated in Figure 9b.

$$J(d) = J_S \cdot e^{-d/\delta} \tag{4}$$

$$\delta = \sqrt{\frac{2\rho}{2\pi f \mu_r \mu_0}} \tag{5}$$

$$R = \rho l / A \tag{6}$$

The efficiency as a function of the electrical conductivity is presented in figure 9c, also considering the frequency-dependent proximity and eddy current losses in the litz coil. The exact values are obtained for one particular case of a TF inductor with a strand diameter of 0.1 mm for the wire, but the behavior and shape of the curve is valid for most inductor designs. The results are computed for three cases: workpiece thicknesses and frequencies of 1 mm and 20 kHz, 1 mm and 50 kHz, and 2 mm and 20 kHz to illustrate the influence of different parameters. Figure 9d shows the efficiency as a function of the frequency for a number of different materials. The setup is the same as for figure 9c and the workpiece thickness is 1 mm. From the plots it is clear that leakage due to a relatively large skin depth versus the material thickness significantly lowers the efficiency.

Another important aspect of induction-heating systems is the need to compensate for the reactive power by adding a capacitance, C, in series or parallel to the inductor, L. If there is good electromagnetic coupling between the currents in the coil and the workpiece, the excitation frequency is not very critical. To avoid significantly reducing the active power, low coupling requires that the system run close to resonance, f_{res}, determined by Equation 7. For a certain setup, a small frequency change can reduce the output power by more than one order of magnitude. A high coupling factor is also important because of the relationship between the excitation voltage, V_{out}, the quality factor, Q, and the voltage across the inductor, V_L, in a

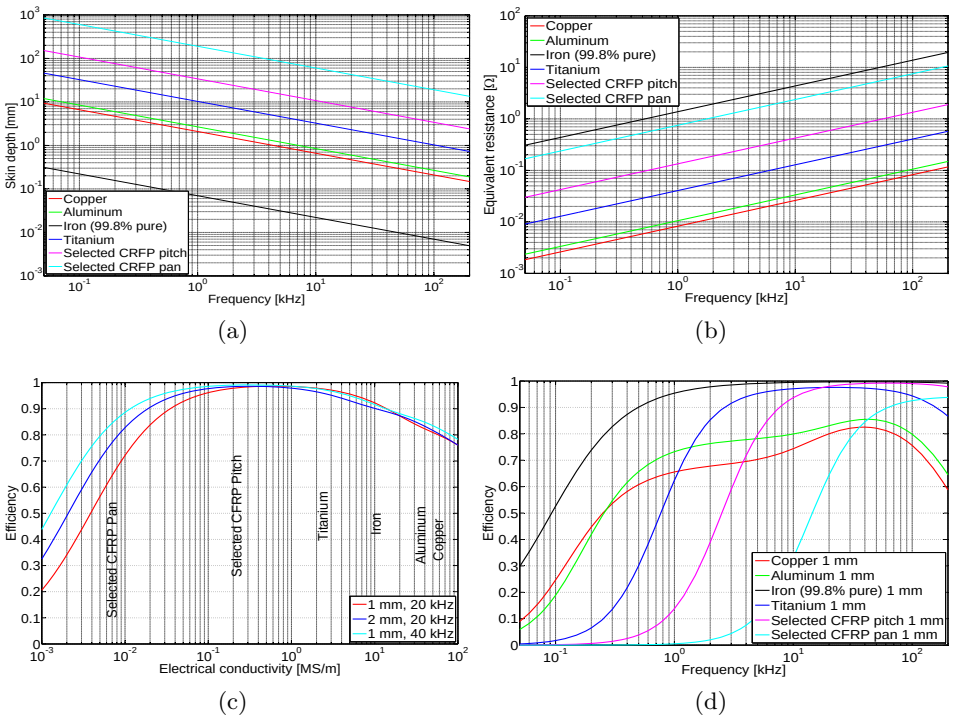

Figure 9: Important properties related to the heating efficiency.

series resonance circuit, Equation 8, since a high peak voltage increases the risk of an electrical breakdown.

$$f_{res} = \frac{1}{2 \cdot \pi \sqrt{L \cdot C}} \tag{7}$$

$$V_L = V_{out} \cdot Q \tag{8}$$

Proper impedance matching is important in order to use the full power of the inverter, which is why transformers are commonly used. Since materials have different equivalent resistances, according to Figure 9, it is difficult to effectively heat different materials using the same setup. Due to saturation effects, the differences between materials with high magnetic permeability and other materials are not as great as shown in the figure, but depend on the output power.

The heating from an inductor is generally highest near the coil, with some exceptions. Since all current paths must be closed, this allows for

heating even at a certain distance from the coil, a capability that is used in selected applications [13]. By adding a core material, the reluctance can be locally reduced with a significant improvement of the heating power due to larger flux density at constant current. The core material also enables the heating pattern to extend to areas not in the immediate neighborhood of the coil, which is not easy to obtain efficiently otherwise the smaller the distance between the inductors, the better the system's efficiency, this also depends greatly on the inductor design.

4 Soft magnetic materials

In many electromagnetic components, soft magnetic materials (SMM) are used to provide a path for the magnetic field, to control the flux and improve the efficiency of the product. [14] [15] [16] [17] For transformers and electric machines, the most common material is laminated steel, while many high-frequency applications, such as switched-mode power supplies, electrical filter components, high-frequency or pulse transformers, and ignition coils, use soft ferrites. All types of SMM have different properties that make them suitable for specific applications. In addition, within a group of materials, the properties can vary depending on the exact geometry and composition.

SMMs are materials that can conduct magnetic flux i.e. have a relative permeability[1] significantly greater than one and cannot be permanently magnetized, unlike hard magnets. For alternating fields, it is important to be able to guide not only the magnetic flux, but also to ensure high electrical resistivity perpendicular to the flux direction. Induced currents in the flux concentrator both counteract the functionality and create undesired losses, similar to losses that create heat in the workpiece of an IH system. In the same way as hysteresis losses need to be considered when calculating the total heating power of permeable workpieces in IH, the hysteresis loop must be small for SMMs used to conduct magnetic flux, both from the efficiency perspective and, most of all, from the thermal design perspective.

The most important technical properties of a SMM are magnetic permeability, anisotropy, and losses. The permeability is highly dependent on the magnetic flux density due to saturation effects, which need to be considered when designing the flux concentrator. In addition, anisotropy plays an important role in the equivalent permeability, since electrical barriers are often used to prevent resistive losses, and significantly reduces the value in a certain direction. The losses, W, are largely dependent on two properties, magnetic flux density, B, and frequency, f, and a common way to compare different materials and to calculate the losses under given working conditions is to define three variables, k_0, α, and β, in a Steinmetz model, Equation 9. In addition, the temperature affects the properties of the SMM, primarily the permeability, which attains a relative value of one when the temperature reaches the Curie point. In this work, the influence of temperature on the flux-concentrating material is disregarded, but its effect on the magnetic properties of the workpiece must be considered, being of major importance

[1] The term *relative permeability* refers to the value relative to vacuum

in many induction heating applications.

$$W = k_0 \cdot f^{\alpha} \cdot B^{\beta} \tag{9}$$

In this section, the properties of the most common groups of SMMs are summarized and compared from an induction-heating perspective, delineating their advantages and limitations for different heating applications. Properties of interest are:

- Losses i.e. hysteresis and resistive losses at high frequency
- Permeability
- Saturation
- Isotropy
- Thermal conductivity
- Temperature resistance (e.g. deterioration and Curie point)
- Manufacturability, machinability
- Cooling potential
- Cost

Figure 10 summarizes the properties of several SMM groups regarding permeability and saturation, while Figure 11 illustrates the properties of several magnetic materials regarding coercivity and remanence, showing the properties of hard magnets as a reference.

4.1 Laminated steel

The most common core material used in electromagnetic components is laminated steel, which is used in most electrical machines, transformers, and other low-frequency applications. The material was also commonly used in induction-heating applications when grid frequency was the natural choice, but has since been replaced with alternative materials when frequencies above approximately 10 kHz are required. Laminated steel, often referred to as electrical steel, is an alloy of iron and silicon, sometimes with small amounts of added aluminum, manganese, etc. and with a low carbon content[20]. The intention is to provide high magnetic permeability, low hysteresis losses, and high resistivity. The insulating layers, usually made

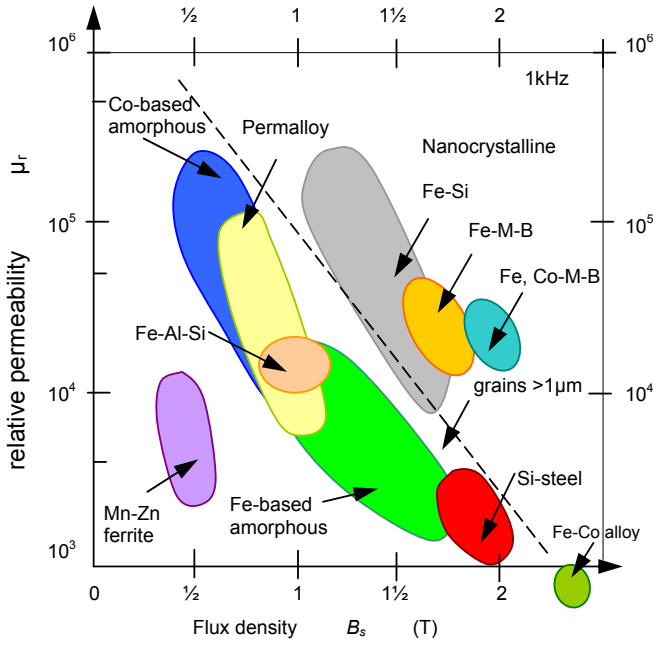

Figure 10: Properties of several soft magnetic material groups regarding relative permeability and saturation [18].

of resin or varnish, are applied in-plane with the magnetic fields to prevent eddy currents from being induced. These currents degrade the performance of the material and create resistive losses in the form of heat. Thinner laminates are required for higher frequencies. In addition, different kinds of non-organic insulation materials and oxides can be used [21]. The insulation material is often the limiting factor with regard to temperature. The Curie temperature of the material is much higher than the service temperature of any used varnish.

Silicon is added to reduce the losses in the iron, increase the magnetic permeability, and lower the magnetostriction, the latter being a major source of vibration and noise. From an electromagnetic point of view, the optimal silicon content is 6.5%, at which point the magnetostriction is completely eliminated and the losses and permeability reach local minima in a positive way (Figure 12). The drawback of this alloy is its mechanical properties, as the high silicon content makes the material brittle and non-ductile, making it very difficult to produce in the desired shapes. In 1993, the Japanese company JFE Steel Corporation introduced a chemical vapor deposition (CVD) process for manufacturing uniform JNEX and later also JNHF, a gradient

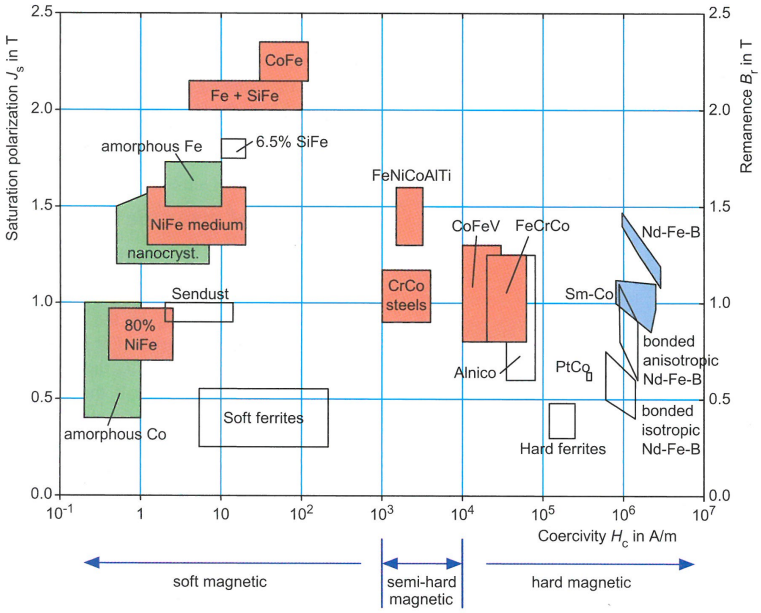

Figure 11: Properties of several magnetic material groups regarding coercive force and remanence [19].

high-silicon iron [23]. Using lamination thicknesses of 50–200 μm of this material, the losses can be kept small enough even at the frequencies of up to 50 kHz [22] typical in induction-heating applications. The laminations feature high permeability, exceeding 20,000 along the laminations [23], high saturation, high temperature resistance, and good mechanical properties compared with alternative core materials. On the other hand, cost, anisotropy, and manufacturability could be regarded as the weak points of this type of material.

Different alloys can have different properties, and the rolling direction, grain orientation, and heat treatment are also important. Annealing can be used to change the microstructure and thereby the electromagnetic properties of alloys, as well as for decarburization, loss reduction, and magnetic aging prevention [19].

4.2 Amorphous and nanocrystalline alloys

By means of the extreme rapid solidification of the melted material, in the order of 10^6 °C/s, into thin structures or ribbons, an amorphous structure can be obtained. The non-crystallographic structure so obtained, sometimes

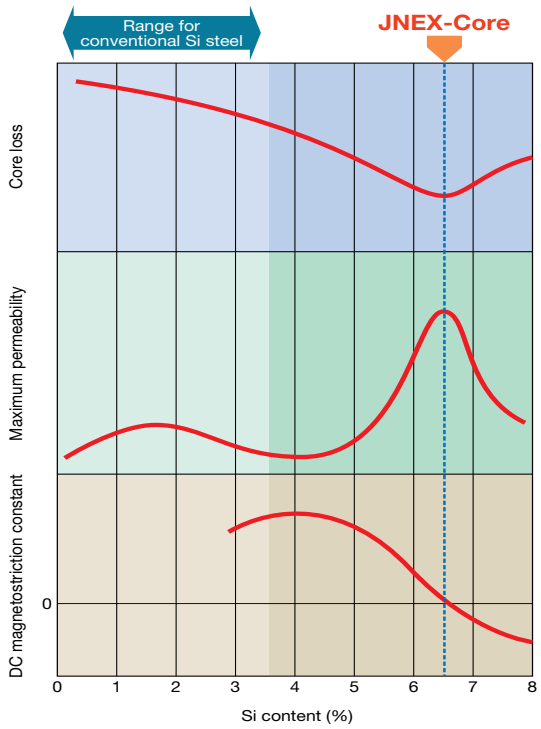

Figure 12: Variation in the magnetic properties of silicon steel by Si content [23].

referred to as metallic glass, exhibits extraordinary properties; by using an appropriate selection of alloys, with a base of iron, nickel, or cobalt, many useful soft magnetic materials can be produced. Their properties are highly dependent on the material composition and a range of qualities is available. One property that can be controlled is the magnetoelasticity, which make this type of material very useful in sensor applications [24]. Other benefits are low hysteresis losses, very high permeabilities, and relatively high saturation and resistivity, all of which are useful in core materials. If the amorphous alloy is exposed to high temperatures, its structure is reorganized into that of a crystal metal and its properties change. The recrystallization temperature depends on the alloy composition, but is typically approximately 400–500°C [19] [25].

By starting with the amorphous alloy and, in a very controlled way, letting parts of the structure transform themselves into a nanocrystalline structure in which the crystals are not allowed to grow more than in the order of 10 nm, the good properties of amorphous structures can be retained and

new positive effects be created. This nanocrystalline material can achieve very small hysteresis losses, very high permeability, high saturation, and zero magnetostriction [18] [19] [26]. Because of the very fast quenching needed to produce the amorphous structure, the thickness of these materials is limited to approximately 5–30 μm. When core components are built, each layer is typically covered by a thin layer of oxide or other insulating material to reduce the interlaminar conductivity, creating a material with extraordinary high-frequency properties. The Curie temperature depends on the exact composition, but can be well above 500°C [19] [26].

Thin ribbons of nanocrystalline material allow for bending without breaking at room temperature, in contrast to high-silicon electrical steel. This makes it possible to build components that require high permeability in all three directions, though in only two dimensions at a time, thus defined as 2.5D. This property makes it very suitable for high-performance high-frequency transformer cores, for example, as used in induction-heating appliances [27].

4.3 Soft ferrites

Most ferromagnetic materials also conduct electricity fairly well, which requires lamination or inter-particle insulation barriers at the microscale to prevent the material from being heated by circulating currents induced by the high-frequency electromagnetic fields. Among the ferromagnetic materials, which behave like ferromagnets when affected by a magnetic field, several oxides are found. Some of these materials, such as magnetite Fe_3O_4, have semiconductor properties with an electrical resistivity many orders higher than that of most SMMs. By adding for example manganese and zinc oxides, materials called soft ferrites with very low losses even at high frequencies, can be produced by sintering to a ceramic compound [19].

Soft ferrites can display a wide range of properties and can serve as core materials at up to hundreds of GHz [25]. The losses at high frequencies are low and soft ferrites are commonly used to concentrate the electromagnetic field, for example in induction cooktops. Soft ferrites can provide high permeability, exceeding 1000, but suffer from low saturation, rarely above 0.5 T and sometimes only half of that. In addition, the Curie temperature is generally lower than for other SMMs, defining the useful temperature limit, although variation within the group is large [19]. The thermal conductivity of soft ferrites is relatively low, in the order of a few $Wm^{-1}K^{-1}$ [28].

Soft ferrites are produced using powder metallurgy methods by means of compaction and sintering. Their ceramic properties make machining prac-

tically impossible, so production is limited in size and to net shapes only. Even so, a large range of geometries and sizes are available on the market, as shown in Figure 13.

Figure 13: Soft ferrites of various sizes and shapes [29].

4.4 Soft magnetic composites

Soft magnetic composites (SMC), sometimes known as magnetodielectric materials (MDM), are a group of flux concentrator materials with 3D properties suited for high-frequency applications. Such materials are made from soft magnetic particles usually covered with a thin electrically insulating layer (Figure 14) and held together using an organic or inorganic binder. The components are generally formed at high pressure to achieve high permeability and good thermal conductivity [30]. Some SMCs are semi-sintered to obtain the desired properties.

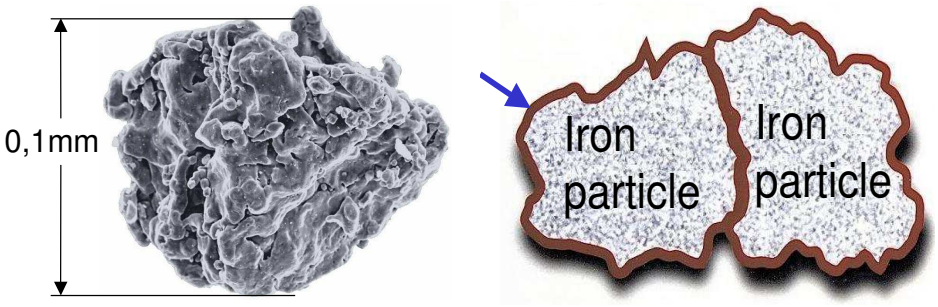

Figure 14: SMC particles: Left: Scanning electron microscope image of water-atomized powder [31]. Right: Image of pressed powder structure including insulating layer [31].

The particles, often produced as atomized powder or flakes, vary in shape and size. Like other SMMs, the particular alloy of the powder greatly deter-

mines the final properties of the SMC. As small insulated particles cannot induce significant eddy currents independent of the field direction, the losses can be small; however, the insulation significantly limits the permeability of the material. Thick insulation layers, preferred at high frequencies, are advantageous not only for the losses, but also for the dielectric strength of the material, as they prevent short circuiting. Generally, the lower the losses at high frequency, the lower the permeability of the material (Figure 15). Depending on particle size, insulation, composition, etc. the complete frequency range from DC up to many MHz can be competitively covered [6].

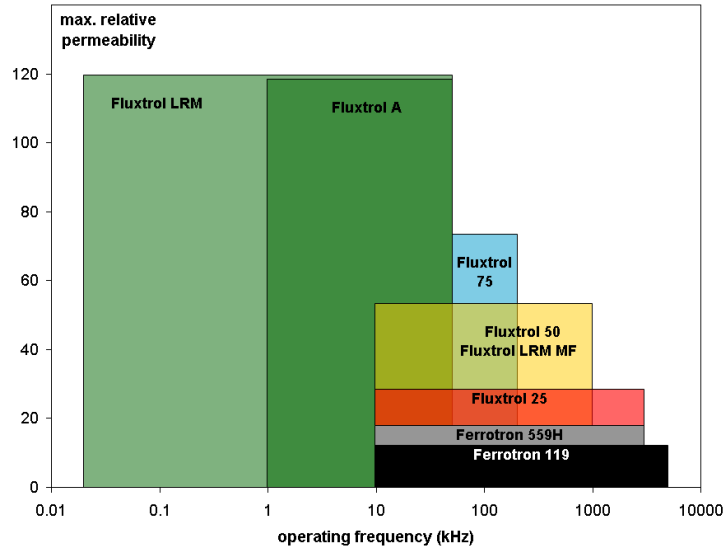

Figure 15: Comparison of different SMC materials from Fluxtrol Inc. [6].

Normally, but not necessarily, the particles are ductile and are deformed during pressing, which increases their permeability and thermal conductivity. The particular binder used is important for the mechanical properties of SMCs. Materials containing organic binders are generally machinable, while inorganic binders generate a more ceramic-like structure able to handle higher temperatures but with limited machinability. Due to the pressing, SMCs usually have anisotropic properties, dependent on the pressure, geometry, particle shape, etc. yet they are nearly isotropic compared with laminated structures. As for the soft ferrites, the pressure required during pressing limits the maximum size of individual components [30].

In polymer-based SMCs, the binder is the weakest point from a thermal perspective, limiting the use of such materials to a maximum of 150–250°C,

far below the Curie temperature. Depending on the application, thermal insulation, cooling, etc., the service temperature is often enough for IH purposes [30]. As the thermal conductivity of most SMCs is relatively high, often 20 or more [30] [32], efficient cooling is possible.

4.5 Soft magnetic moldable composites

To produce high-efficiency induction heaters for large-scale applications, such as band heating, in-tool heating, and the general heating of large structures, the development of a new core material was initiated. Early inductor designs using litz coils surrounded by soft ferrites or SMC material meant high material costs, significant manufacturing costs, as hundreds of small, standard-sized components had to be assembled to form individual units, and highly complex cooling solutions. In addition, the fact that most industrial induction heaters are unique in design makes it difficult to develop or use standard components for optimal results. Given this background, it was desirable to have a material without size or geometric restrictions, with reasonable losses at induction-heating frequencies, and with sufficient isotropic permeability for IH applications. The production aspects of this material have been the main focus. This material has been developed over many years at Lund University, Industrial Production, together with industrial partners.

SMCs, though accepted and well known for decades, are limited in terms of the produced size and are difficult to produce with integrated components, due to the high pressing forces required during manufacturing. The developed moldable material was a breakthrough, and to distinguish this SMC from others and to emphasize its key feature, i.e., *moldability*, a new name was suggested, soft magnetic moldable composite SM^2C. The SM^2C material has been developed parallel to the development of the induction-heating technology. The material's properties and manufacturing processes have been gradually improved, along with new requirements for heater design and manufacturing.

The basic SM^2C is a mixture of 6.5% silicon–iron powder and a binder, typically low-viscosity epoxy (Figure 16). The powder is produced using gas atomization, which generates spherical shapes but allows only moderate control of the particle size distribution. To achieve a maximum packing density, an optimal combination of different particle size fractions can be calculated. In practice, different particle sizes are obtained using sieving; this allows the separation of particle fractions by using gradually finer meshes, the smaller the steps, the narrower and more uniform the distribution. Rejecting cer-

tain size fractions increases the production cost but allows for better packing density. Some of the fractions can be coated to provide electrical insulation, and the powder can also be annealed to reduce losses. Ideally, the different fractions should be uniformly mixed before molding, but in practice this is almost impossible to achieve. Given the range of variables, it is difficult to find the best combinations in terms of permeability, hysteresis losses, and resistive losses. Binder amount and type, curing temperature, and molding principles as well as the parameters within each of these factors affect the result, making the production process even more complex.

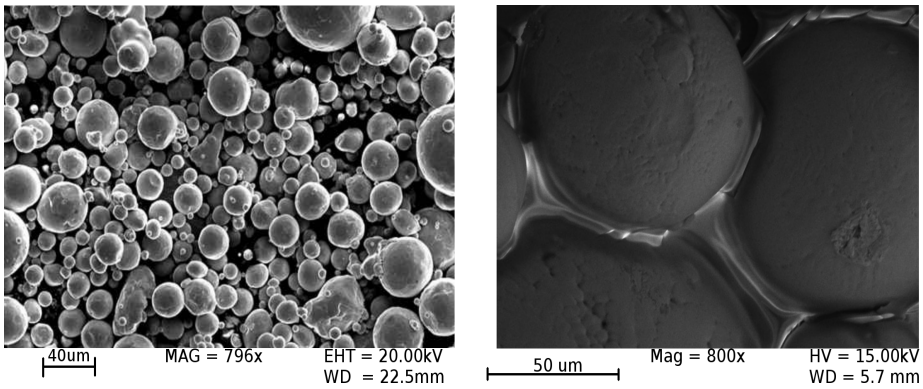

Figure 16: Gas-atomized silicon–iron powder. Left: Free particles. Right: Bonded with epoxy to form an SM^2C component [33].

Methods that have been tested for packing the binder–powder particle mixture are pure gravitation, vibration, pressing, use of magnetic fields, and rotation at different g-forces [34], the latter having resulted in a material and processing patent [35]. The different methods produce different results and which is best in a particular application depends on various aspects, such as the geometry of the die.

The silicon–iron particles are non-ductile and cannot be deformed during molding, which makes the packing density fairly low and limits the thermal conductivity to approximately 3.5 $\mathrm{Wm^{-1}K^{-1}}$. The bridges between the particles also limit the permeability to less than 20 [33].

As a very small cross-sectional area links the flux through the structure in the most advantageous way, given the existence of areas where the coated particles more or less touch each other, a small saturation effect is present even at low flux densities where these areas locally reach high flux densities, which virtually increases the gap between the particles (Figure 17).

As the small powder particles 50–400 μm in diameter cannot conduct

currents in any direction, the frequency-dependent losses are caused mainly by hysteresis effects as long as the frequency is not too high (Figure 17). The frequency limit is highly dependent on the particle size and distribution, so inappropriate particle size selection can increase the losses substantially.

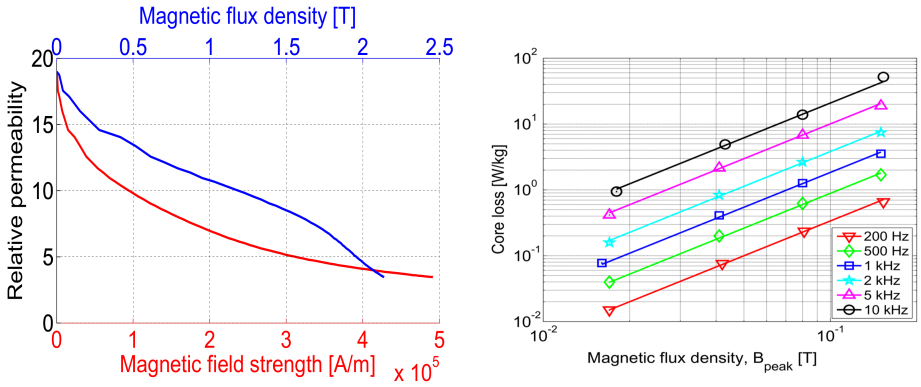

Figure 17: SM^2C material properties. Left: Permeability as a function of flux density. Right: Losses at different frequencies and flux densities [33].

Compared with other SMMs, he SM^2C material has some major advantages; primarily that it can be moulded into practically any size and shape. In addition, the material is machinable and easy to combine with alternative SMM inserts that can increase both the thermal conductivity and permeability in critical regions[35]. The effect on the thermal conductivity of inserting other SMCs into the mold has been investigated by Strindberg [36], who obtained attractive cooling power effects that can also be obtained by embedding laminated steel or wires.

A master's thesis [37] has evaluated different binding systems for SM^2C and established epoxy to be the mechanically best solution. The work also identified ceramic alternatives that can handle very high temperatures, providing more or less the same electromagnetic properties but at the expense of mechanical strength. The ceramic SM^2C material features good compressive strength and has been successfully tested in an induction-heating setup, but cannot handle large tensile stresses without support; however, it still is a good alternative in many high-temperature applications. In addition, porous structures made using ceramic binder can be used to transport gas for cooling purposes [37].

4.6 Comparison of soft magnetic materials

It is obvious that all currently available materials have important technical limitations regarding permeability, small losses at high frequencies, high saturation or isotropy. Three of these properties can be obtained, which enables most induction-heating applications to be realized, the best choice of material depending on the particular application, desired cost, and complexity. Table 1 summarizes some important properties of the different SMM groups from a general perspective, where 5 is excellent and 1 is merely adequate. Note that the properties might vary significantly within a group. The ranking is based on IH applications at 20 kHz, and for anisotropic materials the properties refer to the preferred direction. Cost is excluded from consideration, since comparing the bulk price gives no information about the cost of the finished component, for which the electromagnetic and manufacturing properties must be considered, both of which are dependent on the particular application.

Type \ Property	Permeability	Saturation	Isotropy	Losses	Thermal conductivity	Temperature resistance	Size limitation	Machinability
Laminated steel	5	5	1	3	5	5	4	2
Nanocrystalline alloys	5	4	1	5	4	4	4	1
Soft Ferrites	4	1	5	4	2	2	2	2
SMC	3	5	4	4	4	3	2	4
SM^2C	2	4	5	4	2	3	5	5

Table 1: Summary of SMM properties, assuming an IH application at 20 kHz.

As can be seen from Table 1, the SM^2C material is not the best from an electromagnetic perspective, but has considerable advantages for large and complex structures and small series production due to its manufacturing principle. In applications requiring high permeability, for example very-high-power-density equipment such as handheld heaters, the properties are inadequate. One major advantage of SM^2C is its easy integration with components made of other materials, making it suitable as the base material of a

compound structure. Combined SMMs probably constitute the best solution for many applications in terms of cost and performance, as the most suitable material can be positioned where it is most useful, providing unique properties. As the cost of an inductor is often related more to the manufacturing cost than to the costs of the constituent components, the cost information in Table 1 does not give a completely balanced comparison. In addition, both the production and material properties are continuously improving, and the SMCs have especially improved over the last decade [30] [33]. Figure 18 illustrates the losses at a particular flux density and frequency, the working point being selected based on available data.

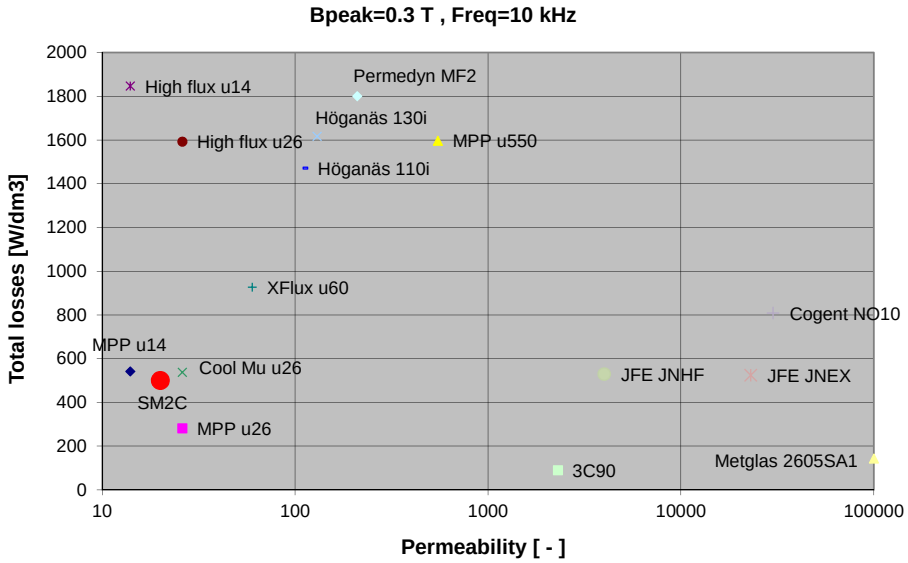

Figure 18: Comparison of the losses experienced by various SMMs at a particular frequency and magnetic flux density.

5 The GreenHeat concept

Most industrial implementations of induction heating use fairly low-efficiency inductor designs, in which a significant amount of power is transformed into heat in the electrical conductor rather than inside the workpiece. The many technical, economic, and historical reasons for this constitute a great challenge. In view of the huge energy saving potential and great opportunities for companies interested in replacing alternative heating and production processes with induction heating, Mistra and SSF invested in the GreenHeat project. The project sought to develop a concept for producing heating inductors featuring very high efficiency in a flexible, scalable and feasible way using a moldable flux-concentrating material, later determined to be SM^2C. The conductor, traditionally built with water-cooled copper tubing, was to be replaced with high-efficiency litz wire, and the cooling was to be integrated in the SM^2C. The idea of replacing a naked copper tube with litz wire surrounded by a flux concentrator is not new, but many aspects of the required production process and related opportunities are not described in the existing literature.

5.1 Litz wire

To reduce the skin effect and proximity losses in the coil, a special high-frequency wire called litz wire can be used. The name originates from the German term "litzendraht," meaning braided or stranded wire, which accurately describes the product. Litz wire comprises numerous thin strands, each individually electrically insulated from the rest and braided together in such a way that each strand stays the same distance in the center as on the outer boundary, relatively (Figure 19). The result is a wire in which all the strands have the same high-frequency resistivity, which forces the current to be equally distributed throughout the wire, giving it a much larger active cross-sectional area than that of a solid conductor or normal stranded wire. The insulating layer, typically made of solderable varnish, allows the strands to be joined together at the wire ends by immersion in liquid solder, welding, or using a special hot crimping tool; in contrast, non-solderable insulation usually requires stripping or cleaning before joining [38] [39].

Litz wires are generally made by twisting or braiding bundles of thin strands to achieve the desired cross-sectional area. For higher frequencies, thinner strand diameters are required. The optimal dimensions depend on many considerations and usually represent a tradeoff between cost and losses [41], but the particular application also plays an important role. Since

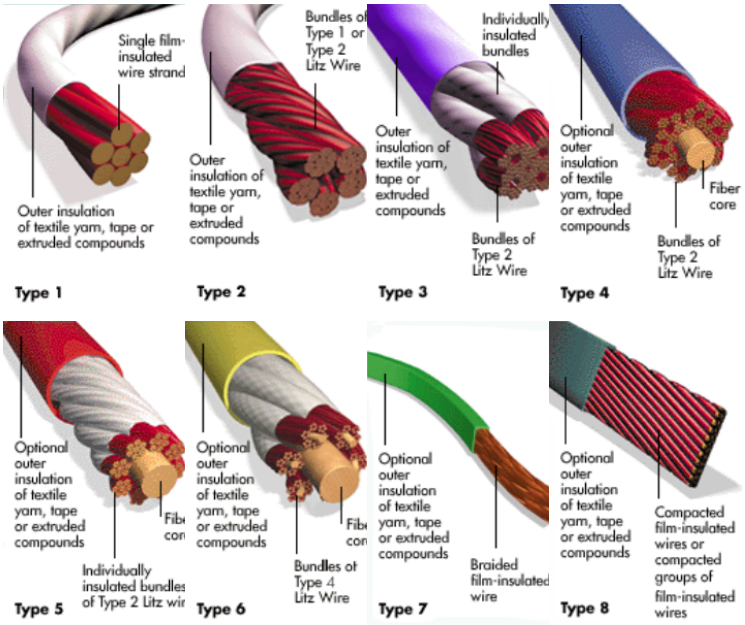

Figure 19: Different types of litz wire [40].

each strand is electrically insulated, the insulation layer consumes proportionally more space as the wire diameter decreases, which reduces the fill factor. Another property that affects the fill factor is the twisting, which also consumes space (see Figure 20) and makes the effective length of each strand longer. The shorter the pitch (i.e. the harder the twisting), the larger the DC resistance but the easier it is to obtain desirable high-frequency properties [42]. The recommended strand diameter is a function of frequency and relates to the relative values of the AC and DC resistance, for example, yielding the results shown in Figure 20 [43]. A rule of thumb is to use the strand diameter that, at the actual frequency used, results in a multi-turn litz coil with a peak phase angle of φ, i.e. the point at which the wire resistance increases linearly with the frequency.

The insulating layer on each strand can be made of polyvinyl, acetal, phenolic resin, polyurethane, nylon, polyester, polyamide, polyimide, polytetrafluoroethylene, ethylene tetrafluoroethylene, epoxy and combinations thereof, depending on the temperature class, dielectric requirements, chemical environment, and shape [44]. The first layer is sometimes complemented with a bondable plastic or thermoset resin to facilitate the production of the finished coils. The bondable alternatives allow for good mechanical properties and fast curing without adding an extra component. Outside the

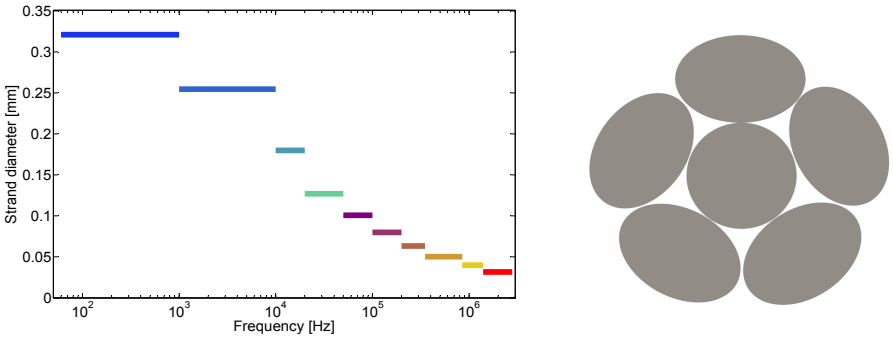

Figure 20: Litz wire. Left: Optimal strand diameter. Right: Illustration of effect of twisting on the cross-section [42].

litz wire, an extra insulating layer can be used comprising fluorinated ethylene propylene, polyvinyl chloride, polyethylene terephthalate, polyimide or kapton, as well as mineral or fiber additives such as mica tape, glass fiber, Dacron or Nomex [44].

In applications in which the production cost is paramount, for example in many domestic induction heaters, the strands in the wire may be twisted in a way that is suboptimal from a performance perspective, in what is sometimes referred to as "fake litz." Nevertheless, this type of wire is frequently used for induction coils and still offers a huge improvement over solid conductors. Investigations of the high-frequency properties of traditional, non-insulating multi-strand wire indicate slightly reduced losses compared with the corresponding solid wire, though it is still not suitable for induction-heating applications.

Unlike solid conductors or tubing, litz wires allow the permeation of the electromagnetic fields, which offers new opportunities but must be considered in the design. An accurate bulk model of the litz wire can be obtained using a complex permeability value, in which the proximity and skin effect losses are grouped together as a function of the magnetic flux density. In addition, the resistive part can be determined, all values based on the properties of the litz wire, namely, strand diameter, fill factor, and equivalent electrical conductivity [45] [46] [47]. Using a bulk model saves both memory and computational time in finite-element simulations and allows for 2D models incorporating wire twisting or braiding.

The important properties of the (litz) wire can be summarized in eight major categories:

- Losses (resistive, proximity, and eddy current losses) at high frequency

- Cooling potential
- Temperature resistance and deterioration
- Dielectric properties and electrical insulation
- Perpendicular thermal conductivity
- Electromagnetic field permeability
- Manufacturability
- Cost

The losses and cooling possibilities must be matched to avoid overheating, which is defined by the temperature resistance of the wire. The maximum temperature is often limited by the electrical insulation, which defines the coil's dielectric properties. Thick insulation prevents voltage breakdown, but creates thermal barriers that complicate cooling and create thermal hotspots in the coil. The field penetration will increase for smaller strand diameters and for lower fill factors of the coil. The finer the strands and the smaller the cross-sectional area of the wire, the easier it is to form the wire into the desired shape. For most applications, however, one must also consider cooling, which is the greatest challenge with the use of litz wire instead of tubing.

5.2 Thermal design and cooling

Probably the most performance limiting factor in technical equipment is temperature. Assuming a continuous process, this limiting factor depends on the efficiency and cooling, and on the maximum temperature and possibly the surrounding conditions. Using water cooled copper tubing as the conductor causes severe losses, but the tube can resist high temperature, limited only by the melting point of copper (exceeding 1000° C), and can be efficiently cooled using flowing water. The specific heat capacity of water is 4.18 kJ/kg·K and the heat of vaporization is 2.26 MJ/kg, which means that water could potentially cool a system exceeding 400 kW at a flow rate of 0.6 m^3/h (typical of ordinary tap water) if all the volume is converted into 100°C steam. This enormous cooling potential has made this design the dominant one, especially in applications dealing with large power densities and high workpiece temperatures. In high-temperature applications, the radiative power increases by a factor of four with the temperature according

to Stefan Boltzmann's law (equation 10), is an important consideration in terms of the shielding or extra cooling of the coil (σ is Stefan Boltzmann's constant, 5.670×10^{-8} W/m^2·K^4). This effect is sometimes used to indirectly heat non-conductive materials using induction [2].

$$P = \sigma A T^4 \tag{10}$$

Another important property of ferritic materials is the Curie temperature, at which all magnetic properties disappear, thereby significantly changing the impedance of the system. [48] Lower workpiece resistance caused by the increase in skin depth means lower efficiency and thus larger losses at constant output power. The resistivity, however, increases with rising temperature, somewhat improving the efficiency as long as the skin depth is significantly less than the workpiece thickness. In addition, copper has a positive temperature coefficient of resistivity, approximately doubling the losses with a 250°C increase in temperature, emphasizing the importance of proper coil cooling.

The applications in focus in this work have mainly involved low temperature heating, i.e. up to a few hundred degrees C, which is why the temperature-resistance of the inductor materials and the thermal radiation from the workpiece have been of secondary importance. Instead, performance in terms of efficiency and heating pattern has been the main objective, as well as manufacturability, component size, and aspects related to particular applications; nevertheless, the thermal design has been crucial, because even small power losses can cause high temperatures if the cooling is insufficient. In the research group, considerable effort has been spent on the thermal design, thermal conductivity of the various materials, and, most of all, the heat transfer between these materials. In addition, it has been challenging to integrate the cooling while maximizing the power density without degrading the materials after substantial operation time.

As the basis for this work, commercially available litz wire with a transverse thermal conductivity of 0.5 W/m·K was used. The SM^{2}C material used has a thermal conductivity of approximately 3.5 W/m·K. These two components defined the framework of this study, and were then combined in many different ways with complementary structures and cooling solutions. Parallel to this, new materials were developed at Lund University, based on desired properties obtained from simulations of induction-heating equipment or from unprejudiced research. As different properties are sometimes conflicting, work progress entailed ranking the properties in order of importance and finding thresholds rather than an unconditional optimum,

resulting in ongoing iteration between design and material science. The type of induction heater depends greatly on the material properties; a large, fairly-low-power-density heater emphasizing uniformity has completely different requirements from a small handheld heater or from a tube heater used for surface hardening or quenching with a very high power density.

The physical designs are of two types: water cooled and air cooled. Air-cooled units are used mainly for low-power-density applications, up to a few thousands kVA/m^2, and may be cooled solely by natural convection, fans, or other forced-air designs. Water-cooled heaters use a channel system for tap water or a closed setup; in the latter case, low-viscous oil or a mixture of water and alcohol, or the like, is used. These heaters can be used with a power density of up to approximately 10 MVA per m^2 without becoming overheated; with an improved cooling capacity, the thermal density can be significantly improved.

Fan cooling is a simple and very cost-effective method used in much electronic equipment to control the temperature, but the low volumetric c_p of air limits the cooling capacity even at fairly high flow rates. By using litz wire in combination with SM^2C, the losses in the coil are reduced from approximately 50 % to only a few percent or less in most applications, making it possible to cool with air. To maximize the efficiency and minimize the stray magnetic fields, it is crucial to use the regions nearest the workpiece for electromagnetic purposes. With good thermal coupling between the litz wire and the SM^2C (Figure 21), the cooling can instead be performed on the back of the inductor [49]. Depending on the voltage levels and the electrical insulation of the wire, there might be a risk of dielectric problems; this issue is investigated in [50].

Figure 21: Coil surrounded by a molded flux concentrator made of SM^2C material [50].

By exploiting the manufacturing benefits of SM^{2}C, complex shapes can easily be created according to the preferred design. Figure 22 shows a CAD model as well as photographs of a manufactured prototype inductor with cooling flanges. The molding was performed in a silicone die and a number of replicas were later produced and assembled into a prototype machine for evaporating forming lubricants [49].

Figure 22: GreenHeat inductor: Left: Naked coil. Center: Finished inductor. Right: CAD model [49].

The inductor was successfully tested and evaluated according to the expected loads of the application machine (Figure 23). Due to high losses in the power electronics and the subcritical dimensions of the transformer, the overall efficiency of the system is not extraordinary, though it still represents a marked improvement over copper tubing coils. When comparing the data with those obtained using a naked coil, the importance of the SM^{2}C is obvious, almost doubling the output power at about constant losses. The experiments were performed using natural cooling only; at increased power, the losses increase faster for the naked than the molded coil, due to the temperature difference between them that favor the encapsulated coil.

Though the heater was never pushed to the limit of power density, the difference in working temperature between natural convection and forced-air cooling proves the functionality of the molded flanges (Figure 24). A lower wire temperature means reduced losses and thus increased efficiency.

It is sometimes advantageous to have a compact heating unit or a unit in which one can conveniently connect the inductor to an existing liquid cooling system rather than using fans. To achieve the same efficiency and output power as in air-cooled units, the liquid cooling channel system must, like the flanges, be located on the back of the inductor. In the frequency range primarily used in the applications considered here, most of the losses are generated inside the coil rather than in the core material. In addition, the losses that actually occur in the SM^{2}C are generally highest near the

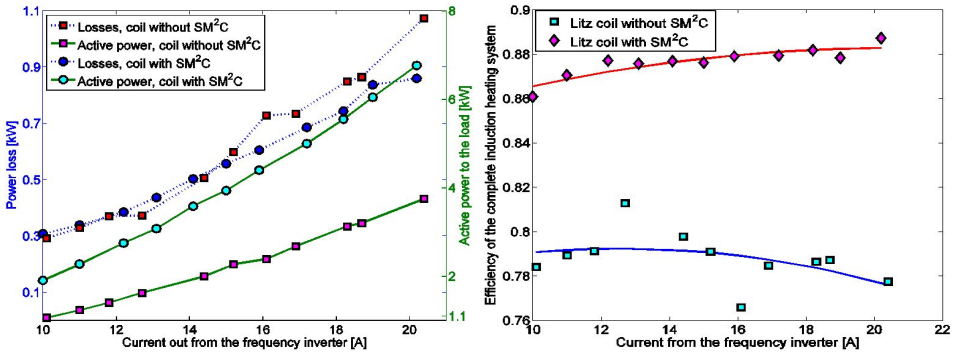

Figure 23: Comparison between a naked coil and a coil molded in SM^2C. Left: Heating power and losses. Right: Efficiency [51].

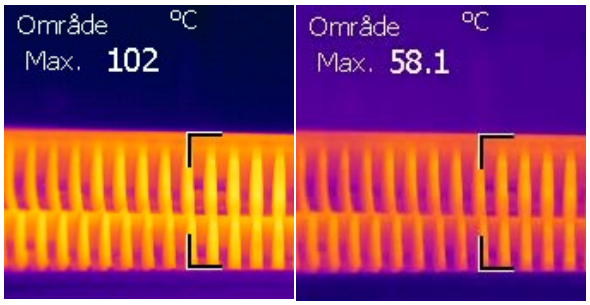

Figure 24: The steady-state temperature of the cooling flanges on the back at the nominal heating current. Left: No forced cooling applied, just natural convection. Right: Cooling with forced air [49].

coil, where the magnetic flux density reaches the highest values. To increase the cooling power, the channel system is preferably located in close contact with the wire, between the coil and the SM^2C on the back of the unit, only marginally reducing the efficiency.

Regarding water cooling, a master's thesis by Strindberg [36] investigated the importance of the material surrounding the channels by comparing the cooling power of plastic tubing with that of stainless steel tubes, both molded into a block of SM^2C. The results were compared with those channels made of wax, which was eventually melted and completely removed from the cured composite. The cooling effect is about double with the use of stainless steel rather than plastic tubing at constant water flow. The test objects with channel walls made of SM^2C, i.e. those made using wax cores, produced the best cooling results, a few percent better than with stainless steel. None of the three materials excels in all respects, however. The molded channels

are the most complicated to produce and to connect to the cooling system without risk of leakage; in addition, there is potential for corrosion if the silicon–iron particles come into contact with water. Integrating a stainless steel tube involves two problems: the first is losses due to induced currents in the electrically conductive material, which degrade the performance; the second is that of handling the high voltage potential that, depending on the design, can be induced across the tube ends. The plastic tubes are easy to shape and integrate into the construction, though they result in a significant reduction in cooling power compared with the other two approaches; even so, this has so far been the preferred solution for use in inductors.

To maximize the cooling where it is needed the most, a litz wire with a thin channel in the center, like a copper tube, would be desirable for producers of IH equipment. One such solution is presented by Paya et al. [52]; however, the selected design with a stainless steel tube in the center (Figure 25) significantly increases the losses when the frequency increases, limiting the frequency range, and counteracting the reason for using litz wire.

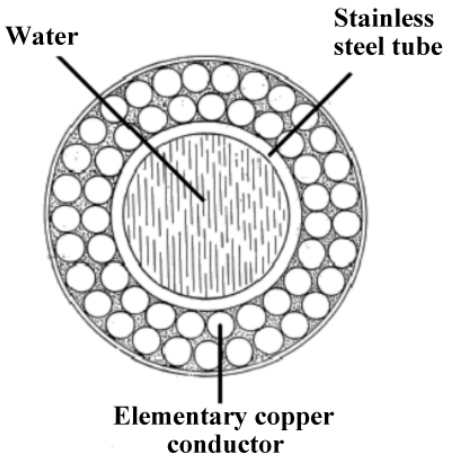

Figure 25: Example of water cooled litz-like or multi-strand wire [52].

5.3 High-temperature applications

Today, heating steel above the Curie temperature is exclusively done using induction coils made of water-cooled tubing or the like. The consensus among producers of induction-heating systems is that litz wire cannot handle these conditions due to a combination of radiative heat and significant losses

in the coil. With a complex and expensive setup it is certainly possible, using thermal shields, to build a litz-based system that can heat workpieces above the Curie temperature–at least for selected geometries. This change in technology for high-temperature applications cannot be justified until competitive alternatives exist that are easy to build and guaranteed to work. The same challenges also apply to high-power-density heating applications.

The required solution is to produce a litz wire with improved cooling capabilities. As discussed earlier, integrated cooling channels are one option, but it is also important to increase the thermal conductivity transverse to the wire, i.e. between the strands. Today, the insulating layer on each strand, usually made of a material with a thermal conductivity below 1 W/mK, is thicker than actually needed. Even with the thermal conductivity of copper, i.e. approximately 400 W/mK, the transverse values cannot exceed 0.5 W/mK with a reasonable packing density. There is generally a correlation between the dielectric strength of the strands and their thermal conductivity; however, the voltage difference between the strands is very small and occasional short circuits are not disastrous as long as there are not too many. The optimal layer thickness depends on several factors and must be thoroughly investigated, but can doubtless be significantly reduced from current values. One factor that affects the required thickness of the insulation layer is the packing density, which is also closely related to the transverse thermal conductivity. Even minimal pockets of air greatly degrade the heat transport. The steps needed to advance from the existing litz standard to a product with completely new capabilities are illustrated in Figure 26: starting with the original cross-section, first the insulation thickness is reduced, then the thinly insulated strands are compacted to form a solid wire, and finally a cooling channel is integrated in the center of the compacted wire.

Another way to improve the system performance is to increase the service temperature, which requires materials that can resist much higher temperatures. One candidate for this is wire made of aluminum with insulation made of aluminum oxide, a material combination with significantly better thermal properties than those of varnish-coated copper. This makes coils that can theoretically resist temperatures up to at least 600°C without becoming damaged. The oxide layer can be created effectively and with good control of thickness, evenly distributed around the wire. A thin layer still provides relatively high dielectric strength and allows for higher thermal conductivity, a better fill factor,[2] and therefore higher currents. The dielectric

[2]Refers to the ratio between the electrically conductive area and the total cross sectional

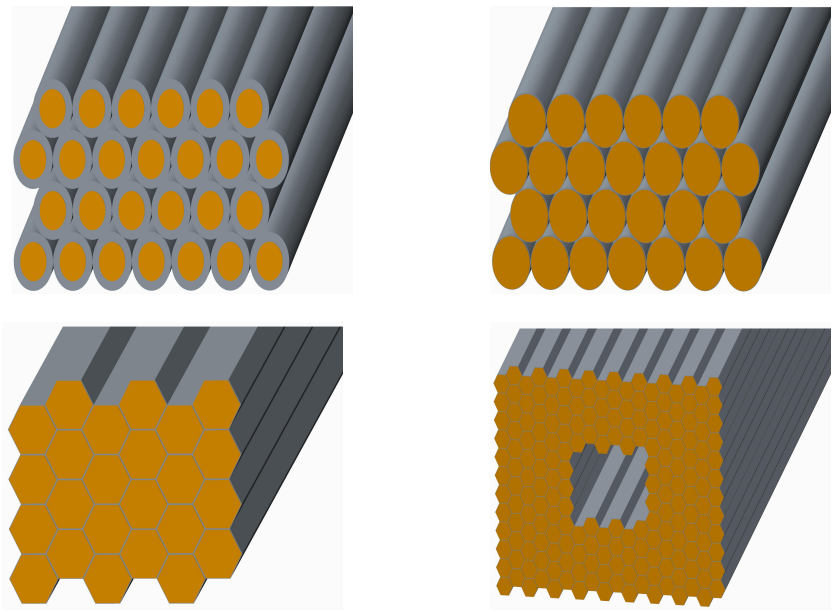

Figure 26: Cross-sections of litz structures showing the steps needed to advance from the current design to high-performance solutions.

strength of the anodized layers varies depending, for example, on the type of anodizing, frequency, and layer thickness, and values of 10–35 kV/mm are found [53]. These values have been confirmed by experiments. A selection of results focusing on anodization time is presented in Figure 27, showing a process for rapidly depositing thin insulation layers that would be usable in litz applications. In addition, a cross-section of the oxide layer is shown, in this case, almost 15 μm thick.

Drawing out thin aluminum wires is not as easy as for copper due to its mechanical properties, though it is still possible, and aluminum wires with diameters as small as 0.1 mm are commercially available [54]. The cost of aluminum is significantly lower than that of copper, resulting in a cost reduction of approximately 50% for the finished magnet wire per kg, including the production cost of a wire more than three times as long. Since aluminum has approximately 60% higher resistivity than does copper, an increased cross-sectional area is required to keep the DC resistance constant. A larger skin depth for the aluminum, however, allows for a 25% larger diameter with the same high-frequency properties, resulting in the same number of strands independent of the material selection. As aluminum wire is about one quarter

area of the coil.

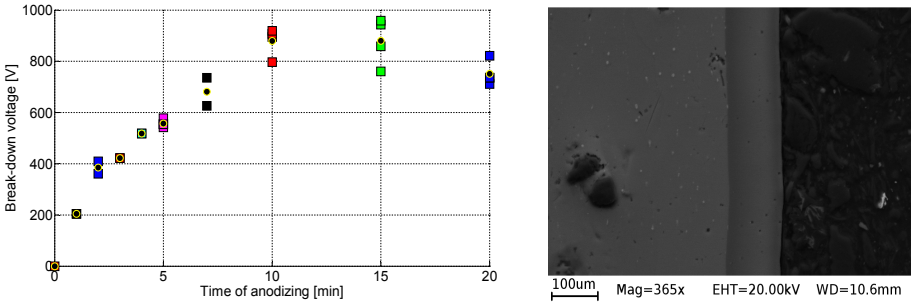

Figure 27: Left: Dielectric strength of some anodized aluminum samples [55]. Right: SEM image of a typical oxide layer.

the cost of copper wire per unit length for the same resistance, aluminum or copper-clad aluminum (CCA) wire is today commonly used as the conductor material in electrical equipment, though the insulating layer is exclusively made of traditional coatings such as enamel or varnish. There are also aluminum wires with an oxide layer covered by varnish, the oxide serving several purposes, for example, as a primer for adhesion. The main reason for not using aluminum oxide for insulation purposes is its brittleness. Aluminum oxide features high hardness and wear resistance, but thermal expansion of the wire or deformation from bending, etc. creates cracks that expose the conductor to any liquid present and severely reduces the dielectric strength in moist air. Figure 28 shows a number of scanning electron micrographs of anodized aluminum wires, illustrating different types of cracks as well as the transitions between wires after being deformed towards each other. The wire is 0.4 mm in diameter and the oxide layer is approximately 3.5 μm thick, both values being greater than is optimal for litz wire applications. By using only thin oxide layers, crimping off the wire ends will allow for good electrical contact through all the strands without cleaning, given that the outer coating layer of the wire confers solderable properties. Resolving a few challenges related to aluminum litz wire would make it economically competitive, not only for particular applications but in most areas of IH due to its properties and affordability.

For the core material, there are alternatives that can withstand temperatures up to the Curie point of approximately 700°C. Using a thermal barrier or, in extreme cases, a water-cooled screen between the inductor and the workpiece allows heating to very high temperatures with enhanced cooling of the coil and possibly also of the core material. The thermal coupling between coil and core material significantly affects the cooling design.

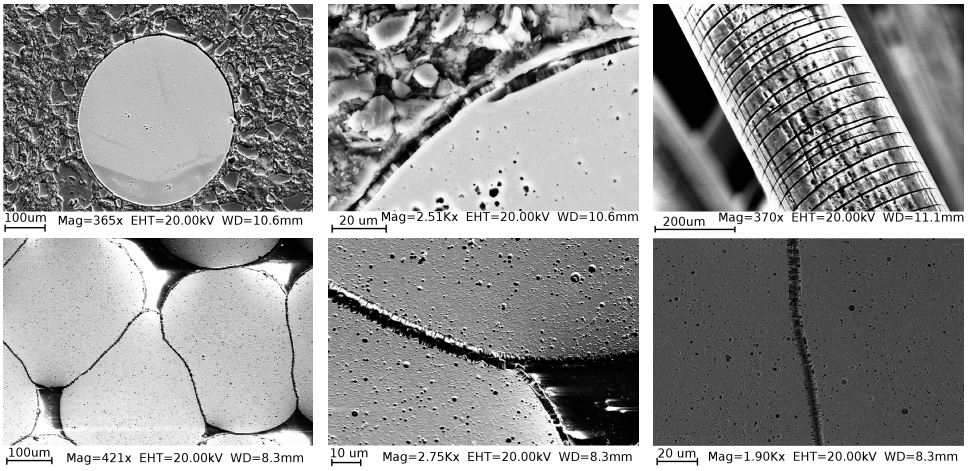

Figure 28: Aluminum wire with aluminum oxide coating.

6 Control system and power electronics

The control and power electronic system used in most of this work and exclusively in the multi-coil experiments is described in detail by Frogner et al. [56]. The system was developed based on a need for accurate control of the switching pulses, full availability of current and voltage measurements, and great versatility. The system is built around two identical variable-frequency drives (VFD), each based on full-bridge MOSFET architecture and ready for the expansion of independent channels in the future. A personal computer is used for monitoring and to coordinate all parts of the system; it uses several data-acquisition cards and a compact RIO (cRIO) from National Instruments to interface with sensors and control signals. The temporal accuracy of the switching pulses has been limited to 20 MHz in the present work, which is sufficient for the evaluated setups and in the explored frequency interval. The system accuracy is not limited to 20 MHz, however, and also features excellent real-time control using the field-programmable gate array (FPGA) built into the cRIO, if required. One of the most important tools for evaluating the experiments is an IR camera, also connected to the system. The data acquisition and the processing of the data from the sensors is described in more detail in chapter 7. All experiments were carried out using a ferrite pot-core transformer for galvanic insulation and adaption of the impedance and using phase-advancing capacitors connected on the secondary side, in series with the inductor. A block diagram of the system is presented in Figure 29 and an image of the setup in Figure 30.

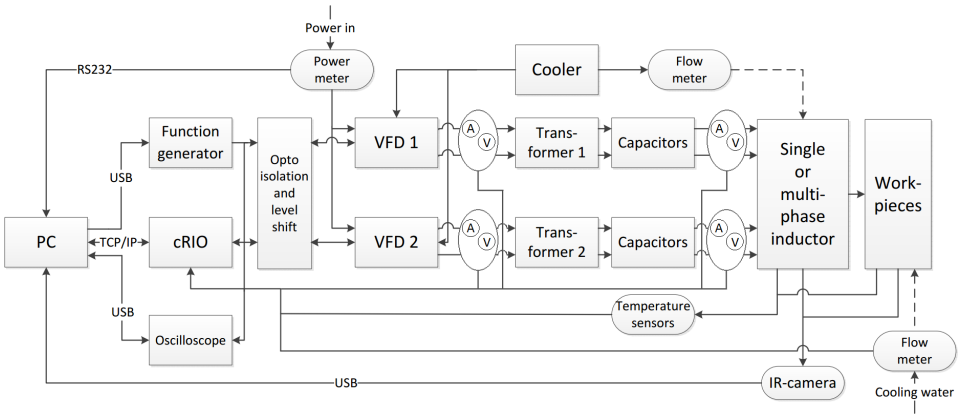

Figure 29: A simplified block diagram of the experimental setup.

The shape of the voltage from the system is crucial for the modeling and results. The transistors allow for large voltage derivatives and the voltage

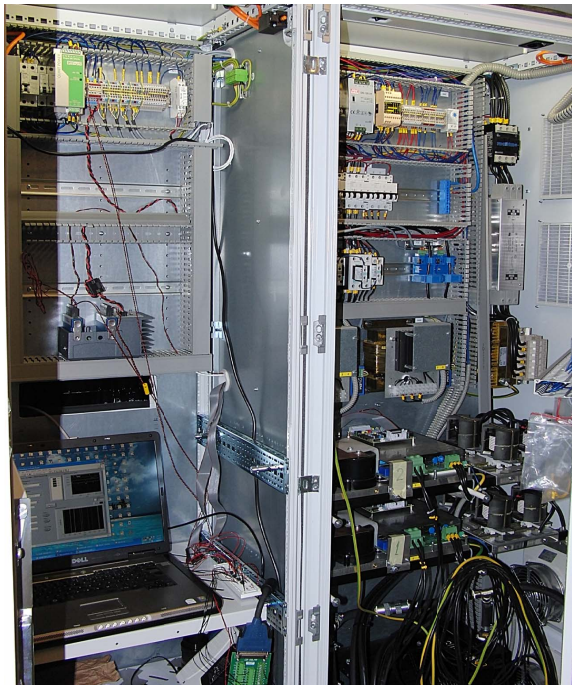

Figure 30: The developed power control system.

shape can be approximated as the theoretical square wave generated by the digital control signals. Figure 31 visualizes the shapes of the voltages and illustrates the definition of *voltage phase shift*. The duty cycle is defined as the on time of the transistors divided by the period time. The short rise times may cause electromagnetic compatibility issues, so the cables must be properly shielded. For the experiments, hard switching was used, which creates unnecessarily large losses and transistor loading, but allows for any type of investigation of the system dynamics.

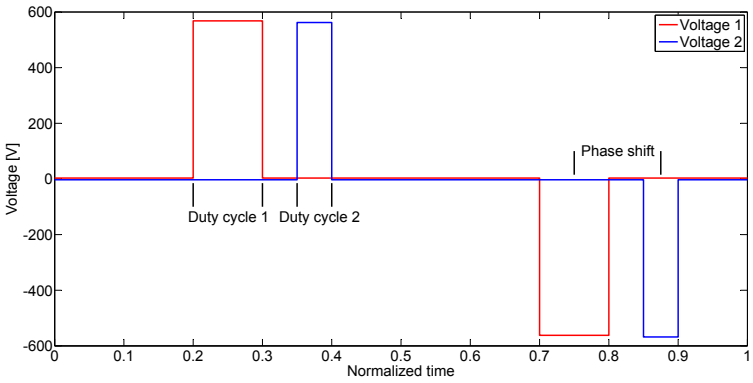

Figure 31: An idealized image of the voltage waveforms, including definitions of properties.

7 Measurement tools

In processes involving induction heating, several properties are of interest, many of which are difficult to measure and even more complicated to observe in real time. In this work, only the most basic properties are considered, i.e. voltages and currents throughout the system and the temperature pattern and absorbed power of the workpiece. This section explains the complexity and challenges of obtaining accurate results regarding these properties and describes the development of an automatic measurement tool capable of performing real-time analysis of the heating results. This work is a key to the investigation and to the future optimization of multi-coil heaters, in order to feed back the results of the advanced current control. Integrated temperature sensors and flow switches, for example, are used for system monitoring and to protect individual components, but not particularly for investigative purposes.

7.1 Current and voltages

The voltage is of great interest when monitoring what happens in the system and, together with the current, is used to calculate the active and reactive powers (equations 11 and 12). Using a differential probe, the voltage can easily be measured with a bandwidth of 25 MHz or more using a data acquisition system. To measure the current, a closed-loop current transducer is a convenient tool that has been used during this work. This type of sensor (e.g. the LEM LA55-P) has a bandwidth of up to 200 kHz and can represent currents up to 40 kHz well, including harmonics. However, the experiments revealed a significant disadvantage of this setup, the unstable behavior due to a small but obvious and unpredictable phase shifts of fast signals. The position of the wire as well as its surroundings may cause a phase shift of a few degrees, and a shift of one degree can change the power by several percent. This small change could, for example, represent the difference between a realistic efficiency of 98% and a measured value exceeding 100%. Much effort has gone into this, without finding a universal solution other than changing the measurement principle. Ultra-low-inductance shunt resistors are now being implemented, a migration motivated by independent studies [57][58]. The measured active and reactive powers are defined according to Equations 11 and 12, respectively.

$$P = \frac{1}{T} \int_{t}^{t+T} v(2\pi f\, t) \cdot i(2\pi f\, t)\, dt \tag{11}$$

$$Q = \frac{1}{T}\int_{t}^{t+T} v(2\pi f\, t)\cdot i(2\pi f\, t - \pi/2)\, dt \tag{12}$$

7.2 Heating pattern and output power

The heating pattern answers the fundamental questions when it comes to uniform heating and allows for easy comparison with simulations. The other important property is the efficiency of the system, often measured using energy balance in one way or another. A common method involves a water cooled workpiece and when the setup reaches steady state, the absorbed power is calculated as the flow rate times the difference in water temperature. The problems with these type of measurements are a time consuming transient phase, often tailor made workpieces for each inductor design, unknown power leakages affecting the accuracy and also the fact that the heating pattern and efficiency can not be measured at the same time. Calculating the absorbed power of a thin workpiece based on thermographic data allows for very fast measurements, also to be used for dynamic analysis of the process.

The thermographic method of measuring the absorbed power faces a number of challenges in order to be reliable, some of them related to accurate temperature measurement of every infinitesimal area of the workpiece surface, other related to the temperature distribution inside of the workpiece in relation to the surface temperature. The emissivity is probably the largest source of error, more or less requiring metal surfaces to be painted or specially tuned cameras to be used. There is primarily one problem that complicated accurate thermographic acquisition of metal surface; the low emissivity at useful wavelengths, Figure 32. The high reflectance means that the radiation from other warm object risk to interfere with the real temperature but also a variation of the emissivity can be a problem. The value is sensitive to the temperature according to Figure 32 but also oxide layers etc.

Based on the approach that heating of workpieces that are relatively thin in comparison to a combination of skin depth and thermal conductivity can be approximated by the surface temperature through the complete thickness, dynamic measurements of absorbed power can be performed with reliable results. [59] To allow for an IR-camera position not perfectly above the center of the workpiece the work has resulted in automatic corner detection followed by a projective transformation to make all pixles the same size. Using the Prewitt edge detection method followed by a Hough transform

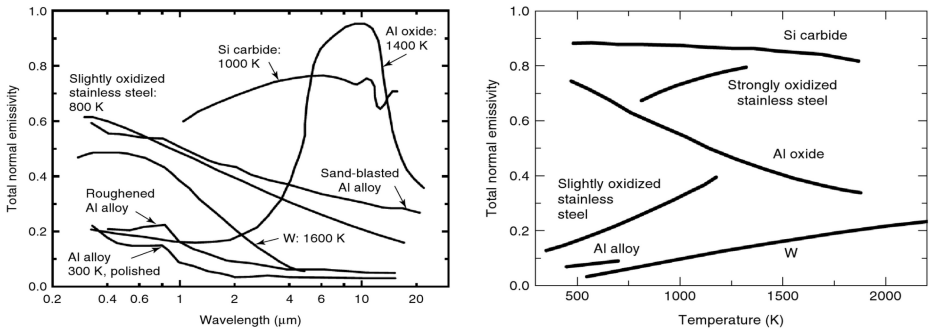

Figure 32: Variations of emissivity. Left: Different wavelengths. Right: Different temperatures.

for line detection, the corners of the workpiece can be found by solving a linear equation system for straight lines intersection, shown in Figure 33. In Figure 34 an example of the projective transformation is shown.

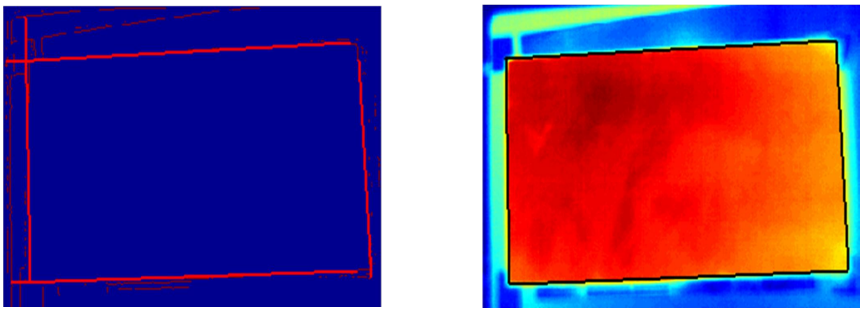

Figure 33: Left: Detection of edges and lines of a recorded thermography. Right: Identified frame using automatic detection.

To investigate the heating pattern and output power, the induction heater is turned on for a short amount of time while recording the temperature, examplified in Figure 36.

The actual energy in the workpiece and thereby the applied power can then be determined by integrating the temperature over the entire workpiece and scaled with the thermal mass according to Equation 16 and 15. For the experiment if Figure 36, the corresponding result is presented in Figure 35.

$$\Delta E = \int_0^t P(t)\,dt = m \cdot c_p \cdot \Delta\overline{T} \tag{13}$$

$$P(t) = Z \cdot \rho \cdot c_p \int_X \int_Y \frac{dT}{dt}(x, y)\,dx\,dy \tag{14}$$

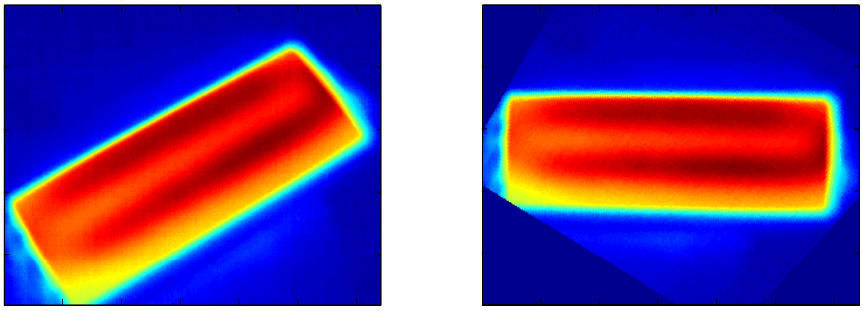

Figure 34: Left: Raw data picture from industrial heater. Right: Same picture after projective transformation [59].

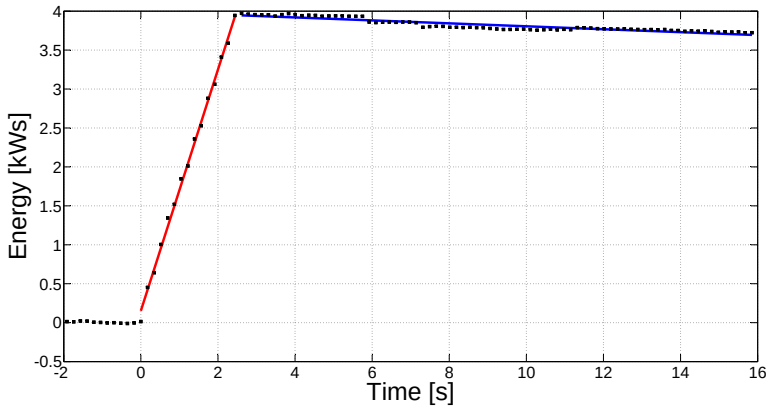

Figure 35: The energy of the workpiece during and after heated by induction, adjusted to start at zero energy [59].

$$P(t) = Z \cdot \rho \cdot c_p \int_X \int_Y \frac{dT}{dt}(x, y)\, dx\, dy \tag{15}$$

$$\Delta E = \int_0^t P(t)\, dt = m \cdot c_p \cdot \Delta \overline{T} \tag{16}$$

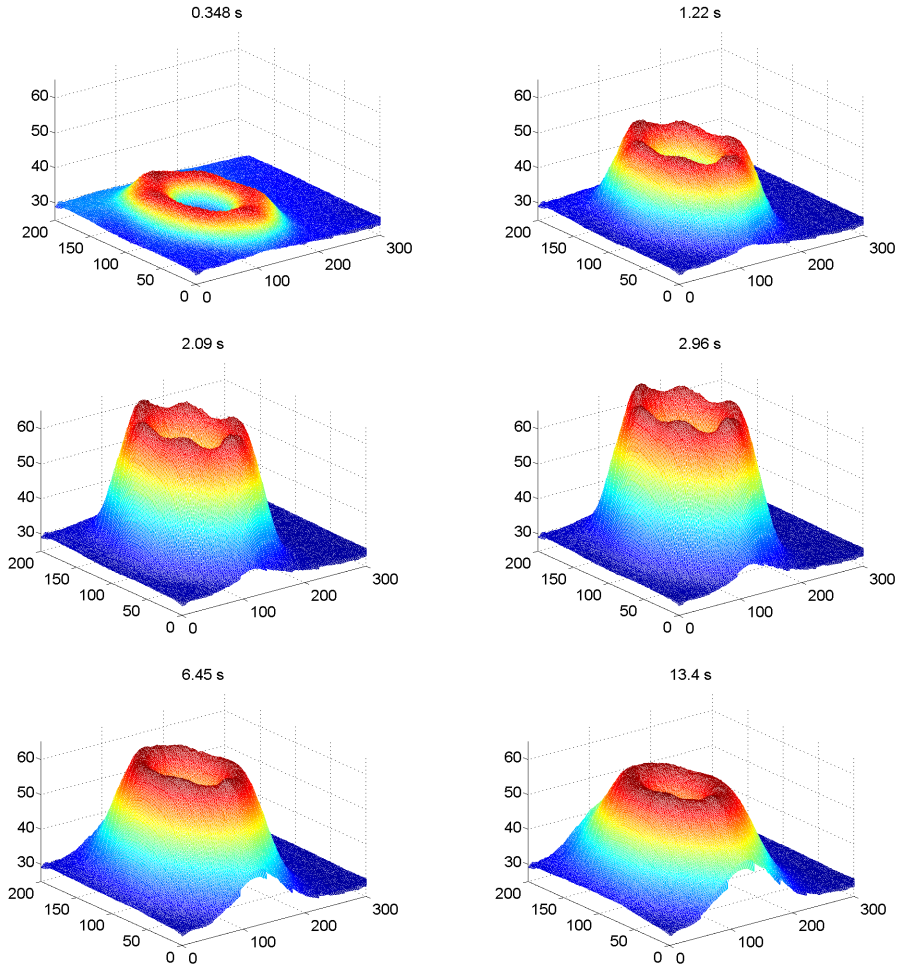

Figure 36: Recorded temperature of the workpiece at different times, x- and y-axis being in millimeters and z-axis in degrees Celsius [59].

8 Travelling-wave induction heating: theory and practical issues

The GreenHeat technology offers new possibilities for inductor design and thereby spatial controllability and heating pattern. Combining the new materials with concepts for uniform induction heating yields interesting results and outlines ways to develop increasingly efficient methods of production. This section focuses on travelling-wave induction heating as one of these methods.

8.1 History and Background

In the 1970s, single-coil solutions for induction heating experienced problems supplying enough power for certain applications. Today, the power electronic drive distributes the loading of the different phases from the grid, which was not the case in the 1970s, when problems arose due to highly unbalanced loads [4] [60]. A solution to this challenge was to use three-phase heating inductors, working with a travelling electromagnetic field in a way similar to a linear motor. A main application of this kind of system was in heating of billets, and the original patent for travelling-wave induction heating was approved in the mid-1970s [61]. The patented solution has parallel wires with an integrated flux concentrator of laminated steel (Figure 37), a design that has been the model for most research in the field [62]. Even at that time, temperature uniformity was an important consideration and double-sided heating was suggested for the best results, arranged in such a way that the main current loops would be represented by circumferential circulation rather than in-plane currents [61] [60] [63].

When modern power electronic frequency inverters entered the market, single-coil solutions became popular again and TWIH was almost forgotten. Nevertheless, TWIH still has qualities in terms of temperature uniformity superior to those of TFIH, and interest in it has been reborn in recent years [64] [65][66]. Most research into TWIH has been limited to analytical analyses or simulations [67] [68] [69] [70] [71], often disregarding significant parts of the complexity and presenting optimal solutions based on simplified models that are clearly unrealistic and impractical. In addition, very interesting aspects of TWIH have been described, as have new findings about other multi-coil induction-heating methods; the present work continues in this path, contributing one piece of the puzzle of induction heating. Two earlier studies, one theoretical and one practical, are of particular interest. The first one, conducted by Ali et al. [72], compares the power density of

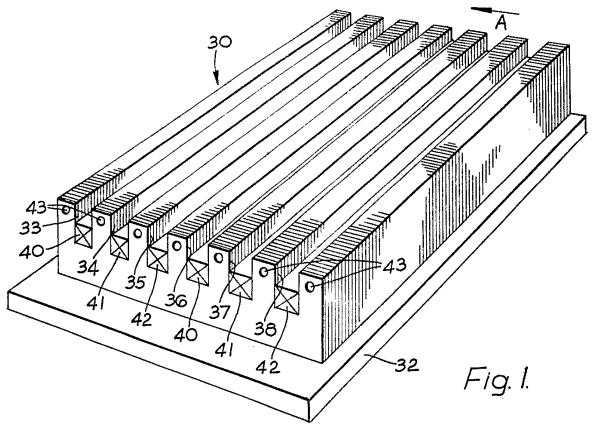

Figure 37: Original design for a travelling-wave inductor [61].

a cross-section of the inductor obtained using analytical calculations with those obtained from FEM simulations. The work clearly illustrates the characteristic asymmetry of TWIH systems (Figure 38), a finding that has been verified several times but not demonstrated in high-quality experiments until the present work. The other work, performed by Sekine et al. [73] [74] and Tomita et al. [75], is one of very few studies presenting experimental results regarding single-sided TWIH heating. The experimental platform used in that study could be improved, as could the heating results (Figure 38); nevertheless, it presents some informative findings somewhat similar to those presented in this thesis.

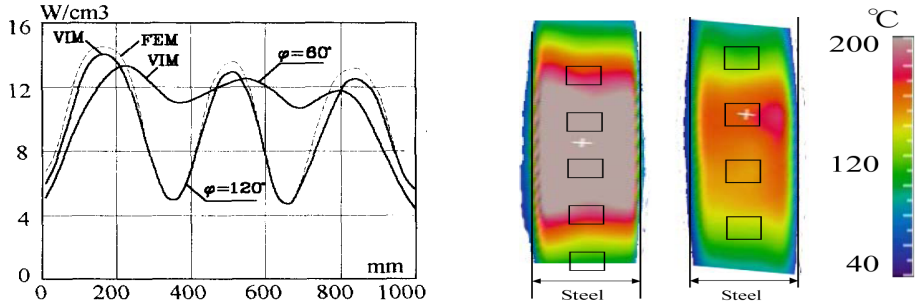

Figure 38: Left: Simulated power density of a three-phase travelling wave configuration. Right: Thermographic image of travelling wave heating.

8.2 Principle

The idea of TWIH is to generate an alternating magnetic field that moves like a wave along the inductor using two or more coils carrying currents with well-defined phase shifts. Instead of creating areas where the resulting electromagnetic field becomes zero due to cancellation, the heating pattern becomes significantly more uniform, to some extent similar to the relative movement between the inductor and the workpiece [76]. The wavelength, λ, or pole pitch is one parameter that affects the heating pattern, and it must be long enough relative to the air gap not to lose efficiency. The speed of the travelling magnetic field is proportional to the product of the wavelength and the frequency. TWIH is sometimes divided into short-pitch and full-pitch types [75] (Figure 39), depending on the coil configuration. The short-pitch type uses separated windings and has shown itself to be a good alternative, for example, when the gap is large [73]. The full-pitch configuration has interlaced windings and is the type considered here.

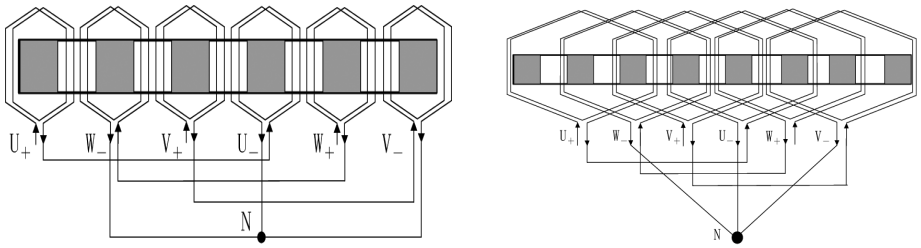

Figure 39: Examples of short-pitch and full-pitch TWIH coil confugurations [73].

Generally, more phases allow for a more uniform heating pattern [72], but many phases also mean increased manufacturing and control complexity, and likely more expensive power electronics. In addition, several conceptual designs have been presented with the same aim: to produce more uniform heating [77] [79] [78]. Two examples of such designs are illustrated in Figure 40, a vernier inductor [80] and slot wedges [81], both of which aim to split the power-density peaks into many smaller peaks located near each other. In the figure, 1 indicate the core material, 2 are the coils and 3 is the workpiece. Due to the thermal conductivity of the workpiece, power peaks in close vicinity will float together giving a uniform temperature pattern. The concepts are interesting but lack experimental validation and rely only on simplified models, for example, ignoring saturation effects. Also the air gap becomes very critical for these type of designs.

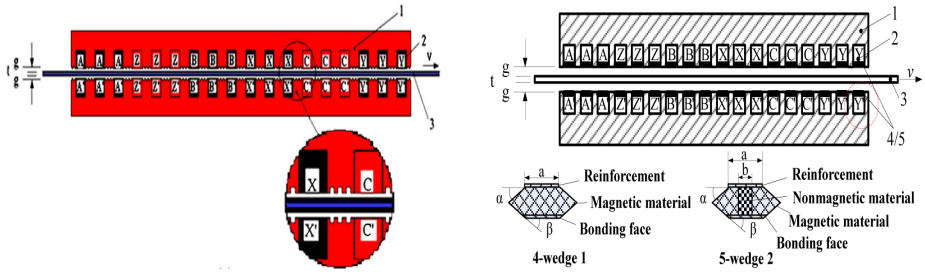

Figure 40: Vernier inductor [80] and slot wedges [81].

8.3 Inductor design

The design of the first travelling-wave inductor was based on two identical TF coils with the same geometry as previously used in this project. The two coils were interwoven into one unit (Figure 41) and later equipped with a surrounding SM^{2}C core. The same geometry was used to allow for direct comparisons between the different inductor types. Unlike solid conductors, the litz wire allows the electromagnetic field to penetrate the compact structure, which is crucial to this kind of design, referred to as *slotless* [82].

Figure 41: Left: Single phase TF coil. Right: Two phase TW coil.

Parallel to the production of the slotless inductor, a design with SM^{2}C teeth was realized, also based on the advantages of convenient comparison between different models rather than on optimization. Slots of the same width as the wire were inserted in the center of each pole of the design, and the straight parts of the coils were covered with the core material (Figure 42). Leaving the coil ends surrounded by air instead of SM^{2}C minimizes the inductance and allows for planar modeling. The particular selection of one slot in each pole and no slots between the poles might be unique, but many similar designs have previously been evaluated.

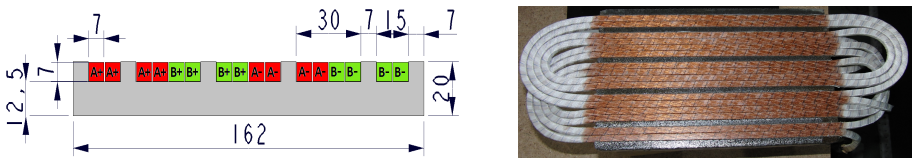

Figure 42: TW coil with SM^{2}C teeth.

Travelling wave inductors made with litz wire are extremely rare, but not unknown, and at least one other research group has tested such an inductor for the uniform heating of long structures [73]. However, as far as is known, what is unique in the present work is a TWIH setup based on only two coils—since the principle originates from using a three-phase grid signal, this was the natural choice of phases. Existing research demonstrates that the use of even more phases could provide even more uniform heating [72], but no study of two-phase systems has been found. The reason for investigating a two-phase system, known to provide less uniform heating and to require more complex power electronics than a three-phase system, is its simplicity. Given the selected design, only the two-phase system can achieve perfect symmetry between the phases, while the center winding of a three-phase inductor exhibits dynamics differing from those of the other two. In addition, when it comes to the number of adjustable parameters, phase shift control, and compensation for mutual inductance, etc., the two-phase inductor is simpler. To fully understand a system, the best approach is often to start simply and increase the complexity in stepwise fashion, as was done here with the selected number of phases.

While the two initial inductors were being tested and before realizing the full complexity of the system, a three-phase version was also built (Figure 43), though it remains untested. It was found to be crucial that the inductance of each coil should be the same, so as not to cause undesired behavior, so a second generation of two-phase slotted inductors was developed. Two identical inductors were built, with one end of each coil lying on top of the other in each inductor, respectively, unlike in the first generation. The new inductors (Figure 43) were made without an outer border of core material to allow the units to be assembled into a single larger, modular inductor. The reason for building two identical units was also related to an experiment with current decoupling, described in section 8.9.

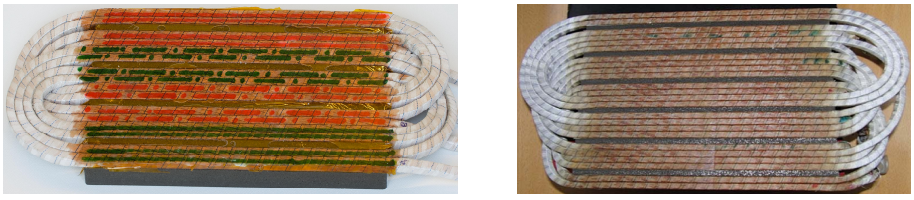

Figure 43: Left: New version of two phase TW coil. Right: Three phase TW coil.

8.4 Coupling effect

An increasing proportion of induction heaters being developed uses more than one coil. There are two main reasons for doing this: a larger demand for generic heaters and an increased requirement for uniform and controlled heating. In domestic appliances, for example, customers demand products in which each cooking zone can efficiently handle several sizes of vessels and not be too sensitive to exact vessel positioning [76]; the same principle applies to industrial applications. With a well-distributed heating pattern, product quality can be improved and processing time reduced. There are many reasons for using multi-coil solutions, but they exact a cost in terms of increased complexity due to mutual coupling. Independent of the inductor type and control principle, the same problems occur in all designs. The commonly used measure to define the interaction is mutual inductance, M, defined as the geometric average of the inductances, L_i, of all the coils times the coupling factor, k (equation 17).

$$M = \sqrt{L_1 \cdot L_2} \cdot k \tag{17}$$

Much effort has gone into this area in recent years, with a focus on analytical modeling [83] [84] [85] and identifying system parameters [86] [87]. One common way of describing the interaction between the currents of the coils is based on the impedance matrix representation, Equation 18:

$$\begin{bmatrix} \overline{V}_1 \\ \overline{V}_2 \\ \vdots \\ \overline{V}_n \end{bmatrix} = \overbrace{\begin{bmatrix} \overline{Z}_{11} & \overline{Z}_{12} & \dots & \overline{Z}_{1n} \\ \overline{Z}_{21} & \overline{Z}_{22} & \dots & \overline{Z}_{2n} \\ \vdots & \vdots & \ddots & \dots \\ \overline{Z}_{n1} & \overline{Z}_{n2} & \dots & \overline{Z}_{nn} \end{bmatrix}}^{Impedance\ matrix} \cdot \begin{bmatrix} \overline{I}_1 \\ \overline{I}_2 \\ \vdots \\ \overline{I}_n \end{bmatrix} \tag{18}$$

Due to the resonant behavior of IH systems, the impedance matrix features a huge frequency dependency. TW inductors have a mutual inductance of approximately 1/5 of the inductance of each coil, i.e., a coupling factor of approximately 0.2 within the selected frequency range of 10–40 kHz when measured unconnected (Figure 44). The coupling factor increases to approximately 0.5 at resonance when connected to the system, as illustrated in the same figure. From the plots it is obvious that the resonance and thus the coupling are dependent on the output power and also that the phase shift of the induced current is significantly dependent on the excitation frequency.

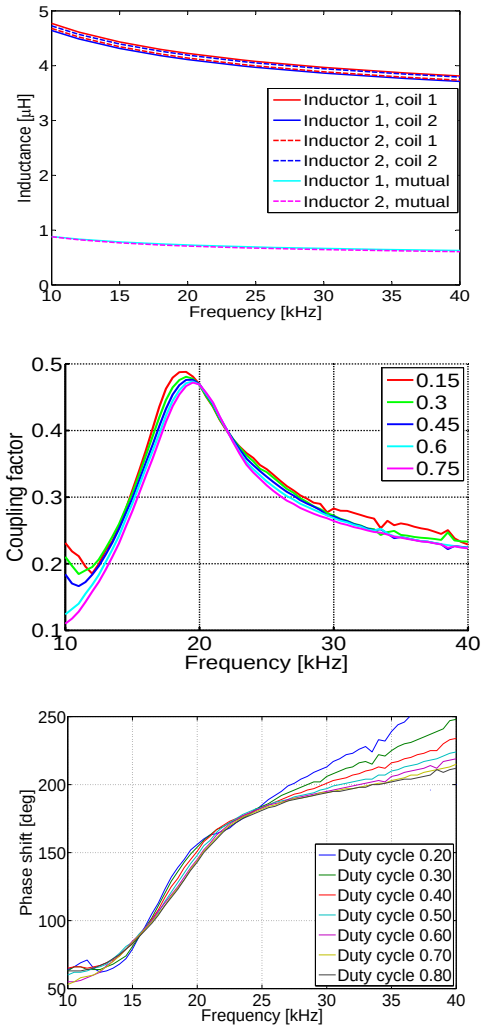

Figure 44: Top: Inductance and mutual inductance. Center: Coupling factor. Bottom: Phase shift of induced current.

8.5 Simulations

The power distribution of two-phase TW inductors was thoroughly investigated using electromagnetic simulations based on finite-element analysis (FEA). The coil ends were neglected and 2D planar models were developed. The freeware program Finite Element Method Magnetics (FEMM) was used in this study due to its simplicity, accurate results, and useful interface with

Matlab (OctaveFEMM [88]), but most of all because of its well-developed bulk model representation of litz wires [89] [47]. By building on or modifying the FEM model from Matlab, a fully automated parameter study could be performed, sweeping the current amplitudes and phase angle for each inductor type. The simulations were performed with linear and nonlinear workpiece materials to investigate the effect of saturation. Since nonlinear models typically require 10–100 times more computational time to converge than do linear models, their benefits must be considerable to justify their use. Due to the low magnetic flux densities involved in such applications, the results are the same independent of the complexity of the SM^2C material, so a linear representation is preferred. For highly permeable workpiece materials, on the other hand, the field concentration near the surface justifies the use of nonlinear representation—at least at higher power levels. The mesh size for the workpiece is particularly important for achieving reliable results, and a clear breakpoint was found at two triangles per skin depth. By using a fine mesh around the line segment defining the workpiece surface, the most critical regions can be very accurately computed without increasing the number of nodes more than necessary. Since a 2D representation can be used in this case, memory requirements are not an issue with a workstation computer, which allows for some margins in the meshing. A simple and common method to investigate the current or power density in the workpiece is to extract the magnetic flux density or surface current density along a line at the boundary of the workpiece; however, this method is very sensitive and requires a fine mesh to work. Instead, the workpiece was divided into a number of pieces, typically 0.5 mm wide, over which the total current or power can be accurately integrated. Figure 45 shows the post-processed model of the first-generation TW inductor and the resulting power density in cross-section when linear and nonlinear workpiece materials are used at current densities of 4 and 10A/mm^2, respectively. The currents are the same in size and have a phase shift of 90°. The selected workpiece material is steel 1010, found in the materials library of FEMM.

By using the Matlab support for parallel computing, i.e., matlabpool and parfor loops, many instances of FEMM can be opened and running in parallel on different cores. With automatic pre- and post-processing of the models available, a library of Matlab functions was developed that can update the geometry or other parameters, such as frequency or material properties, based on previous results. These functions were useful tools for investigating the influence of various parameters, and can easily be used together with built-in functions, such as *nlinfit*, for optimization purposes; these built-in functions were only briefly tested.

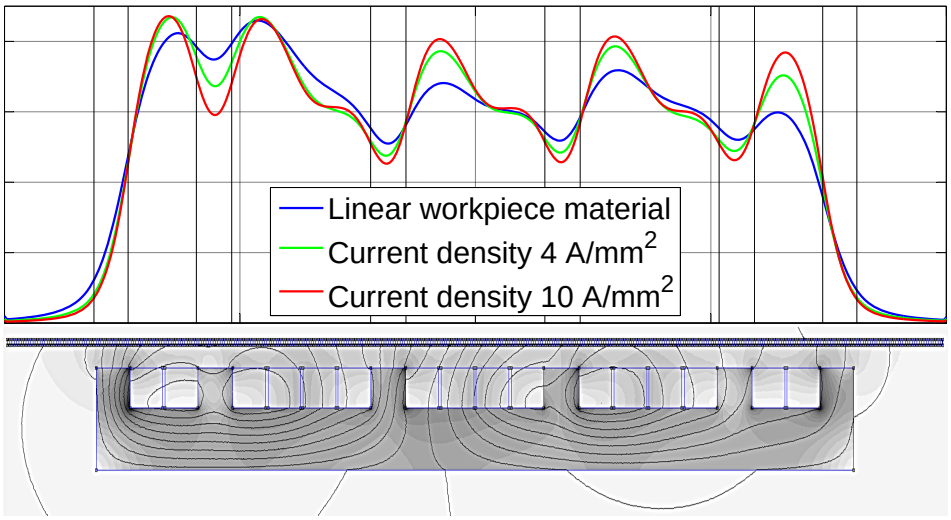

Figure 45: Bottom: Simulation model of first generation of inductor design with magnetic field lines. Top: Power density using linear and nonlinear workpiece material at different current densities in the winding.

Figure 46 shows the power density of the two slotted inductors for phase shifts of 0–180 degrees. Removing the SM^2C from the outside of the coils as well clearly decreases the power along the edges. It is also obvious that the power generation dips locally at the slots, i.e., in the regions where there are no coils. These power dips are also present when running only one of the phases.

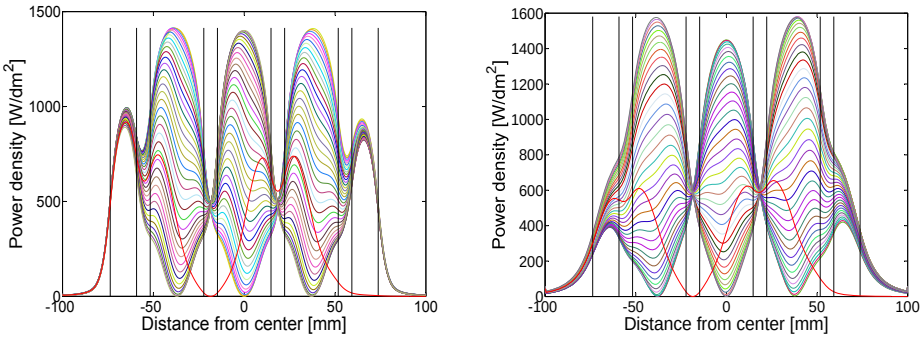

Figure 46: The power density of the two studied slotted inductors.

The corresponding power density as a function of the phase shift for the slotless inductor is shown in Figure 47. In this case as well, there are two nodes where the output power density is almost independent of the

phase shift. The nodes correlate well with the position of the slots of the other inductors. Another interesting result is obtained by adding the power density to the mirror pattern, to create a symmetric result. In the linear case, this means that the resulting power pattern is the same independent of the phase shift and is the same as when running one coil at a time. In Figure 47, the graph represents this symmetric heating pattern for the second generation slotted inductor.

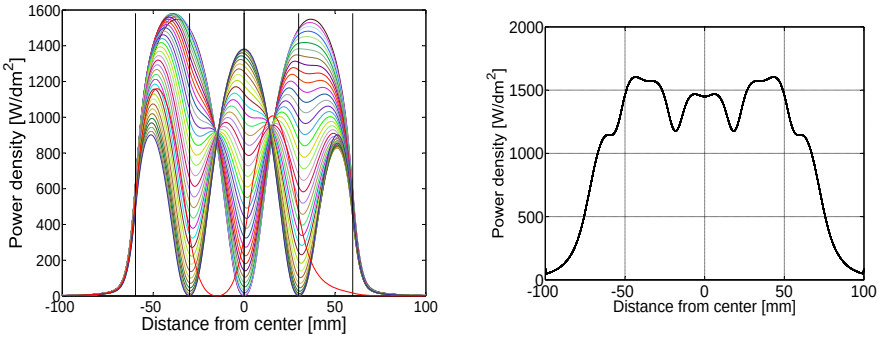

Figure 47: The power density of the slotless inductors.

By using a nonlinear representation of the workpiece material, more realistic results can be obtained, as shown in Figure 48. The graph shows a fairly uniform heating pattern, representing the first-generation slotted inductor.

Figure 49 explains how the heating pattern depends on the number of wave lengths of the inductor, this is important information e.g. when building large systems. The result is a peak in one of the ends, but otherwise small periodic waves.

The planar simulation models could provide all the information about the electromagnetic behavior required for the selected inductor geometries. For problems requiring 3D simulations, there are several tricks to reduce the memory usage, though they reduce the reliability of the solutions. When analyzing the thermal effects, on the other hand, all expected properties lie in the same order of magnitude. The mesh size needed in order to accurately resolve the temperature pattern, can appear as in Figure 50. So as not to neglect the electromagnetic analyses, the thermal aspects were left to co-researchers to analyze.

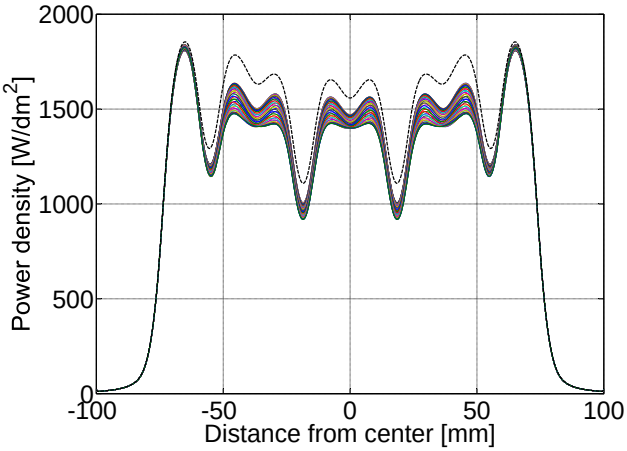

(a)

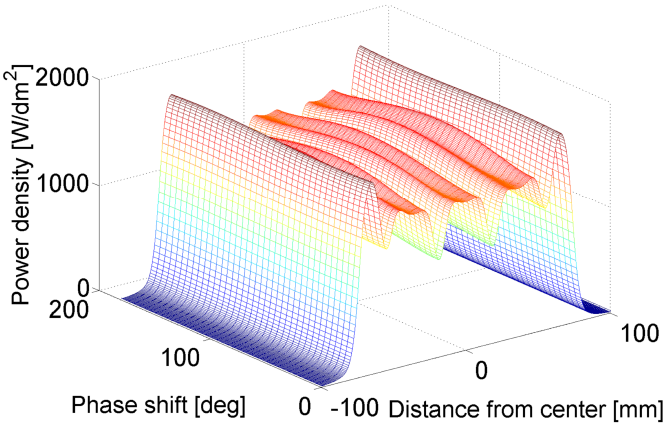

(b)

Figure 48: Heating pattern of the slotted inductor.

8.6 Analytical work

Analytical models play an important role in fully understanding the reasons for or underlying theories of a certain behavior. Analytical models can be empirical, physical, or combinations thereof. Empirical models have their origin in data of any kind and need not be related to physical laws or known relationships. Due to the complex behavior of real dynamic systems, the

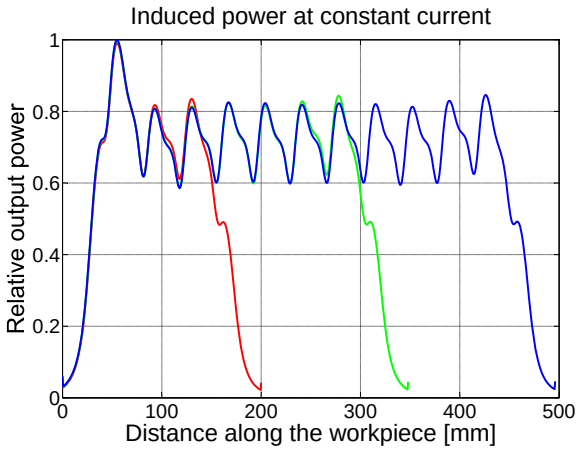

Figure 49: Simulated power density along the workpiece for three different sizes of the inductors.

development of physical models is challenging and often requires substantial simplifications. During the thesis work, analytical models were developed to link the currents in the coils to the voltages from the power electronics. The TWIH system was approximated by a simplified LCR scheme with two parameters according to Figure 51 [90]. The component values were fitted to experimental data obtained from frequency sweeps of the 10–40 kHz range using a Hameg HM8118 LCR meter.

The simplified model can be described using a set of five differential equations, relating the currents to the voltages according to Equation 19.

$$\begin{cases} u_0 = R_{12_{eqv}} \cdot i_{01}(t); \\ u_0 = L_{12_{eqv}} \cdot \dfrac{di_{02}(t)}{dt}; \\ u_0 = u_p(t) - \dfrac{\int_0^t i_1(t)dt}{C_1} - L_1 \cdot \dfrac{di_1(t)}{dt} - R_1 \cdot i_1(t); \\ u_0 = u_s(t) - \dfrac{\int_0^t i_2(t)dt}{C_2} - L_2 \cdot \dfrac{di_2(t)}{dt} - R_2 \cdot i_2(t); \\ i_{01}(t) + i_{02}(t) = i_1(t) + i_2(t). \end{cases} \quad (19)$$

Solving the equations yields the results presented in Figure 52; however, the time-dependent signals were not the primary interest, but rather the indirect information derived from them. Those results are presented in sections 8.8 and 8.10. The solutions are sensitive to resonances but, overall,

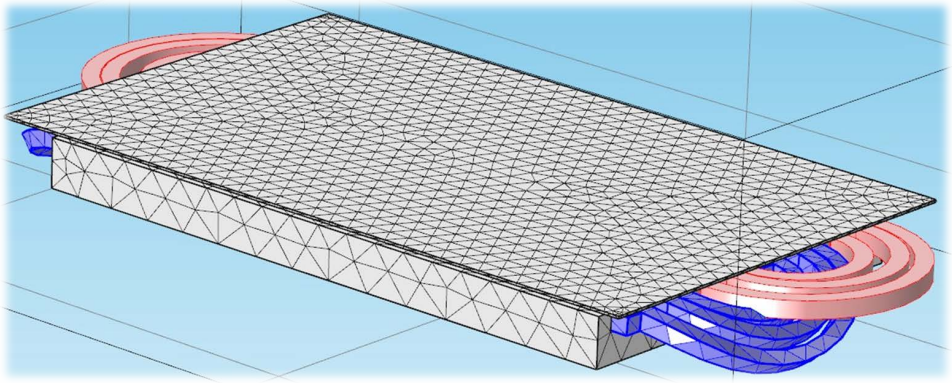

Figure 50: Simulation model for thermal analysis.

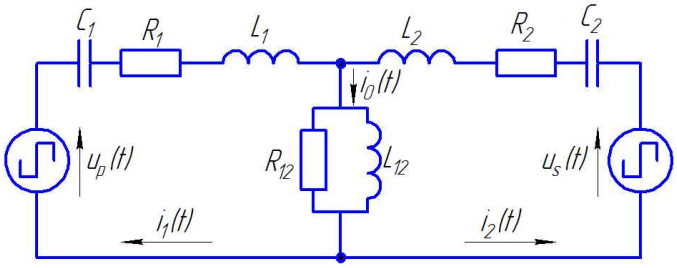

Figure 51: RLC circuit model of currents in coils [90].

coincide well with the experimental results.

8.7 Experimental work

Based on the experimental platform described in section 6 and using the developed measurement tools described in section 7, TWIH setups were extensively tested and measured. By running the system at different duty cycles, voltage phase shifts, and frequencies, the dynamic behavior was investigated. Most of the experiments were performed using a water-cooled workpiece and recording the currents and voltages obtained for each setting. The most important signals were the inductor currents (i.e., on the secondary side of the transformers) and the voltage across the inductor. The sensor signals were sampled simultaneously at 1 MSamp/s and, for most frequencies, further resolved by assuming the repetition of each period. Using this method, one period with a high equivalent sample rate was obtained and saved for further processing for each set of parameters.

In order to investigate the heating pattern, the water-cooled workpiece

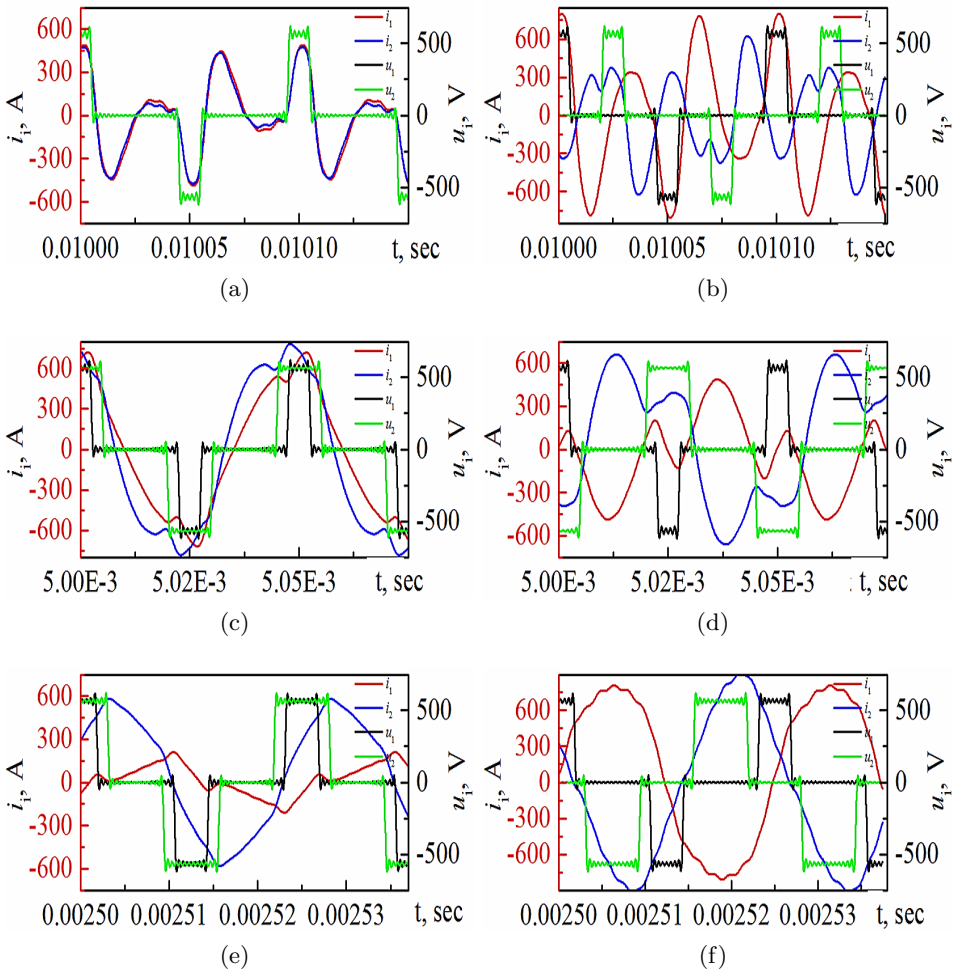

Figure 52: Time dependencies of input voltages, $u_p(t)$ and $u_s(t)$, and calculated currents, $i_1(t)$ and $i_2(t)$, in the inductor coils at various frequencies, f, and voltage phase shifts, ψ. (a) 10 kHz, $dc_1 = 0.2$, $dc_2 = 0.2$, $\psi = 0$; (b) 20 kHz, $dc_1 = 0.2$, $dc_2 = 0.4$, $\psi = 0°$; (c) 40 kHz, $dc_1 = 0.3$, $dc_2 = 0.5$, $\psi = 0°$; (d) 10 kHz, $dc_1 = 0.2$, $dc_2 = 0.2$, $\psi = 90°$; (e) 20 kHz, $dc_1 = 0.2$, $dc_2 = 0.4$, $\psi = 180°$; and (f) 40 kHz, $dc_1 = 0.3$, $dc_2 = 0.5$, $\psi = 270°$ [90].

was replaced by a 1.5-mm-thick, black-painted sheet of similar material. With the dynamics already known, proper settings of the power electronics could be assigned and the heating pattern and output power investigated using thermography [51]. At equally sized currents and a phase shift of 90°, a fairly uniform heating pattern could be produced within an area of the same size as the inductor, shown in Figure 53.

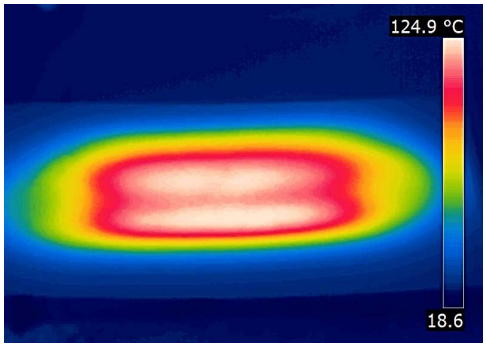

Figure 53: Heating pattern at equal current amplitudes and 90° phase shift.

To investigate the influence of the phase shift on the heating pattern, a series of measurements was performed in steps of 10°. The heating pattern was defined as the power generation in the workpiece along a line in the center of the inductor, perpendicular to the coil. Running the system for a short time only and with a fairly small change in temperature minimized the influence of the thermal conductivity on the heating pattern. The output power pattern was then determined from the temperature difference at each position. To reduce the influence of noise and other uncertainties, the results are calculated as the average over 20 lines, all near the center of the workpiece. The result of the power distribution as a function of the phase shift is shown in Figure 54. As indicated, the phase shift adds an extra degree of freedom for the temperature control, also shown by Pham et al. [91].

8.8 Working points and optimal control

TWIH uses well-defined current amplitudes and phase shifts to create the expected power generation. In a non-circular finite wavelength heater, there is mutual inductance between the coils, as described earlier. This interaction between signals complicates the generation of currents at a given amplitude and phase shift, meaning that finding the desired working points is not straightforward. The working points for the two-phase heaters are defined as two equally sized currents with a phase shift of ±90 degrees.

During the present work, large parameter studies were performed using a huge number of data generated both by the analytical model and experimentally. Using functions for automatically interpolating data in several dimensions, parameter values corresponding to certain conditions can be identified with high accuracy. The sought-after parameters are the fre-

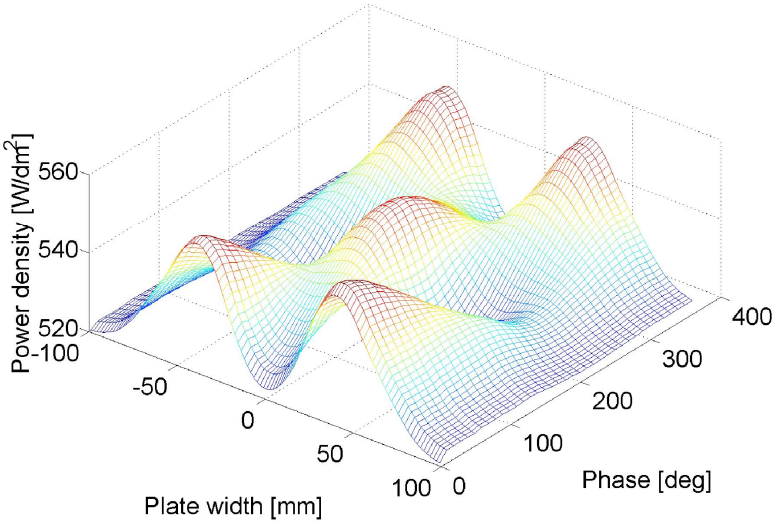

Figure 54: Measured power density along the workpiece for equally sized currents at different phase shift.

quencies, voltage duty cycles, and phase shifts that can be controlled in the system. The first condition is currents that are equally sized in terms of RMS value, limited to a selected frequency range and a given combination of duty cycles. In the study, only frequencies of 10–40 kHz were of interest. Based on experimental data, an example of the amplitude working point, indicated with black dots, is shown in Figure 55. Similarly, results could be extracted from the analytical model shown in Figure 56.

The second property to identify was the current phase shift of $\pm 90°$. The phase shift is easy to define for a sinusoidal signal, but as soon as the signals contain harmonics it is no longer obvious. A current phase shift equal to zero was defined as settings at which the correlation between signals is the highest, i.e., equation 20. N is the length of the signal and $|\bullet|$ denotes the distance between two sets of points with the coordinates $max[abs((I_1 * I_2)[n])]$ and N. The results using experimental and analytical data, respectively, are presented in Figure 57.

$$\varphi = \frac{2 \cdot \pi \cdot |max[abs((I_1 * I_2)[n])], N|}{N} \tag{20}$$

To find what controllable settings correspond to both the identified amplitude and current phase shift, the results were projected onto the frequency–voltage phase shift plane shown in Figure 58. Only the intersections between

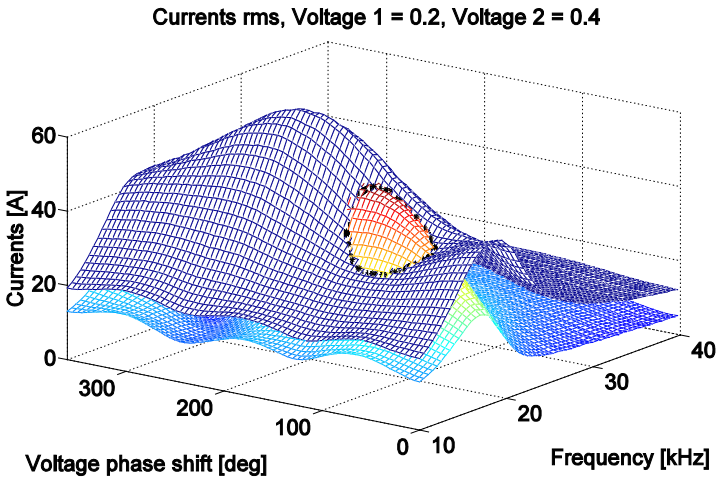

Figure 55: Current 1 and 2 for different settings. The intersection is marked with black dots [90].

the curves meet the requirement of being working points. Each properly selected combination of duty cycles generates two working points, each producing its own current amplitude value.

By plotting the projected results for different combinations of duty cycles in a single diagram, the desired results appear as two curved lines in the 3D space, one at a 90° and the other at a 270° current phase shift, according to Figure 59, assuming one of the voltages to be constant. These results are obtained from the measured data, but the same procedure can also validly be used with the analytical results, though the uncertainties of the two-parameter model make its results too approximate to be practically useful for the purposes of this research.

The bigger the differences in the applied voltage duty cycles, the larger the currents generated, according to Figure 60. Starting with equal duty cycles and reducing one of the voltages means an increased current, indicating a negative system impedance. This behavior results from mutual coupling combined with a step towards the resonance frequency.

The working points are closely related to the system dynamics and even a small change, for example, because of increased workpiece temperature, can alter the generated heating pattern. Based on known system behavior, combined with proper starting points, automatic current control can be implemented. With a poorly selected starting point combined with a generic control algorithm, there is the risk of positive feedback, as investigated in similar systems by Fujita et al. [92].

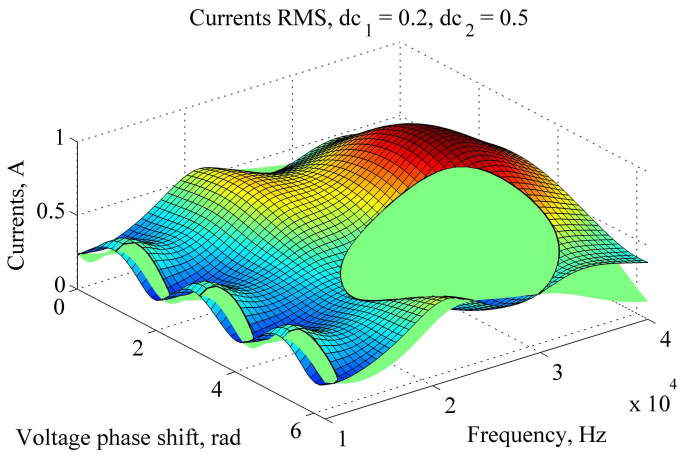

Figure 56: Current amplitudes as function of frequency and voltage phase shift at duty cycles dc_1=0.2 and dc_2=0.5 respectively [90].

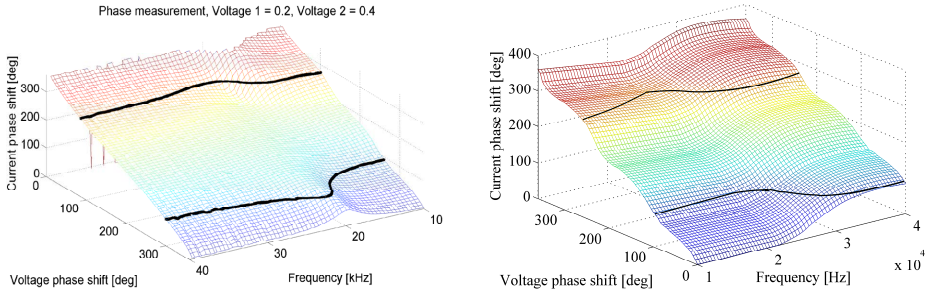

Figure 57: Current phase shifts, $\pm 90°$ marked with black lines. Left: Experimental data. Right: Data from analytical model [90].

8.9 Reduction of mutual coupling

Based on experimental data or theoretical models, it is possible to find proper working points for TWIH systems. Due to variations in relative position between inductor and workpiece, actual temperature, etc., the dynamics might change, producing a different heating pattern from that expected. Different setups and working points have different sensitivities to variations in properties and the currents can be kept stable using automatic control, though this increases the complexity and the mutual coupling may reduce system efficiency [11]. Considerable effort has been spent on reducing the cross terms of the impedance matrix [87], and one way of doing this is to use decoupling transformers [11] [93]. These transformers increase the cost but,

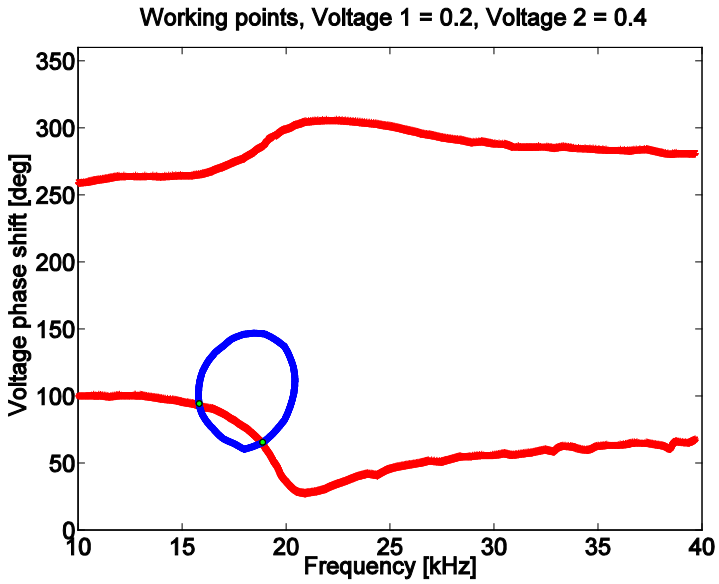

Figure 58: Projected settings generating equally sized currents, blue and a current phase shift of $\pm 90°$, red. The intersections of the curves illustrate the desired working points [90].

more importantly, reduce the power factor and cannot perfectly follow the dynamic coupling affected, for example, by saturation effects and temperature. For systems that can be based on two identical and independent TW inductors, on the other hand, the currents can be decoupled without a need for external components. The dynamic behavior is the same independent of current amplitude, temperature, frequency, etc., as long as the inductors serve similar processes [94]. The effects of connecting coils of two more or less identical inductors in series and parallel, respectively, on the mutual coupling were investigated (Figure 61).

The relationship between the voltages, V, and currents, I, within a single inductor, i, can be formulated as in equation 21, where k represents the complex coupling factors between two coils, j. Each section of the coil is divided into positive and negative parts depending on the direction of the current, indicated with a sign index (see equation 22). Z is the impedance imposed

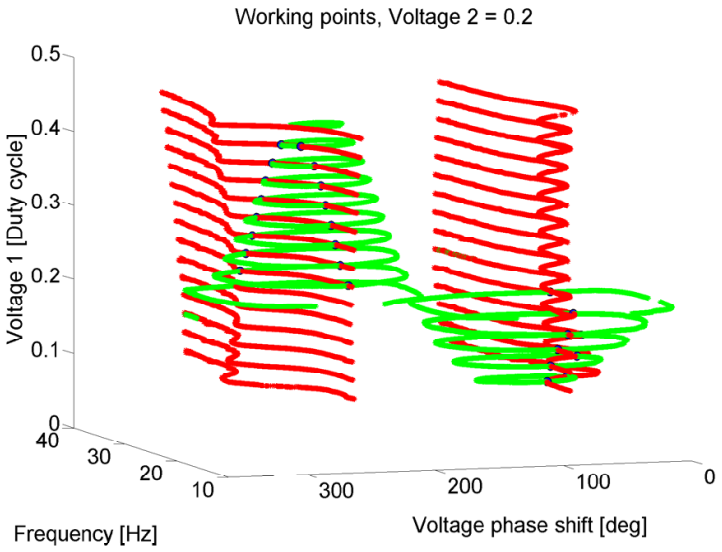

Figure 59: Working points for different combinations of duty cycles [90].

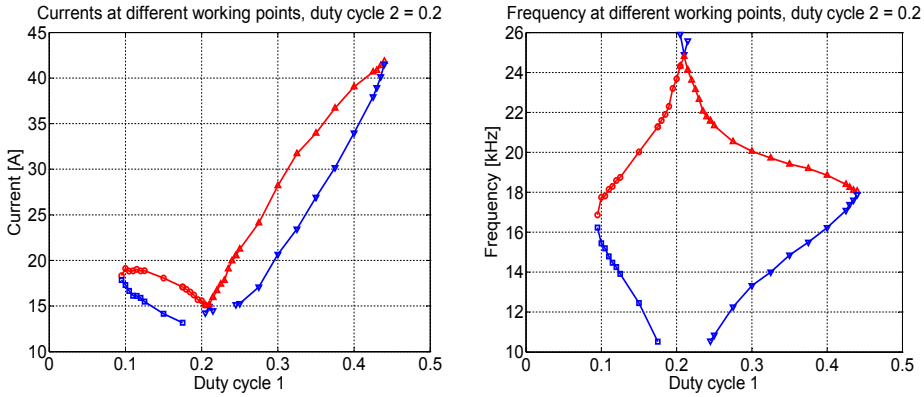

Figure 60: Current amplitude and corresponding frequency at the working points for different combinations of voltage duty cycles.

by each part of the coil in the inductor, which is considered symmetric.

$$\begin{bmatrix} V_{i1} \\ V_{i2} \end{bmatrix} = \begin{bmatrix} I_{1+} & I_{2+} & I_{1-} & I_{2-} \\ I_{2-} & I_{1-} & I_{2+} & I_{1+} \end{bmatrix} \cdot \overbrace{\begin{bmatrix} Z_1 \\ -k_{12}Z_1 + k_{23}Z_2 \\ Z_2 \\ k_{14}Z_1 - k_{12}Z_2 \end{bmatrix}}^{Z} \tag{21}$$

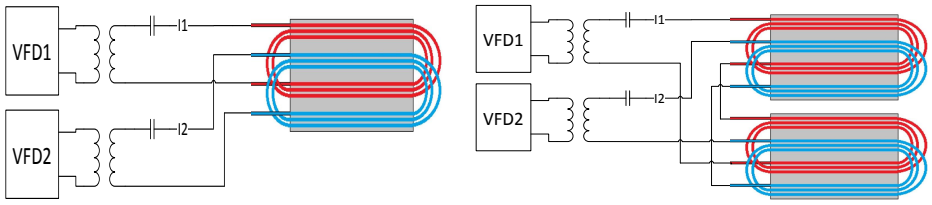

Figure 61: Connection of the coils to the variable-frequency drives. Left: Original setup. Right: Setup for a series or parallel connection [94].

$$I_{j+} = I_{j-} = I_j \tag{22}$$

For serial connection of the two inductors, the resulting voltage sums accordingly (equation 23):

$$\begin{bmatrix} V_1 \\ V_2 \end{bmatrix} = \begin{bmatrix} V_{11} \\ V_{12} \end{bmatrix} + \begin{bmatrix} V_{21} \\ V_{22} \end{bmatrix} \tag{23}$$

Eight series and eight parallel connections were identified according to Figure 62 and experimentally tested. Defining the positive end of one the VFDs as the reference phase, 0°, and the positive end of the other VFD as 90°, the negative ends automatically correspond to 180° and 270°, respectively. The phase shifts of each configuration and thereby the wave directions can be defined as shown in Table 2.

0°	90°	180°	270°	0°	90°	180°	270°	⟹	⟹
0°	90°	180°	270°	0°	270°	180°	90°	⟹	⟸
0°	90°	180°	270°	180°	90°	0°	270°	⟹	⟸
0°	90°	180°	270°	180°	270°	0°	90°	⟹	⟹
0°	90°	180°	270°	90°	0°	270°	180°	⟹	⟸
0°	90°	180°	270°	90°	180°	270°	0°	⟹	⟹
0°	90°	180°	270°	270°	0°	90°	180°	⟹	⟹
0°	90°	180°	270°	270°	180°	90°	0°	⟹	⟸

Table 2: The phase shifts of each configuration and the corresponding wave direction of each inductor.

Analyzing the impedance vector, Z, for the different configurations according to equations 21–23 eliminates the cross terms for configurations 2,

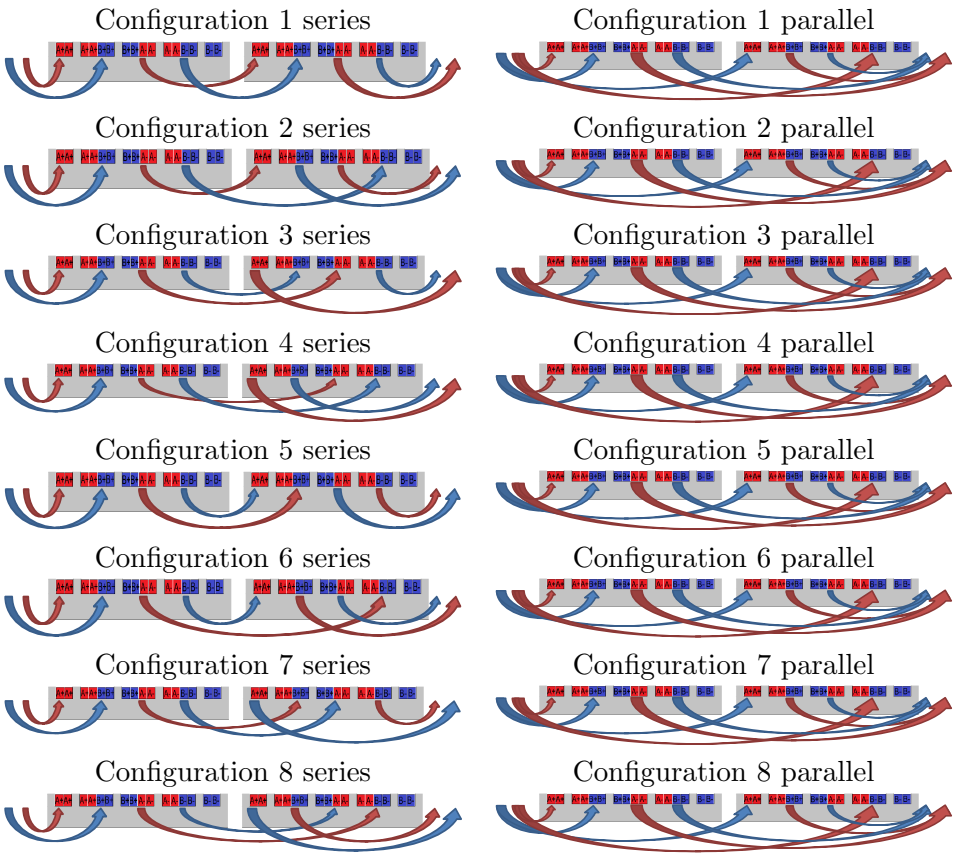

Figure 62: Connection schematics of the eight series and eight parallel unique configurations of two, two-phase travelling-wave inductors, shown in cross-section.

3, 6, and 7, independent of whether the connection is series or parallel, assuming that the inductors are perfectly equal. Equations 24 and 25 show the results of the configuration 2 series. The resulting impedance is doubled for each phase according to basic circuit theory; in the case of a parallel connection, it accordingly becomes half the original value. The changed inductance affects the resonance frequency if not compensated for by the value of the resonant capacitor.

$$Z = \begin{bmatrix} Z_1 \\ -k_{12}Z_1 + k_{23}Z_2 \\ Z_2 \\ k_{14}Z_1 - k_{12}Z_2 \end{bmatrix} + \begin{bmatrix} Z_1 \\ k_{12}Z_1 - k_{23}Z_2 \\ Z_2 \\ -k_{14}Z_1 + k_{12}Z_2 \end{bmatrix} = \begin{bmatrix} 2Z_1 \\ 0 \\ 2Z_2 \\ 0 \end{bmatrix} \tag{24}$$

$$\begin{bmatrix} V_1 \\ V_2 \end{bmatrix} = \begin{bmatrix} I_{1+} & I_{2+} & I_{1-} & I_{2-} \\ I_{2-} & I_{1-} & I_{2+} & I_{1+} \end{bmatrix} \cdot \begin{bmatrix} 2Z_1 \\ 0 \\ 2Z_2 \\ 0 \end{bmatrix} \tag{25}$$

Due to uncertainties in inductor manufacturing and possibly due to stray inductances in the cables, the compensation for the coupling varies between the various configurations theoretically doing the same job. These differences are illustrated by the mutual inductances presented in Figure 63, also showing the results of the configurations where the cross terms are not cancelled.

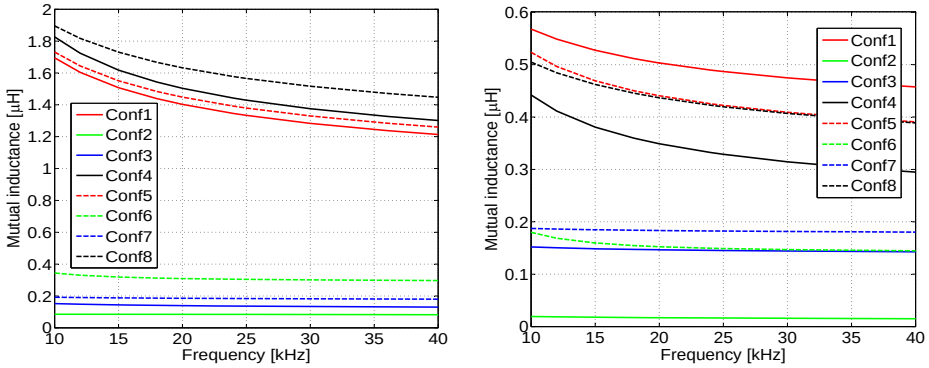

Figure 63: Mutual inductance of the different configurations. Left: Series. Right: Parallel.

For the best configuration, the coupling factor is reduced by approximately 95%. Figure 64 compares the currents between configurations 1 and 2, only one coil being excited.

Decoupling the currents significantly simplifies the control, since the current in each coil can be adjusted using the corresponding voltage without affecting the current in the other coil. The interference between the electrical properties from using one and two inductors in series according to configurations 1 and 2, respectively, is shown in Figure 65.

Some concluding remarks about the decoupling are as follows:

- This type of decoupling can eliminate the interference between currents, independent of surrounding conditions, if designed properly.
- Series or parallel connections work equally well; the best choice depends on the desired system impedance.

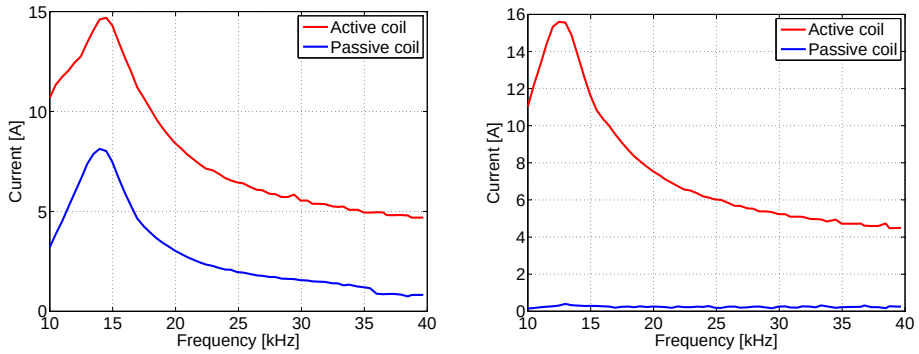

Figure 64: Current in active and passive coils of two inductors connected in anti-series. Left: Configuration 1. Right: Configuration 2.

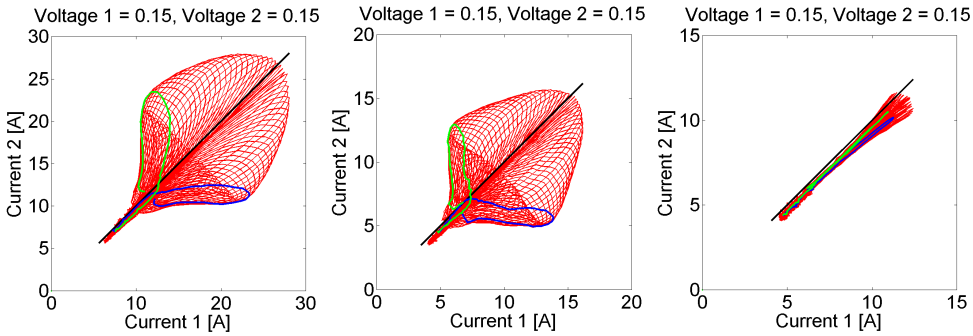

(a) One inductor (b) Configuration 1 series (c) Configuration 2 series

Figure 65: Currents measured in each phase at constant voltage amplitude but at different frequencies and with different phase shifts. The black line indicates that the currents are equal in amplitude; the green and blue curves indicate a phase shift of $\pm 90°$.

- The relative accuracy of the inductor properties is more important than the absolute accuracy.
- Coils with few turns have a relatively greater inductance uncertainty stemming from production variations and cabling than do coils with many turns.
- The heating patterns of the two inductors are similar only for a current phase shift of $\pm 90°$; an increased phase shift in one inductor reduces the value correspondingly in the other.

A simple way to reduce the coupling is to make inductors with many

poles or wavelengths. Since the mutual coupling is due to the asymmetry caused by the outer poles, solutions with many poles have relatively less mutual coupling.

8.10 Results and comparison

Generally, there are good correlations between the modeled and experimental results; to simplify comparison, selected plots from each section were moved here. Figure 66 compares the power density distribution along a cross-section through the center of the inductor, perpendicular to the coils, as a function of different current phase shifts; the results are obtained from FEM simulations and measurements, respectively. To improve the quality of the images, the data were linearly interpolated before being plotted.

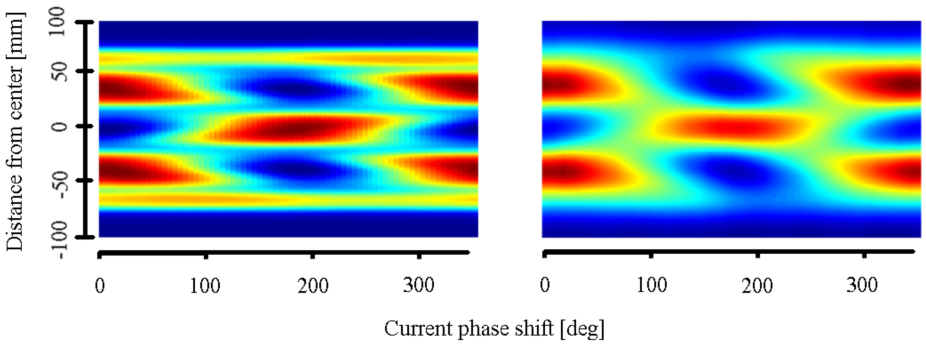

Figure 66: Left: Simulated power density distribution. Right: Measured power density distribution.

By extracting the power density distribution of the settings related to TWIH, i.e., 90° and 270°, the results are as shown in Figure 67. The very good correlation between the simulated and measured results is an important finding of this work. The results are normalized so that the peak value equals one for each curve. A more appropriate adjustment would likely be to normalize the results according to equal area, though the interference between the graphs would made the figure less ordered. These results experimentally and qualitatively verify the asymmetry related to TWIH and confirm that model works as expected. Compared with the simulated results, the experimental results indicate some averaging effects, not considered in the model, caused by the thermal conductivity of the workpiece.

The output power as a function of the phase shift is shown in Figure 70, which also indicates a good correlation between modeled and real-world re-

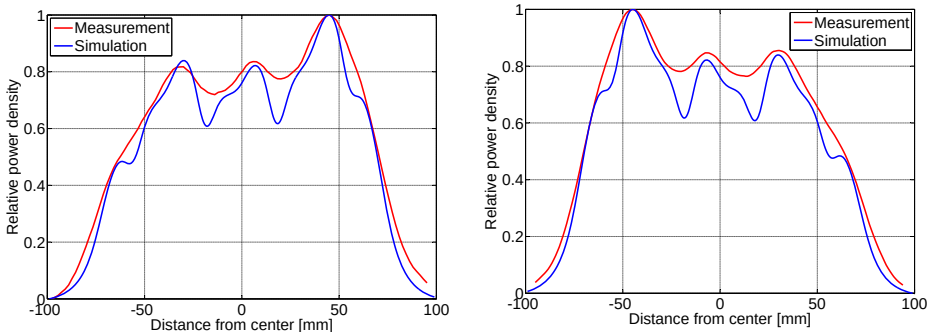

Figure 67: Simulated and measured power density distribution. Left: Phase shift of 90°. Right: Phase shift of 270°.

sults. By reducing the measurement uncertainty, an even better correlation could likely be obtained.

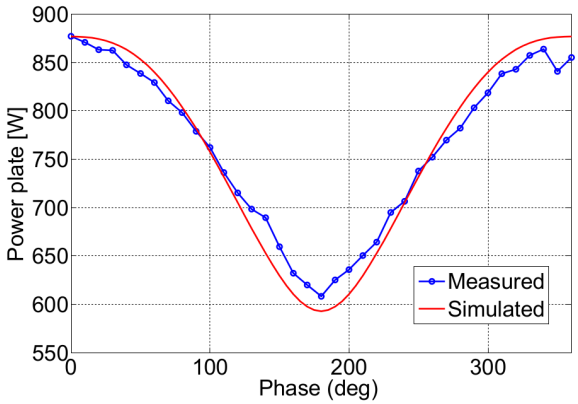

Figure 68: Simulated and measured output power at constant current amplitude but different phase angles.

Decoupling the currents using an anti-series or anti-parallel connection significantly simplifies the control, since the current in each coil can then be adjusted using the corresponding voltage without affecting the current in the other coil. The behavior of the decoupled system resembles that of a single-coil system. The decoupling works well independent of the setting, though from a practical point of view, only the ±90° current phase shift can feasibly be used, as seen in Figure 69. Any other phase shift produces different heating patterns from the two inductors.

Combining currents with an alternating ±90° phase shift always pro-

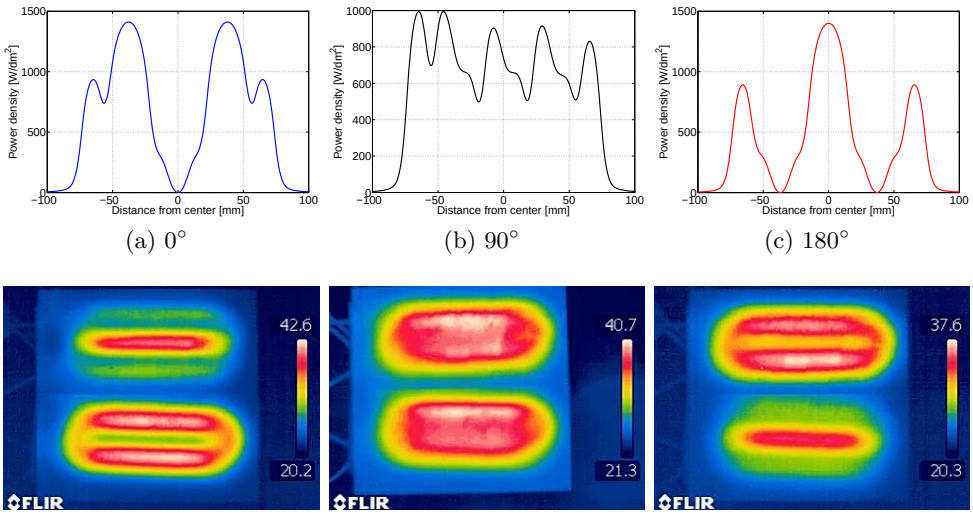

(a) 0° (b) 90° (c) 180°

(d) 0° (e) 90° (f) 180°

Figure 69: Thermographic images of induction heating using 0°, 90°, and 180° phase excitation and configuration.

duces symmetric results in the decoupled system. The heating pattern as a function of the current phase shift from 0 to 180°, given that the same negative phase shift is used half of the time, produces the results shown in Figure 70. As concluded in section 8.5, when disregarding saturation effects in the workpiece the results are the same, independent of the phase shifts; for saturation, the modeled results are somewhat similar to the experimental results.

By plotting the currents versus eachother for different frequencies and voltage phase shift yields the results in Figure 71, showing clear similarities of the behavior between the analytical and experimental results. The resonance frequency is marked with black circles, showing a maximized interference. The red/magent and blue/cyan markers indicate a frequency well below the resonance and well above resonance respectively.

8.11 Alternative geometries

This work has proven that TWIH can provide a fairly uniform heating pattern over a certain area in accordance with simulation models. The TWIH inductors used for verification serve as a simple lab platform but suffer from large inactive areas that are not practically useful due to coil ends and end

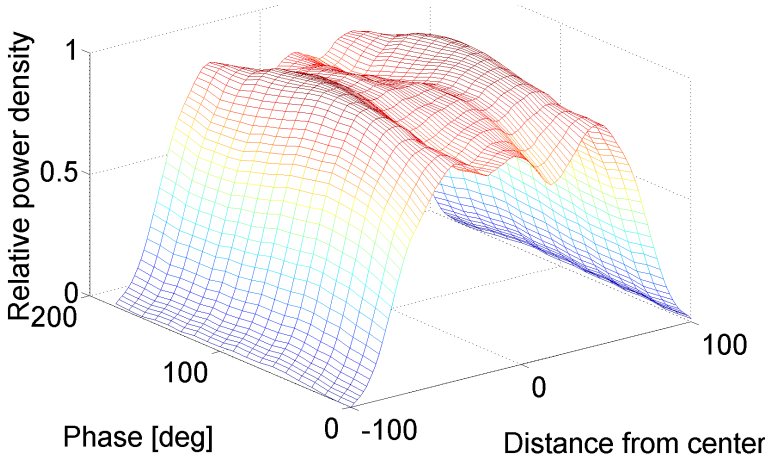

Figure 70: The heating pattern as a function of the current phase shift from $0 - 180°$.

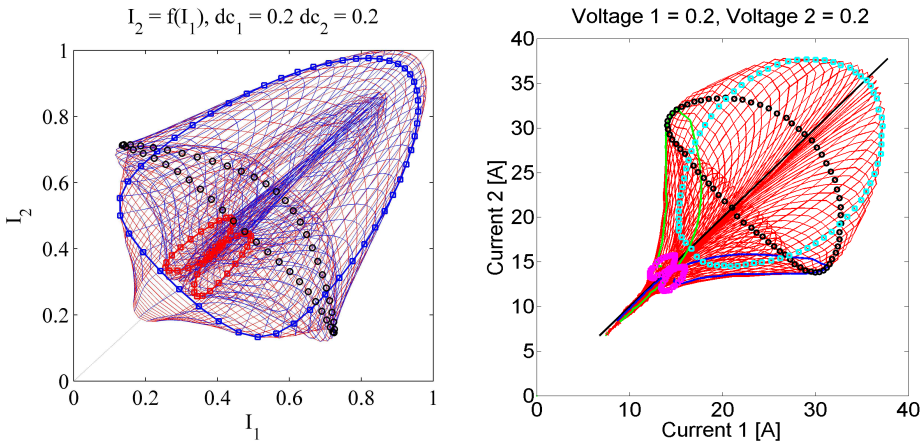

Figure 71: Left: Analytical solution. Right: Results.

effects. One way to extend the useful area relative to the boundaries is to build larger units or to combine several inductors to form one larger inductor. Increasing the number of wavelengths reduces the interaction between the currents, making the inductor more suitable for large surfaces. Figure 72 shows the principle of building modular units. The larger heating pattern in the figure is obtained by multiplying the heating pattern generated by one inductor, as shown, and rebuilding it as it corresponds to three wavelengths. By itself, the combined heating pattern provides no scientific information, though simulations yield similar results.

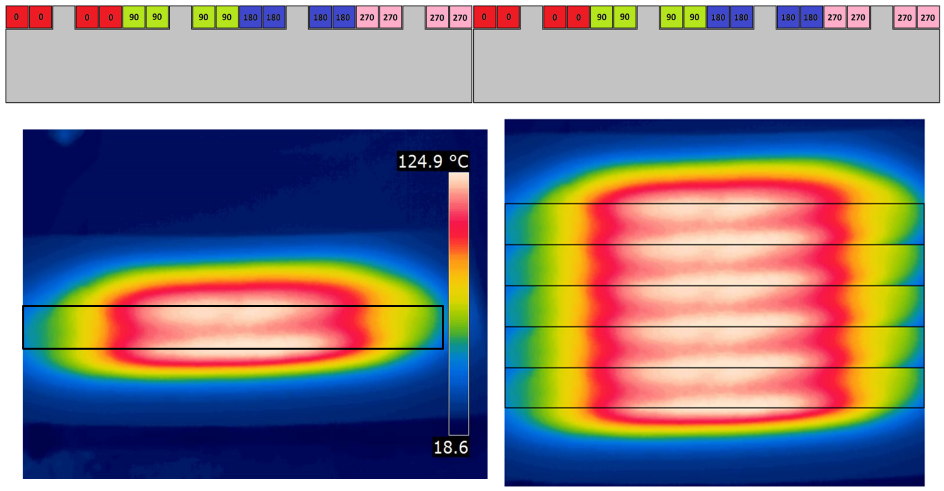

Figure 72: Left: Heating pattern generated by one inductor. Right: Heating pattern from several modular units.

The temperature pattern shown in Figure 72 can certainly be improved according to Figure 69e, but the spatial controllability is limited to one direction, i.e., the wave direction. By exploiting the permeability of the litz wire to electromagnetic fields, more flexible 2D inductor design solutions can be developed (Figure 73). Though in their infancy, 2D inductors based on litz wires with a strand diameter of 0.2 mm have been experimentally tested with successful results.

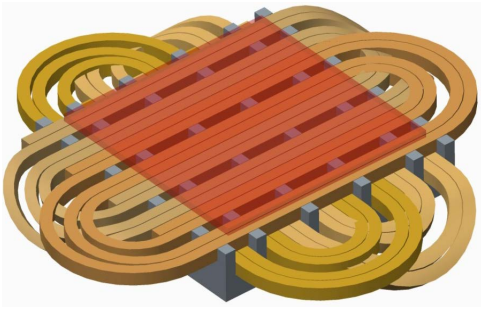

Figure 73: 2D inductor design based on litz wire.

The coil ends are an important to eliminate for three reasons: they contribute inductance, reducing system efficiency; they cause undesired edge effects [95]; and they consume space. A solution that solves the problem is the *labyrinth inductor* shown in Figure 74. It can be constructed in a

rectangular or round shape for any number of phases, in slotless or toothed forms, as illustrated. The sharp corners are complicated to produce from finished wires but can easily be made using multilayer printed circuit board (PCB) coils [96] [97] [98]. The flexibility of PCB coils in terms of their locally adjustable wire area and width allows for compensation for the power density, which is usually reduced at corners, for example. In the center of the inductor, travelling wave "collision behavior" arises, as described in section 8.5, not to be confused with cancellation. The labyrinth inductors, though yet to be scientifically tested and constituting future work, still serve a purpose: they justify simulation work related to wave collision and justify industrial interest in TWIH for built-in applications as well, such as in-tool heating.

Figure 74: Different conceptual coil designs in order to eliminate coil ends.

9 Surface heating using longitudinal field inductors

One of the most common coil configurations for induction heating is the longitudinal field configuration due to its high electromagnetic coupling and good ability to distribute power uniformly. These properties are related to geometries in which the coil can completely surround workpieces, such as shafts, gears, and wings, and in which workpieces, such as tubes and valves, can completely surround the coil. Little published work treats the heating of flat or curved surfaces where the coil does not surround the workpiece as illustrated in Figure 75. This configuration is still used to some extent by industry. This section investigates the heating pattern obtained using this technology and under what circumstances it can work properly.

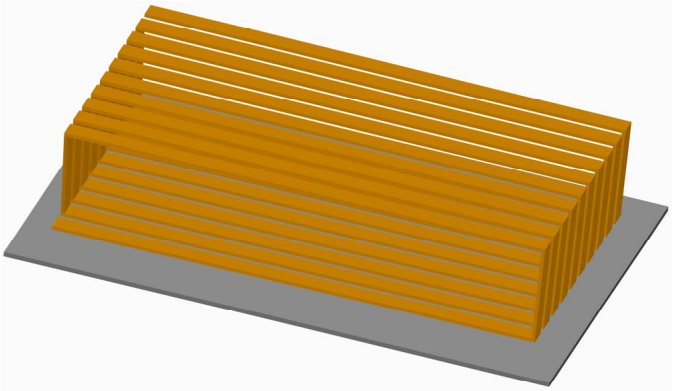

Figure 75: Illustration of LF-coil above a workpiece.

9.1 Electromagnetic simulations

According to Kirchoff's law, the sum of currents flowing into each point must be zero, which means that all current loops must be closed. To numerically investigate what happens to the current paths in the workpiece at the ends of the coil and at the edges of the workpiece, 3D simulations are necessary. While simulation models always simplify the real world, 2D simulations can often represent the problem accurately with reasonable memory useage without applying numerical tricks. For 3D problems, the memory requirements are a huge problem when working with problems concerning physical phenomena involving large differences in size. A parametric simulation model of the LFIH system was built in COMSOL Multiphysics using

two major simplifications. An impedance boundary condition was applied to the workpiece (equation 26) approximating all currents induced to flow on the surface, suitable for small skin depths. This means that the workpiece, which otherwise would have required a mesh size of less than 10 μm along the surfaces, must not be meshed at all for the electromagnetic simulation. $\vec{n}$ denotes a unit normal vector, H the magnetic field strength, ω the angular frequency, σ the electric conductivity, ϵ the permittivity, and j is $\sqrt{-1}$. The distribution of the dissipated power, P_d, is insted calculated based on the surface current density, J_S, using Equation 27, where E^* represents the complex conjugate of the electrical field.

$$\vec{n} \times \vec{H} + \sqrt{\frac{\varepsilon - j\sigma/\omega}{\mu}} \vec{n} \times (\vec{E} \times \vec{n}) = 0 \tag{26}$$

$$P_d = \frac{1}{2} \vec{J_S} \cdot \vec{E^*} \tag{27}$$

The other critical part of the model is the wire, which was approximated using line currents. Two versions of the model were made, one in which the coil was surrounded by air and one with a core of SM^2C, each with a 4-mm gap between coil and workpiece. These models are shown in Figure 76. By using the symmetries, the memory requirement could have been reduced by approximately 75%.

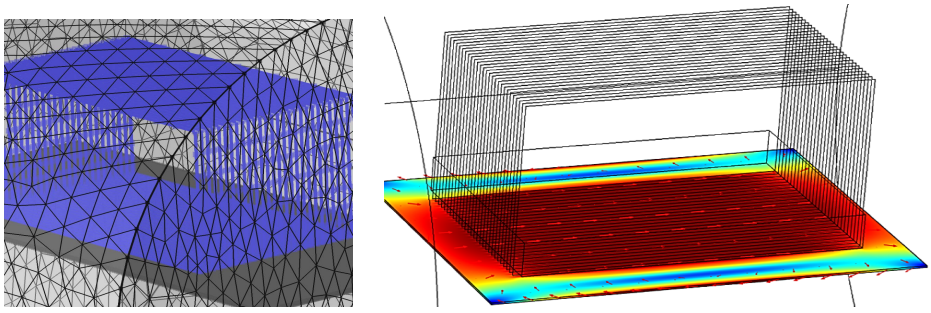

Figure 76: 3D simulation models of LFIH setups for outside heating. Left: Without core material. Right: With SM^2C core material.

For each of the two models, simulations were performed using workpiece dimensions ranging from 200 x 96 mm to 300 x 360 mm, corresponding to 100–150% of the coil length and 80–300% of the coil width. The different dimensions were selected based on realistic applications, to investigate how size influences the return paths of the currents. It is particularly interesting to observe the relative dimensions that force the currents to cross to the

opposite side of the workpiece and how this affects the heating pattern. Carbon steel EN 235JRG2 was selected as the workpiece, as it has a very small skin depth relative to the workpiece material at the frequency used, i.e., 20 kHz. After post-processing of the simulation results, the surface current density and paths can be shown for each side of the workpiece dimensions. Figure 77 shows the current densities using the inductor with SM^2C core for the workpiece 1.25 x 1.5 times the coil size.

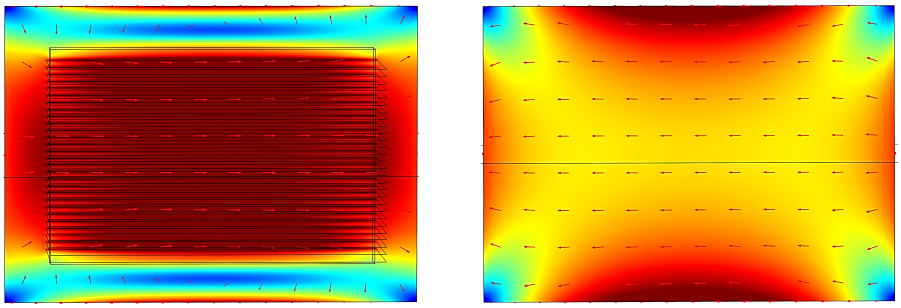

Figure 77: Current density and directions on the top and bottom surfaces, respectively, when using a SM^2C core; the workpiece is 250 x 180 mm.

9.2 Thermal analysis using time stepping

COMSOL Multiphysics was developed to handle coupled simulations by solving problems iteratively. In the present case, this means that the current creates power losses that heat the workpiece, which in turn affects the temperature-dependent resistivity that determines the heating power. The plan was initially to use the opportunities afforded by the software, but due to the small changes in temperature that were actually of interest in this case, the simplifications had a much larger impact than did the temperature. The significantly increased memory needed for coupled and transient simulations, combined with already large memory usage for steady-state solutions, could not justify use of a more complex model. In addition to the memory usage, the impedance boundary condition also further complicated the processing. Instead, the current densities and power losses on all six surfaces of the workpiece were exported for further computation in Matlab.

From earlier study [51] it is known that the temperature in a thin workpiece is fairly uniform throughout the thickness. Approximating the power generation in 2D using projection, in which the short ends are therefore assumed to generate power only along the boundaries, allows the temperature to be calculated at each point of the workpiece using time stepping. All

exterior cooling effects were neglected, meaning that the generated energy stayed inside the workpiece, which is a good approximation if the time is short and the temperature change small. The equilibrium is defined by the standard equation for energy conservation 28.

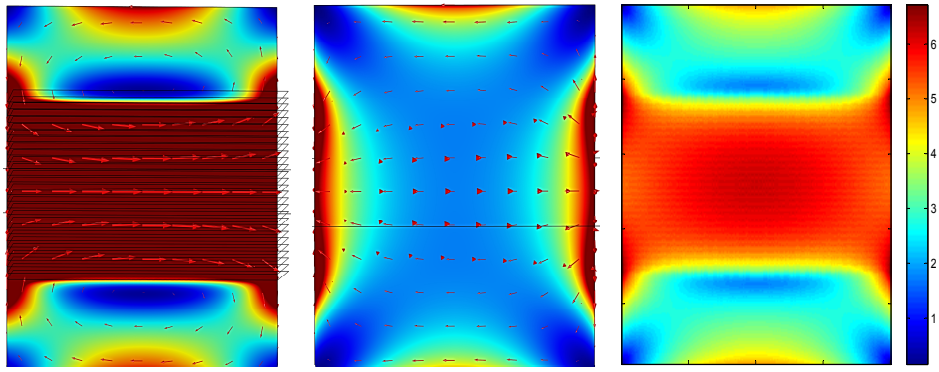

Figure 78: Power density along the top and bottom surfaces and the total projected power density in MW/m^3; the workpiece is 200 x 240 mm and the arrows indicate current directions.

The power generation was interpolated to a uniform square grid on which the temperature was calculated. In each time step, the updated temperature matrix was based on the previous temperature plus the supplied power converted into temperature by scaling with the thermal mass. The thermal conductivity of the plate was considered by calculating the thermal gradients based on the eight surrounding mesh points using distances of one unit and the square root of two units, respectively. The results of the computations were presented and compared with the measurement results in 9.3.

$$\rho c_p \frac{\partial T}{\partial t} - \nabla \cdot k \nabla T = Q(T, A) \tag{28}$$

9.3 Experimental results and comparison

Two LF inductors of a design similar to those modeled in the simulation environment were manufactured. The testing was performed using several workpieces of different dimensions in accordance with the models. To limit the effect of thermal conductivity in the workpiece material, the experiments were performed by applying a high power for a short time while recording the development of the temperature pattern using thermography. The heating reveals the regions where the induced currents are concentrated and the regions where the resulting current approaches zero. Figure 79 compares the

simulated and measured results of the heating for workpieces of the same length as the coil but 80, 120, 200, and 300% of the coil width, respectively. These results correspond to the inductor without core material.

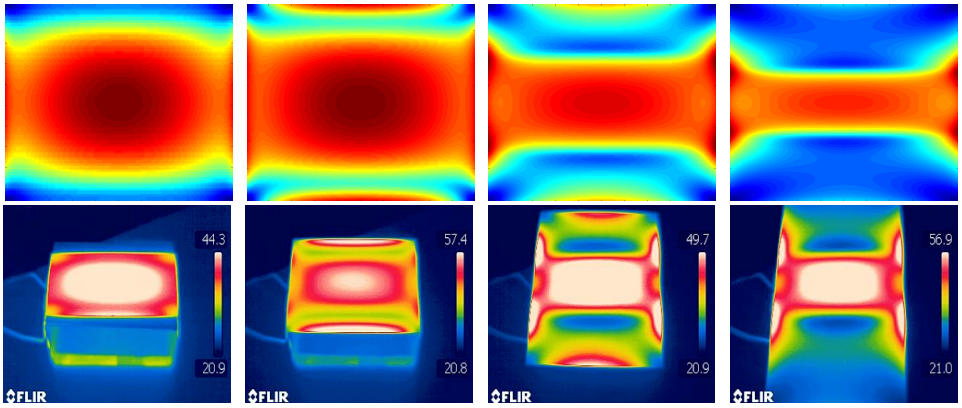

Figure 79: Simulated and measured temperature pattern for different workpiece dimensions obtained by outside LFIH.

By extracting the temperature profile along lines crossing the center of the workpiece perpendicular to the coil (Figure 80), one can conclude that the temperature pattern is significantly more uniform than with transversal flux heaters, though still far from uniform, and that the heating pattern is greatly dependent on the workpiece dimensions with a peak power density along the center and, for selected dimensions, along the edges as well. In the figure, solid lines represent workpiece lengths of 200 mm and dotted lines 300 mm, the larger workpiece, the higher the total output power generated. A drawback of this design is that areas of the inductor not covered by the workpiece or similar material add inductance that limits the power factor and degrades system performance. A solution would be to shield the open areas using a cooled copper mantle, for example, which would also reduce stray magnetic fields coming from these regions of the coil.

Good agreement between simulations and measurements are also obtained using the SM^2C core inductor. Due to the fairly low permeability of the core material, i.e., approximately 15, the differences in heating pattern with and without the core are not extreme, but clearly noticeable for certain workpiece dimensions (Figure 81). In the Figure, a workpiece of 2 x 3 times the active coil size was used and the return paths of the current are apparent.

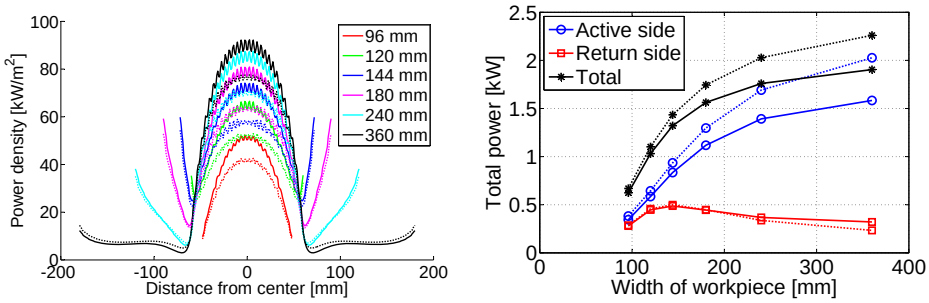

Figure 80: Left: Power density across the center, perpendicular to the coil, of workpieces of different sizes. Right: Total power induced in workpieces of different sizes. Solid and dotted lines represent workpieces with lengths of 200 mm and 300 mm, respectively [99].

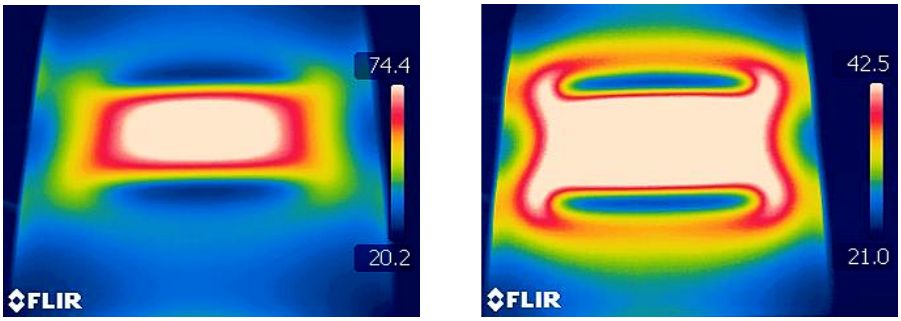

Figure 81: Heating pattern generated by a longitudinal field inductor. Left: Without core material. Right: with SM^{2}C core material. Coils are 200 x 120 mm and the workpieces are 300 x 360 mm.

10 Results and discussion

Induction heating involves many fields of knowledge, not all of which are covered here. However, by taking a significantly broader approach than does most research, cross-disciplinary challenges have been overcome and the developed solutions have been applied in narrower research fields. Though linking theoretical models to real measurements is a key component of research, most studies of induction heating omit the verification step, significantly reducing the value of the results. The present work treats the complete development chain, ranging from problem identification and definition, through model and simulation tool development, to experimental verification and full-scale demonstrators.

A parametric 2D simulation model of two-phase TWIH was developed and experimentally verified, and its results agree very well with measurements. The program enables the modeling of litz wire with a complex permeability bulk property that has been demonstrated to represent the real system with high accuracy. By sweeping the relative current amplitudes and phase shifts in the model, the power distribution, total power, and efficiency can be determined. The influence of the phase shift on the heating pattern and total output power was compared to experimental results. As expected, comparing the modeled power density with the temperature pattern of the real workpiece highlights some averaging effects due to thermal conductivity in the real case, though very good correlation is still obtained.

A challenge when working with mutually coupled systems is handling the current interference, which complicates the current control. The exact settings of the currents are critical in order to obtain the expected output power pattern. Based on a parameter study, various relationships were mapped: between the controllable parameters; between the voltage duty cycles, frequencies, and the properties sought; and between the current amplitudes and phase shifts. From these relationships, proper working points in terms of equally sized currents with a phase shift of $\pm 90^\circ$ could be extracted and successfully tested. Based on these results, a solution for automatic current control can be implemented without the risk of positive feedback—generally a problem in such systems. In addition, a method for decoupling the currents was found, using the anti-series or anti-parallel connection of two equal inductor setups. Using the decoupled system significantly simplified the control and contributed to some of the more important results obtained here.

To automatically investigate the efficiency and temperature distribution of any induction-heating system for flat surfaces, and of TWIH setups in particular, a thermographic tool was developed. By positioning an IR camera to

monitor the workpiece temperature, the system can record a stream of temperature matrices and automatically convert it to useful information. The necessary steps involve automatically identifying the corners of the workpiece and using projective transformation to compensate for the camera position by converting it so that all pixels cover the same given area. The result is the heating pattern of the complete workpiece, which can automatically be converted into supplied energy or power, based on the workpiece properties.

The results of the TWIH study clearly indicate that this principle can provide a nearly uniform heating pattern useful for industrial implementation, especially for heating large workpieces. Unlike most other types of induction heaters, TWIH setups can be built in modules, simplifying the production of very large units. It is useful to apply the method in parallel processes to compensate for mutual coupling, allowing very high efficiency to be obtained with inductors made from litz wire and a suitable core material. In this study, the coil ends consume unnecessary amounts of space; however, other designs, better adapted for various applications, can be developed and some examples are presented in the thesis.

From a scientific point of view, the work has produced a number of unique results, mainly related to travelling-wave induction heating. One of the more important results is the qualitative experimental verification of the heating pattern obtained from simulations. The characteristic asymmetry of TWIH systems was demonstrated analytically and numerically a long time ago [72] but is experimentally verified here for the first time. Two main aspects of the work independently made the verification possible: the work focused on finding working points (i.e., settings that produce a given amplitude and phase shift of the currents) and on decoupling the currents to facilitate generation of the desired currents. Another important part of the work is the development of the automatic measurement system [51], by itself not the most important scientific contribution, but crucial for evaluating TWIH systems.

A comprehensive study of a two-phase TWIH system has, as far as is known , not previously been undertaken. While traditional three-phase systems feature many parameters and very great complexity, the two-phase platform allows for detailed analyses of properties in a way never before presented in published research. The influence of current phase shifts and relative amplitudes on the induced power density distribution is one completely new finding, and the output current as a function of voltage duty cycle and frequency is another. Investigation of the heating results as a function of saturation effects in the workpiece is yet another novel result, saturation effects usually being disregarded without even a comment.

The asymmetric results obtained in TWIH are due to the direction of the travelling wave [72]; this is because of the interaction between the currents, which is not treated here. However, the effects on the heating pattern of multi-wavelength solutions have been analyzed as depending on the directions of the various waves. The results provide a good basis for further investigation of more complex travelling-wave inductor designs, as exemplified in the thesis.

The industrial benefits of the present work are obvious, and this is particularly emphasized by the commercialization of GreenHeat technology. With a significant number of heaters of this type already installed in industrial processes, the usefulness of combining litz wire with SM^2C and integrated cooling has already been verified. Several inductors on the market are based on bifilar winding because of the demands for uniform heating, which demonstrates the need for alternative inductor types, for example the travelling-wave inductor. As demonstrated in the work, multi-coil heaters entail certain complexities, but the heating pattern results can definitely justify their deployment and cost. With a high-efficiency heating solution that can fairly uniformly heat a surface within reach, offering large savings in cycle time and quality, the market is sure to increase.

11 Summary of appended publications

This section summarizes the content of each appended publication and points out the most important findings or contributions to the overall thesis research. In addition, the rationale for each publication is presented in order to situate the work in a larger context. The work presented here took a top–down approach, starting with the applications and then stepwise exploring a few important key features to meet the demands of the applications.

11.1 Paper 1—Industrial heating using energy-efficient induction technology [49]

This paper presents the principles and advantages of building induction heaters based on litz wire and molded flux concentrators. The goal is a high-efficiency, air-cooled unit that can be easily integrated into any machine or directly integrated into a process. The inductor design is a transverse-flux type, common for heating flat surfaces and simple to produce. The advantages of not only producing the flux concentrator in one piece, but of using the opportunity to mold it with cooling flanges to facilitate fan cooling, are demonstrated. The elegant solution of building inductors for low-power applications is successfully tested in an evaporator for removing pressing oil from sheet metal components. The same elegant design also disallows or severely complicates a deeper scientific analysis of the involved materials as well as the construction principle. Thermally coupled 3D electromagnetic simulations of such complex designs without significant simplifications are very demanding and require considerable computer capacity. A better design from an analytical perspective would have been an axisymmetric system, though this would not be as suitable from an industrial perspective.

11.2 Paper 2—Soft magnetic moldable composites: properties and applications [33]

The SM^2C material is a key component of the induction heaters studied and give them some unique properties. This paper presents the manufacturing, composition, and properties of the developed SM^2C material versus other SMMs. The structure of the material is investigated using scanning electron microscopy, which reveals the wetting of the binder and the particle size distribution in a selected region. The measurement principles used to investigate the magnetic permeability and losses, saturation effects, dielectric strength, thermal conductivity, and mechanical properties are explained.

The Steinmetz coefficients are calculated to quantify the influence of the frequency on the losses, which is important in high-frequency applications. A section on applications cites example of products in which the SM^2C material and its properties are suitable, and also cites cases in which the material has been tested but its properties have proven to be inappropriate—at least using existing designs.

11.3 Paper 3—A method for fast characterization of power efficiency in induction-heating processes [59]

Accurately measuring the efficiency of an induction-heating setup may appear simple, but it is actually quite complicated, especially if it is to be performed quickly using a generic tool not adapted to each particular setup in terms of workpiece material, geometry, power level, etc. To allow for the automatic measurement and analysis of both the heating pattern and efficiency, which is required for smooth progress with multiple-coil heaters, a thermography-based tool had to be developed. This paper describes the measurement difficulties and the steps required to advance from raw IR data, via emissivity estimation, projective transformation, and integration of the absorbed energy of the workpiece of a transient operation, to final estimates of the useful power. The input power is calculated by integrating the product of measured current and voltage, which is not always as simple as in this work. Simulations demonstrate the influence of skin depth on the response time of the measurement, which can also handle dynamic effects in a continuous process. The scientific depth of this article may be considered limited as all the steps are already known; nevertheless, it answers some important questions related to the IH process and provides an essential tool for further work, particularly after being complemented by automatic workpiece localization as described in the thesis.

11.4 Paper 4—Analysis of current paths in induction heating of flat sheets using single-sided longitudinal-field inductors [99]

It is commonly known to be nearly impossible to achieve uniform induction heating of an unmoving flat surface, and considerable research has examined this subject by exploring multi-coil solutions based on the transverse-flux design. On the other hand, for heating shafts using longitudinal-field inductors, achieving a uniform pattern is a simple task and is done in many industrial applications. Since all current paths must be closed, 3D simulation is needed

to investigate what really happens to the current paths when reaching the end of the coil or the edge of the workpiece. This paper presents a 3D FEM model created in COMSOL Multiphysics, using approximations such as line currents and the small-skin-depth boundary condition and assuming all currents to be surface currents. The simplifications made it possible to perform the simulations on a high-performance workstation computer. Two inductor designs were simulated, one with an SM^2C core and one without core material for a parametric-sized workpiece. The results were successfully verified in experiments demonstrating that the heating pattern can be nearly uniform, but that the pattern greatly depends on the size and position of the inductor in relation to the workpiece. In addition, the core material exerts an important influence on the results.

11.5 Paper 5—Induction heating using a two-phase travelling-wave setup [56]

To take the step from pure inductor design to optimizing the switching, facilitating convenient current and voltage measurements, and, most importantly, implementing fast control loops and accurately generating synchronized signals, developing a competent power electronic lab platform was necessary. This paper presents the details of the power electronic system and related components, including interfaces with other equipment coordinated using a personal computer. The article also summarizes the research published in the TWIH field around the world and the current status of this work. The paper mostly comprises theoretical analyses, and few practical investigations are described. The published experimental work suffers from the use of primitive analytical equipment, emphasizing the importance of the present work.

The initial results concerning two-phase TWIH obtained at Lund University are presented, including simulated and measured values of the heating pattern in a workpiece cross-section. There is good correlation between the simulated and experimental results, and the characteristic asymmetric behavior of TWIH systems is clearly illustrated. The results are compared with those obtained by running one coil at a time and the problem of mutual coupling is addressed.

11.6 Paper 6—Decoupling of currents in travelling-wave induction heating [94]

Multi-coil solutions for uniform induction heating have been a research area for the last few years and much effort has been dedicated to the coupling problem. Several solutions have been presented, including running the coils at different, optimally selected frequencies [100] and automatically controlling the phase angle between the currents to be zero. Solutions using decoupling transformers have been used to reduce, but not eliminate, the interference. This work presents another solution, also based on decoupling transformation but from the ideal case, in which saturation effects and the frequency selection do not affect the result. The paper evaluates a number of series and parallel connections using two nearly identical two-phase inductors and demonstrates a reduction in the mutual coupling of more than one order of magnitude. More precise manufacturing will improve this even more. This means that the high-efficiency TWIH solution is feasible in industrial applications in which electrical interference is no longer an issue. The paper also illustrates how the current phase angle affects the output power and compares the experimental results with simulations, finding good agreement.

11.7 Paper 7—An experimental parameter study of two-phase travelling-wave induction heating [90]

In understanding and controlling TWIH systems, the dynamics are of great importance. This paper characterizes a two-phase TWIH system in an extensive experimental parameter study, by sweeping the frequency, duty cycles of each coil, and voltage phase shift. The relationships between these control parameters and the currents, amplitudes, and phase shift are presented. The work focuses on the so-called desired working points, referred to as two equally sized currents with a phase shift of $\pm 90°$. The paper also presents a theoretical model based on analytical expressions obtained from LCR circuits, including transformer models representing mutual coupling and the relationship between coils and workpiece, also taking the losses into account. The model is fitted to measured values of the resistance and inductance of the coils of the real inductor as a function of frequency between 10 and 40 kHz, and is well correlated with the real system. The model uses a Fourier transform with ten harmonics to represent the square-wave voltage from the power electronics.

12 Author's contributions to the papers

This section identifies what the author contributed to the various papers and what parts were produced by others.

12.1 Paper 1—Industrial heating using energy-efficient induction technology [49]

The author performed the theoretical work and simulations by himself and wrote most of the text. The author was also involved in designing and manufacturing the induction heater and in parts of the testing. Parts of the testing of the finished prototype were performed by cooperating companies.

12.2 Paper 2—Soft magnetic moldable composites: properties and applications [33]

Most of the writing and work related to this paper were conducted by the coauthors. The author contributed mainly by analyzing the measurements and presenting the corresponding results, including regression analysis of the data to find the Steinmetz coefficients of various materials.

12.3 Paper 3—A method for fast characterization of power efficiency in induction-heating processes [59]

The author produced this paper by himself except for proofreading by his coauthors. The work included manufacturing and arranging the test platform, developing a transient coupled electromagnetic-to-thermal simulation model, conducting experiments, and analyzing results. Most of the work concerned developing software for running the heater, collecting data from the various sensors in a synchronized way, and image processing. Calibration was another key task needed in order to achieve reliable results.

12.4 Paper 4—Analysis of current paths in induction heating of flat sheets using single-sided longitudinal-field inductors [99]

The work related to this paper was performed exclusively by the author, except for proofreading and some minor help from lab personnel when manufacturing the test inductors. The major part of the work was developing

and using a parametric 3D longitudinal-field simulation model. In addition, the simulation results were analyzed and experimental validation was conducted.

12.5 Paper 5—Induction heating using a two-phase travelling-wave setup [56]

The paper was written by the author except for proofreading and minor revisions by the coauthors. The power cabinet was assembled by a cooperating company to a basic standard, and then refined by the author with the installation of transformers, reconfigurable capacitors, sensors, data-acquisition tools, etc. The author tested and analyzed the system and, together with the coauthors and workshop personnel, was involved in designing and manufacturing the inductor. Much of the work done by the author entailed reviewing previous work in the field, illustrated by a number of cited figures.

12.6 Paper 6—Decoupling of currents in travelling-wave induction heating [94]

The paper was written by the author, who also performed the theoretical investigation and simulations. In addition, the experiments were conducted by the author, but later refined by his colleagues and complemented with the experimental validation of the output power as a function of the current phase angle. In addition, a significant part of the inductor manufacturing was conducted by others.

12.7 Paper 7—An experimental parameter study of two-phase travelling-wave induction heating [90]

This paper can be divided into two parts, one analytical and one experimental. The author performed the tasks related to the experimental work, which entailed developing an automatic control and measurement system and analyzing the measured data, and wrote the description of these tasks. Considerable effort was spent identifying working points using methods that produce reliable results independent of the current waveform and harmonic content. The analytical section of the paper was written by one of the coauthors, who also performed the analytical work, which was iteratively developed and refined based on measurements.

References

[1] R. Wrangham, Catching Fire – How Cooking Made Us Human, Profile Books Ltd., ISBN 9781846682865, 2010

[2] D. Miyagi, A. Saitou, N. Takahashi, N. Uchida, and K. Ozaki, Improvement of zone control induction heating equipment for high-speed processing of semiconductor devices, IEEE Transactions on Magnetics, vol. 42, no. 2,pp. 292–294, 2006

[3] H. Fujita, K. Ozaki, N. Uchida, A Zone-Control Induction Heating (ZCIH)System for Semiconductor Processing, Electrical Engineering in Japan, Vol. 171, No. 1, 2010

[4] V. Rudnev, D. Loveless, R. Cook, M. Black, Handbook of Induction Heating, ISBN 0824708482, Marcel Dekker, Inc. 2003

[5] Alfred Muhlbauer, History of Induction Heating and Melting, ISBN 978-3-8027-2946-1, 2008

[6] `http://fluxtrol.com/chap-viii-historical-overview/`

[7] SSAB, Domex 700 MC Hot rolled, extra high strength, cold forming steel, Datasheet: 11-02-03 GB8421 DOMEX

[8] V. Demidovich, F. Chmilenko, P. Sitko, V. Nemkov, I. Rastvorova, Energy effective induction heating of aluminum billets before pressing, Proceeding of International Conference on Heating by Electromagnetic Sources - HES13, 2013

[9] M. Fabbri, A. Morandi, and P. L. Ribani, DC induction heating of aluminum billets using static permanent magnets, Proceeding of International Conference on Heating by Electromagnetic Sources - HES13, 2013

[10] R. Kolleck, R. Veit, M. Merklein, J. Lechler, M. Geiger, Investigation on induction heating for hot stamping of boron alloyed steels, CIRP Annals - Manufacturing Technology 58, pp. 275–278, 2009

[11] H. Fujita, N. Uchida, K. Ozaki, Zone Controlled Induction Heating (ZCIH): A New Concept in Induction Heating, Proceeding of the Power Conversion Conference - Nagoya, 2007. PCC '07, pp. 1498 - 1504

[12] J. Wang, J. Li, Y. Wang, X. Yang, Simulation of Travelling Wave Induction Heating Systems, WAC-2008 - Automation Congress, pp. 1-4, USA, 2008

[13] R. Ernst, D. Perrier, J. Feigenblum, R. Hemous, 3D inductive phenomena modelling, Proceedings of the COMSOL Users Conference, France, 2006

[14] R. S. Ruffini, R. T. Ruffini, V. S. Nemkov, R. C. Goldstein, Enhancing Induction Heating Processes by Applying Magnetic Flux Controllers, ASM 1999

[15] R. T. Ruffini, V. S. Nemkov, R. C. Goldstein, Influence of Magnetic Flux Controllers on Induction Heating Systems, Computer Simulation and Practice, ASM 2001

[16] V. Nemkov, Magnetic Flux Control in Induction Installations, Proc. of Int. Symposium HES-13 "Heating by Electromagnetic Sources", Padua, Italy, May 2013

[17] V. Nemkov, Magnetic flux control in induction heat treating, Proc. of Int. Symposium HES-13 "Heating by Electromagnetic Sources", Padua, Italy, May 2013

[18] B. W. Williams, Power Electronics: Principles And Elements, ISBN 9780955338403, 2006

[19] R. Hilzinger, W. Rodewald, Magnetic Materials - Fundamentals, Products, Properties, Applications, Publicis Publishing, ISBN 978-3-89578-352-4, 2012

[20] ASTM Standards Specification -09, A345, A664, A677, A683, A726, A840, A876, 2009

[21] ASTM Standards Specification -13, ASTM A976-13, 2013

[22] JFE Super Cores - Magnetic Property Curves, JNEX-CORE JNHF-CORE, catalogue Oct.'03-1-2,JUP, Cat.No.F2E-001-00

[23] JFE Super Core (Electrical steel sheets for high-frequency application), catalogue 0708R(0403)1-1 JUP, Cat.No.F1E-002-01

[24] T. Meydan, Application of amorphous materials to sensors, Journal of Magnetism and Magnetic Materials, Volume 133, Issues 1–3, 1 May 1994, Pages 525–532

[25] H. Gavrila, V. Ionita, Crystalline and amorphous soft magnetic materials and their applications: status of art and challenges, Journal of Optoelectronics and Advanced Materials 4 (2002) 173–192.

[26] G. Herzer, Handbook of Magnetic Materials, Volume 10, Pages 415-462, 1997

[27] G. T. Nikolov, V. C. Valchev, Nanocrystalline magnetic materials versus ferrites in power electronics, Procedia Earth and Planetary Science 1 (2009) 1357–1361, The 6th International Conference on Mining Science & Technology, 2009

[28] Magnetic materials producers association, Soft Ferrites, MMPA SGF-98, 1998

[29] Tianjin Huigao Magnetics Co. Ltd., `http://www.directindustry.com/prod/tianjin-huigao-magnetics-co-ltd/soft-ferrite-cores-79831-1036719.html` accessed 2014-01-10

[30] R. Ruffini, N. Vyshinskaya, V. Nemkov, R. Goldstein, C.J. Yakey, Innovations in Soft Magnetic Composites and their Applications in Induction Systems, ASM 2013

[31] C. Pompermaier, Finite Elements performance Evaluation of a Transverse Flux Machine using Somaloy 500 1P, 700 3P and 5P, Presentation at JMAG Users Conference, Frankfunrt, July, 2012

[32] Höganäs AB (publ.), Somaloy® Technology for Electric Motors, Typical Data, `www.hoganas.com/somaloy`, March, 2011

[33] L. Svensson, K. Frogner, T. Cedell, P. Jeppsson, M. Andersson, Soft Magnetic Moldable Composites - Properties and Applications, Journal of Magnetism and Magnetic Materials 324 (2012) pp. 2717–2722, Elsevier

[34] P. Jeppsson, M. Andersson, T. Cedell, M. Alaküla, A. Reinap, Rotocast: A new method to produce optimally packed SMC components, Proceedings of Swedish Production Symposium, Stockholm, 2008.

[35] M. Andersson, T. Cedell, P. Jeppsson, M. Alaküla, Patent SE533657 C2/SE0702311 L, Pulverbaserad, mjukmagnetisk, induktiv komponent samt metod och anordning för tillverkning därav, 2010

[36] H. Strindberg, Termisk analys av integrerade funktionella element i SM^2C, Master Thesis, Lund University, CODEN:LUTMDN/(TMMV-5234)/1-57/2010, 2010 (Swedish)

[37] D. Kihlbaum, Bindemedelsystem för SM^2C-material, Master Thesis, Lund University, LUTMDN(TMMV-5240)1-111/2011, 2011

[38] A. Warner, Working with litz wire, `http://www.allem.com/files/litzw.pdf`, accessed 2013-12-20, also published in Wiring Harness News

[39] Termination Methods for Litz Wire, `http://www.newenglandwire.com`, accessed 2013-12-20, Issue 4, July 2007

[40] OSCO - specialist electronic materials, `http://www.osco.uk.com/products/cable/litz-wire`, accessed 2014-01-09

[41] C. R. Sullivan, Cost-Constrained Selection of Strand Diameter and Number in a Litz-Wire Transformer Winding, IEEE Transactions on Power Electronics, vol. 16, no. 2, 2001

[42] C. R. Sullivan, Optimal Choice for Number of Strands in a Litz-Wire Transformer Winding, IEEE Transactions on Power Electronics, vol. 14, no. 2, pp. 283–291.

[43] HM Wire International Inc., R.1.09.16.2011, Litz Designing Calculations, `http://www.litz-wire.com`, accessed 2013-12-02

[44] HM Wire International Inc., Insulation Film-Enamel Guide, `http://www.litz-wire.com/pdf%20files/Copper_Wire_Film_Insulation_Enameled_Guide.pdf`, accessed 2013-12-02

[45] M. Etemadrezaei, S. M. Lukic, Equivalent Complex Permeability and Conductivity of Litz Wire in Wireless Power Transfer Systems

[46] X. Nan, C. R. Sullivan, An Equivalent Complex Permeability Model for Litz-Wire Windings

[47] D. C. Meeker, An improved continuum skin and proximity effect model for hexagonally packed wires, Journal of Computational and Applied Mathematics, vol. 236, pp. 4635–4644, 2012

[48] H. Kagimoto, D. Miyagi, N. Takahashi, N. Uchida, and K. Kawanaka, Effect of Temperature Dependence of Magnetic Properties on Heating Characteristics of Induction Heater, IEEE Transactions of magnetics, vol. 46, no. 8, pp. 3018-3021, 2010

[49] K. Frogner, M. Andersson, T. Cedell, L. Svensson, P. Jeppsson, J-E. Ståhl, Industrial heating using energy efficient induction technology, 44th CIRP International Conference on Manufacturing Systems, USA, 2011

[50] L. Svensson, M. Andersson, T. Cedell, P. Jeppsson, A. Fröjvik, Electrical isolation of coils in SMC applications, Swedish Production Sumposium (SPS11), 2011

[51] K. Frogner, L. Svensson, M. Andersson, T. Cedell, J-E. Ståhl, A new concept of coil design for industrial induction heating, SPS11 - Swedish Production Symposium, Sweden, 2011

[52] B. Paya, O. Pateau, Y. Neau, Development of energy saving solutions for induction heating devices, International symposium on heating by electromagnetic sources, Padua (Italy), May 18-21, pp. 271-276, ISBN 978-88-89884-13-3, 2010

[53] `http://www-ferp.ucsd.edu/LIB/PROPS/PANOS/al2o3.html` accessed 2013-01-13, refers to Goodfellow Cambridge Ltd., "Metals, Alloys, Compounds, Ceramics, Polymers, Composites", Catalogue 1993/94.

[54] Tongling Jinglong Electric Material Co. Ltd., `http://www.tljinglong.com/en/info.asp?base_id=9` accessed 2014-01-26

[55] C. Högmark, A. Reinap, K. Frogner, M. Alaküla, Laminated Winding with a Rapid Cooling Capability for Electrical Machines, CWIEME, 2012

[56] K. Frogner, T. Cedell and M. Andersson, Induction heating using a two-phase travelling wave setup, Internatinal Journal of Applied Electromagnetics and Mechanics (IJAEM), DOI 10.3233/JAE-141762, 2014

[57] G. C. Bosco, M. Garcocz, K. Lind, U. Pogliano, G. Rietveld, Phase Comparison of High-Current Shunts up to 100 kHz, IEEE Transactions on Instrumentation and Measurement, vol. 60, no. 7, 2011

[58] U. Hetzler, K. Göpfrich, R. Stark, Paradigm change for frequency converters - Shunts instead of current transformers, Elektronik Industrie, issue 1/2, 2005

[59] K. Frogner, T. Cedell and M. Andersson, A method for fast characterization of power efficiency in induction heating processes, SPS12 - Swedish Production Symposium, Sweden, 2012

[60] E. J. Davies, Conduction and induction heating, ISBN: 0 86341 174 6, 2007

[61] E. J. Davies, Patent Specification, No. GB1513241/2, Appl. No. 8847/74, 1974

[62] L. Pang, Y. Wang, T. Chen, New Development of Traveling Wave Induction Heating, IEEE Transactions on Applied Superconductivity, vol. 20, no. 3, 2010

[63] F. Dughiero, S. Lupi, V. Nemkov, P. Siega, Travelling Wave Inductors for the Continous Induction Heating of Metal Strips, Proceedings of the 7th Mediterranean Electrotechnical Conference, pp. 1154-1157 vol 3, Turkey, 1994

[64] Y. Wang, J. Wang, The study of two novel induction heating technology, International Conference on Electrical Machines and Systems, 2008. ICEMS 2008.

[65] J. H. H. Alwash, L. J. B. Qasir, Helical winding induction heating system, Journal of engineering, vol. 13, no. 1, 2007

[66] J. Egalon, S. Caux, P. Maussion, M. Souley, O. Pateau, Multi phase system for metal disc induction heating: modelling and RMS current control, IEEE Transactions. Industry Applications, vol 48, no 5, September/October, 2012

[67] F. Dughiero, S. Lupi P. Siega, Analytical calculation of travelling wave induction heating systems, Proceedings of ISEF - International Symposium on Electromagnetic Fields in Electrical Engineering, pp. 207-210, Poland, 1993

[68] F. Dughiero, S. Lupi P. Siega, Analytical calculation of double sided travelling wave induction heating systems, COMPEL, vol. 14, no. 4, pp. 251-255, 1995

[69] F. Dughiero, S. Lupi P. Siega, Calculation of forces in travelling wave induction heating systems, IEEE Transactions on magnetics, vol. 31, no. 6, 1995

[70] Y. Wang, J. Wang, J. Li, H. Li, Analysis of induction heating eddy current distribution based on 3D FEM, IEEE Region 8 Sibircon, 2008

[71] J. Wang, Y. Wang, Study about temperature modeling of travelling wave induction heating, International Conference on Electrical Machines and Systems, 2008. ICEMS 2008.

[72] A. Ali, V. Bukanin, F. Dughiero, S. Lupi, V. Nemkov, P. Siega, Simulation of multiphase induction heating systems, 2nd International Conference on Computation in Electromagnetics, pp. 211-214, United Kingdom, 1994

[73] T. Sekine, H. Tomita, S. Obata, Y. Saito, An Induction Heating Method with Traveling Magnetic Field for Long Structure Metal, Electrical Engineering in Japan, vol. 168, no. 4, 2009

[74] T. Sekine, H. Tomita, Y. Saito, S. Obata, S. Yoshimura, Induction Heating with Traveling Magnetic Field for Uniform Heating to Flat Metal, PEDS'07 - 7th International Conference on Power Electronics and Drive Systems, 2007

[75] H. Tomita, T. Sekine, S. Obata, Induction Heating Using Traveling Magnetic Field and Three-Phase-Frequency Inverter, 11th European Conference on Power Electronics and Applications, no. 371, 2005

[76] F. Sanz, C. Franco, C. Sagues, D. Paesa, S. Llorente, Flexible Cooking Zones with 2D mobile Inductors in Induction Hobs, IEEE, 2012

[77] Y. Wang, J. Wang, L. Pang, S. L. Ho, W. N. Fu, An advanced double-layer combined windings transverse flux system for thin strip induction heating, Journal of Applied Physics 109, 07E511, 2011

[78] S. L. Ho, J. Wang, W. N. Fu, Y. H. Wang, A novel crossed travelling wave induction heating system and finite element analysis of eddy current and temperature distribution, IEEE Transactions on Magnetics, vol. 45, no. 10, 2009

[79] Y. Wang, J. Wang, S. L. Ho, X. Yang, W. N. Fu, Two novel induction heating technologies: Transversal flux induction heating and travelling wave induction heating, Advances in Induction and Microwave Heating of Mineral and Organic Materials, ISBN 978-953-307-522-8, pp 181-206, 2011

[80] J. Wang, Y. Wang, S. L. Ho, X. Yang, W. N. Fu, G. Xu, Design and FEM Analysis of a New Distributed Vernier Traveling Wave Induction Heater for Heating Moving Thin Strips, IEEE Transactions on Magnetics, vol 47, no 10, 2011

[81] J. Wang, S. L. Ho, W. N. Fu, Y. H. Wang, Design and analysis of a novel traveling wave induction heating system with magnetic slot wedges for heating moving thin strips, IEEE Transactions on Magnetics, vol. 46, no. 6, 2010

[82] L. Pang, Y. Wang, T. Chen, Analysis of eddy current density distribution in slotless traveling wave inductor, International Conference on Electrical Machines and Systems, 2008. ICEMS 2008.

[83] J. I. Rodriguez S. B. Leeb, A Multilevel Inverter Topology for Inductively-Coupled Power Transfer, IEEE Transactions on Power Electronics, vol. 21, no. 6, pp. 1607-1617, 2006

[84] H. N. Pham, H. Fujita, K. Ozaki, N. Uchida, Dynamic Analysis and Control of a Zone-Control Induction Heating System, IEEE Energy Conversion Congress and Exposition (ECCE), 2011

[85] J. Acero, L. M. Burdío, L. A. Barragán, R. Alonso, A model of the equivalent impedance of the coupled winding-load system for domestic induction heating application, IEEE International Symposium on Industrial Electronics ISIE-2007, 2007

[86] H. N. Pham, H. Fujita, K. Ozaki, and N. Uchida, Estimating Method of Heat Distribution Using 3-D Resistance Matrix for Zone-Control Induction Heating Systems, IEEE Transactions on Power Electronics, vol. 27, no. 7, pp. 3374-3382, 2012

[87] M. Souley, A. Spagnolo, O. Pateau, B. Paya, J.C. Hapiot, P. Ladoux, and P. Maussion, Methodology to characterize the impedance matrix of multi-coil induction heating device, Proceedings of International Conference EPM 2009 Electromagnetic Processing of Materials, Dresden (Germany), Oct. 2009.

[88] D. Meeker, Finite Element Method Magnetics: OctaveFEMM, Version 1.2, User's Manual, (`http://www.femm.info/Archives/doc/octavefemm.pdf`,) 2010

[89] D. Meeker, Finite Element Method Magnetics, Version 4.2, User's Manual, (`http://www.femm.info/Archives/doc/manual42.pdf`,) 2010

[90] K. Frogner, O. Gutnichenko, T. Cedell, M. Andersson, An experimental parameter study of two-phase travelling wave induction heating, IEEE Transactions on Magnetics, submitted, 2014

[91] H. N. Pham, H. Fujita, N. Uchida, K. Ozaki, Heat Distribution Control using Current Amplitude and Phase Angle in Zone-Control Induction Heating Systems, Proc. of IEEE Energy Conversion Congress and Exposition (ECCE), 2012

[92] H. Fujita, N. Uchida, K. Ozaki, A New Zone-Control Induction Heating System Using Multiple Inverter Units Applicable Under Mutual Magnetic Coupling Conditions, IEEE Transactions on Power Electronics, vol. 26, no. 7, 2011

[93] R. V. S. Sengar, A. Barve, M. Khmeriya, Optimum Controlling of High Phase/frequency current in a multiple inverter system for Zone – Control Induction Heating, International Journal of Emerging Technology and Advanced Engineering, ISSN 2250-2459, Volume 2, Issue 10, October 2012

[94] K. Frogner, T. Cedell and M. Andersson, Decoupling of currents in travelling wave induction heating, Journal of Electromagnetic Analysis and Applications, (JEMAA), 2014

[95] S. Lupi, M. Forzan, Comparison of edge-effects of transverse flux and travelling wave induction heating inductors, IEEE Transactions on magnetics, vol. 35, no. 5, pp. 3556-3558, 1999

[96] D. W. Baarman, J. K. Schwannecke, W. E. Guthrie, R.A. Wahl and P. Duckworth, US Patent, Printed circuit board coil, US7973635B2, 2011

[97] I. Lope, C. Carretero, J. Acero, R. Alonso and J. Miguel Burdío, Printed circuit board inductors for domestic induction heating, Proceeding of International Conference on Heating by Electromagnetic Sources - HES13, 2013

[98] Printed circuit board implementation of small inductors for domestic induction heating applications using a planar litz wire structure, Proceeding of the Twenty-Eighth Annual IEEE Applied Power Electronics Conference and Exposition (APEC), pp. 2402-2407, 2013

[99] K. Frogner, T. Cedell and M. Andersson, Analysis of Current Paths in Induction Heating of flat sheets using single sided Longitudinal Field Inductors, 15th Biennial IEEE Conference on Electromagnetic Field Computation (CEFC), 2012

[100] Patent: WO2005/043737 A3